Doctoral Dissertation

Development of fluorine induced microporous silica membranes for carbon dioxide separation

(CO_2分離のためのフッ素含有シリカ系多孔膜の開発)

Ikram Rana

Chemical Engineering Program

Graduate School of Advanced Science and Engineering

Hiroshima University

(広島大学大学院先進理工系科学研究科)

September, 2023

Contents

Chapter 3

Chapter 5

Chapter 1

General Introduction

1.1. Background of CO_2 emission and separation

Excessive release of anthropogenic gases, such as carbon dioxide (around 2 billion tons of CO_2 per year), from existing power plants is significantly contributing in the global warming (~ 1 ºC) [1-3]. Fig. 1-1 indicates those sectors which are considered major contributors in the emission of carbon dioxide (CO_2). The production of electricity accounts for 44.4% CO_2 emission and is dominant sector followed by transportation with 24% CO_2 emission, industry 19.4%, and residential sector with 7% CO_2 emission. The dominance of electricity in CO_2 emission is because of extensively utilized fossil fuels to meet the energy requirements. Since electricity producing power plants run by fossil fuels are easy to operate at desired conditions [4, 5]. In similar manners, natural gas streams where CO_2 concentration is about 80% and it must be reduce to 2% to avoid the equipment damage, since CO_2 become very corrosive in the presence of water vapors and consequently it could increase the operational cost [6-8]. Therefore, the increasing CO_2 emission and global concerns regarding climate change has drawn considerable attention of scientific community to overcome this core issue. Hence, in order to protect the environment affected by CO_2 emission, rigorous efforts are required to develop CO_2 capture technologies which account for 90% of CO_2 recovery by limiting the energy requirements up to the 35% in coal-fired power plants as well as the natural gas streams [9-14].

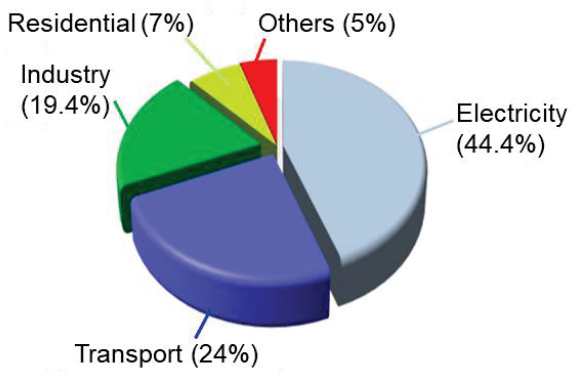

Fig. 1-1. Pie chart depicts the various CO_2 emission sources [4].

On that account, CO_2 capture from bulky industrial wastes is technological and scientifically challenging and target separation performance is being conducted while using following CO_2 capture strategies as shown in Fig. **1-2** [15, 16].

✓ **Oxy-fuel combustion**

This combustion system utilizes the pure oxygen instead of using air to burn the primary fuel gas as shown in Fig. 1-2a. Oxygen mixed with flue gas such as coal gas, biomass, and natural gas to produce flame which burns at higher temperature more efficiently than using air. This system with oxidant environment (95% oxygen) offers significant results with high level of CO_2 recovery containing less N_2 contents in carbon capture and storage system (CCS) technology [16-18].

✓ **Pre-combustion capture**

Pre-combustion CO_2 capture as shown in Fig. 1-2b, involves the process in which primary fuel is desulfurized to obtain higher catalytic efficiency to be used in further steps. After that, primary fuel is mixed with oxygen or air to produce carbon monoxide (CO) and

hydrogen (H_2). This mixture (syngas) then reacted with steam to produce CO_2 and additional hydrogen followed by water gas shift conversion reaction. Membrane gas separation or pressure swing method can be used to capture H_2/CO_2 at high pressure (~80 bar) and temperature (~700 ºC). Target gas (H_2) is suitable to use as a clean energy fuel and remaining CO_2 (30-35%) is stored for various applications and simultaneously to prevent its release in atmosphere [16, 19, 20].

✓ **Post-combustion capture**

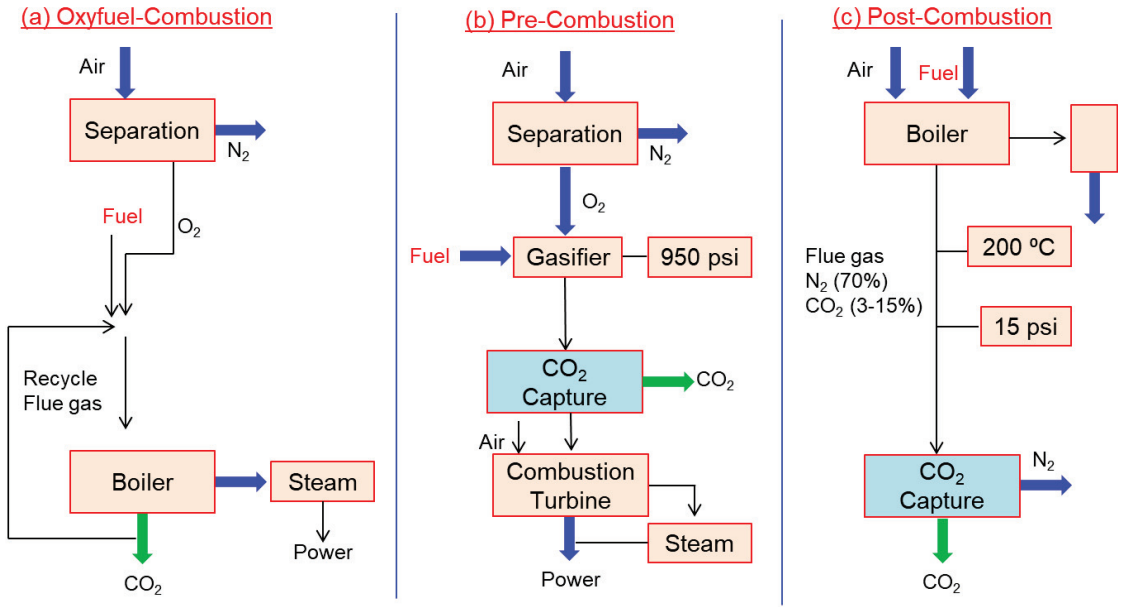

Fig. 1-2. Schematic image of various CO_2 capture processes [15, 16].

Fig. 1-2c shows the post-combustion CO_2 capture system which is considered easy in operation by comparison with other two methods since it can be used in existing power plants without further modifications. Nonetheless, post-combustion process is more

challenging and required vigorous attentions while developing technologies to be used in this system. Since employed separation technology has to be deal with several factors (high temperature, low pressure, water vapors, etc...) which have direct influence on the separation efficiency of the system applied for CO_2 capture. Herein, CO_2 is captured at very low temperature and with low CO_2 concentration from mixture containing CO_2/N_2 along with other possible gases such as SO_2, NO_2, and O_2. Table 1-1 summarizes the various CO_2 capture processes and respective technologies. In particular, post-combustion capture, where target gas (CO_2) is separated at 25 ºC after emission of fossil fuels, is being employed in commonly used amine absorption, cryogenic separation, and membrane gas separation because of low operational cost and low modification difficulty [21-23].

Table 1-1. Various CO_2 capture processes and respective methods [24].

Process	Separation system	Current technology
Oxy-fuel combustion	CO_2/H_2O, O_2/N_2	Absorption
Pre-combustion	CO_2/H_2	Absorption, Adsorption
Post-combustion	CO_2/N_2	Absorption, Membranes

1.2. Current CO_2 separation methods

Following methods are operational to carry out the current needs of CO_2 capture/separation.

1.2.1. Chemical/physical absorption

Amines based absorption is most widely used CO_2 capture method in petroleum, coal-fired plants, and natural gas streams due to its high level (~90%) of CO_2 capture performance. Chemical absorption involves reaction between CO_2 and mono, di, tri, and isopropanol amines [25, 26]. In the process industry, CO_2 containing flue gas absorbed into the amine solution and this solution regenerated followed by the CO_2 desorption at high temperature (120-140 ºC) and low pressure (1.0 bar) [27]. Fig. 1-3 illustrates the annual publication volume consists of amine based absorption [24].

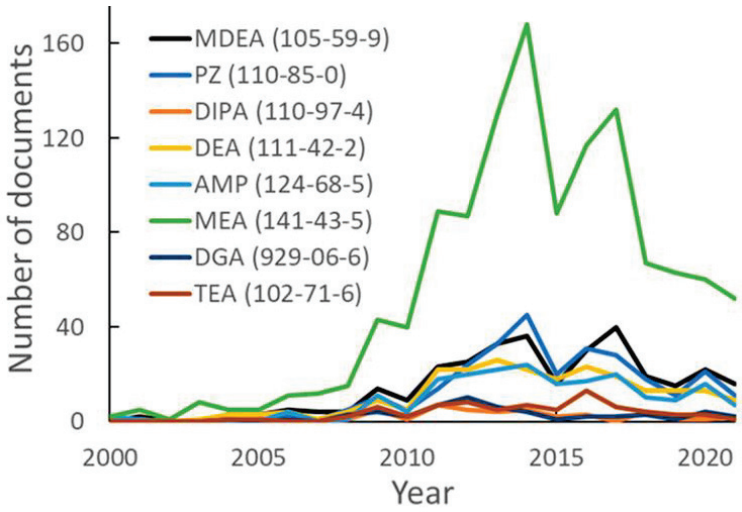

Fig. 1-3. Annual publication related to CO_2 capture using amine based absorption solvents. TEA, triethanolamine; PZ, piperazine; DIPA, diisopropanolamine; AMP, aminomethylpropanol; DGA, diglycolamine [24].

Commonly, primary (monoethanolamine, MEA), secondary (diethanolamine, DAE), and tertiary (N-methyldiethanolamine (MDEA) amines, which offers fast kinetics and strong

chemical reaction for CO_2 molecules, have been utilized extensively as an amine source. There are several advantages such as maturity of amine absorption process, widely commercialized, and modification to existing power plants associate with chemical absorption of CO_2. Despite of strong CO_2 and amine interaction, these amine candidates are appeared to have some drawbacks of low CO_2 loading, energy intensive, corrosive, amine degradation, and system compactness [28-30].

Similarly, physical absorption involves the dissolution of CO_2 and this method is feasible in pre combustion process due to the low temperature and high pressure. Commonly used physical solvents are propylene carbonate, methanol, polyethylene glycol dimethyl ether, and N-methyl-2-pyrrodilone. These solvents are possessing similar CO_2 solubility at ambient temperature. However, some of the solvent such as polyethylene glycol dimethyl ether exhibit low vapor pressure which results in less solvent loss but it also suffer from high viscosity. A recent study reported the physical absorption capacity of propylene carbonate solution which contains 2-methylimidazol and ethylene glycol. The results showed significantly improved CO_2 solubility over methane, nitrogen, and hydrogen. The regeneration of physical solvent is less energy intensive compared to solvents used in chemical absorption [31-35]. Fig. 1-4 shows the publication volume for various physical absorbents and methanol dominates the other three absorbents in both journal publications as well as the patents [24].

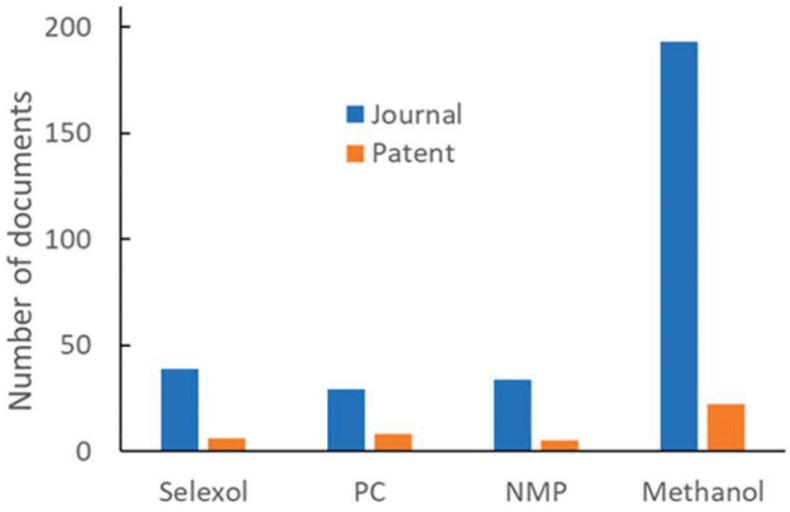

Fig. 1-4. Publication volumes for various physical absorbents used for CO_2 capturing process [24].

1.2.2. Adsorption process

Porous solid absorbents are used in CO_2 adsorption process. This method can be used in pre combustion, post combustion, and direct air capture process. Additionally, solid adsorbents are stable, less hazardous, and easy to handle compared to physical/chemical solvents utilized for CO_2 capture. Most commonly used solid adsorbents are zeolites, carbon, and metal organic frameworks (MOF). These porous adsorbents have some drawbacks such as low uptake, sensitive to moisture, and cost effectiveness. Thus, various studies have focused to improve the uptake of CO_2 as well as the resistance to moisture contents by using these solid adsorbents [36, 37]. Acevedo et al. [38] reported the CO_2 adsorption capacity of activated carbons consists of lignocellulosic material and Cu $(NO_3)_2$. The optimum CO_2 adsorption capacity was ascribed to the ACCu-31073 and further results revealed that obtained activated carbons for CO_2 adsorption is energy efficient. Another

study reported the CO_2 adsorption capacity of activated carbons prepared from African palm shells and later dissolute with NH_4OH and HNO_3. Fig. 1-5 shows the structure of metal organic frameworks (MOFs) used for CO_2 capture in post combustion process [39]. The modified activated carbons demonstrated decreased surface area and pore volume but favorable CO_2 adsorption sites were significantly increased which assisted high uptake of adsorbed CO_2 in respective activated carbons. Table 1-2 summarizes some of the design parameters among membranes and chemical absorption process [5]. It is evident from the data that membrane process possesses promising characteristics from operational flexibility to energy efficiency.

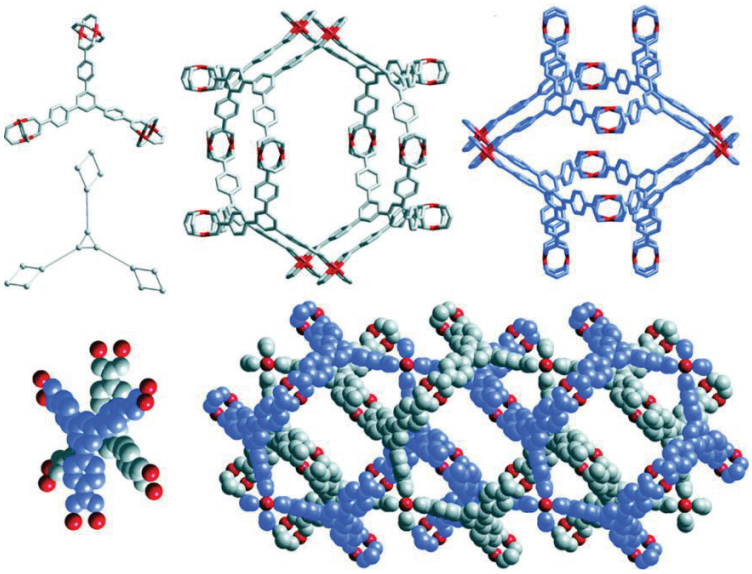

Fig. 1-5. Metal organic framework (MOFs) used for CO_2 capture process [39].

Table 1-2. Comparison among some important design parameters [5].

	Membrane separation	Chemical absorption	Adsorption
Operation flexibility	High	Moderate	-
Startup time	Very short (10 min)	1 h	-
Reliability	100%	Moderate	-
Control requirements	Low	High	-
Ease of expansion	Very high	Moderate	-
Energy requirements	0.5 M/kg_{CO2}	4 M/kg_{CO2}	3.2 M/kg_{CO2}

1.2.3. Membrane separation

Alternatively, membrane which was firstly introduced by Thomas Graham, is of great interest due to the low energy requirements, cost effectiveness, and easy to operate manners compared to previous two methods and these parameters play a key role in the development of membranes to be used for not only gases (CO_2/N_2, CO_2/CH_4, CO_2/H_2) but liquid separation (pervaporation, vapor permeation, and reverse osmosis) results via membranes were found promising as well. However, industrial waste which composed of various gases, possess high temperature that could degrade the membrane separation performance. Therefore, membranes with following characteristics of high CO_2 permeability, high

CO_2/N_2 selectivity, superior chemical/thermal stability, high plasticization resistance, and cost effectiveness would be of great advantage in industrial applications [40, 41].

In fact membrane is an emerging technology but has been explored for pre-combustion (CO_2/H_2, CO_2 > 20%) and post combustion (CO_2/N_2, 5% < CO_2 < 15%) CO_2 capture process. Table 1-3 summarizes advantages and disadvantages of membrane separation process and it apparently shows that membrane separation offers significant results from cost effectiveness to operational flexibility. In principle, membranes act as a selective barrier to separate one or more gases from feed mixture. Generally, CO_2 preferentially pass through the membrane matrix and separation occurred by following the solution-diffusion, molecular sieving, and/or facilitated transport mechanism [5, 24].

Table 1-3. Advantages and disadvantages of membrane separation method [24, 42].

Process	Advantages	Disadvantages
Membrane separation	Easy installation	Material easily compromised
	Small footprints	CO_2 permeability is low
	Simple process	Moderate purification
	Cost effective	Not mature enough
	Energy efficient	

Several studies have reported the membrane performance which consists of two parameters, permeance (P_i) and selectivity ($\alpha_{i,j}$). Permeance (P_i = mol m^{-2} s^{-1} Pa^{-1}), indicates a membrane property which allows the gas species (*i, j*) to pass via concentration gradient,

and selectivity most commonly obtained by the ratio of component *i* and *j* ($\alpha_{i,j} = P_i/P_j$) [43]. However, it has been found that selectivity deviated as a result of interaction among molecules and/or membrane pore walls. Fig. 1-6 depicts overview of various membrane materials and respective separation mechanisms. In polymeric membranes, gas permeation takes place via solution-diffusion (Fig. 1-6b) which defines that no specific pores exist inside a membrane matrix and simultaneously surface shows no affinity for CO_2 molecules. Firstly, CO_2 adsorbed on the membrane surface from permeate side and then diffuse through the membrane matrix. Finally, gases desorbed from downstream side. Facilitated transport membranes offers strong affinity for CO_2 permeating molecules, an opposite characteristic than solution-diffusion mechanism. For instance, extensively utilized amine functional groups facilitate CO_2 transport by following the reversible chemical reaction between CO_2 and amines.

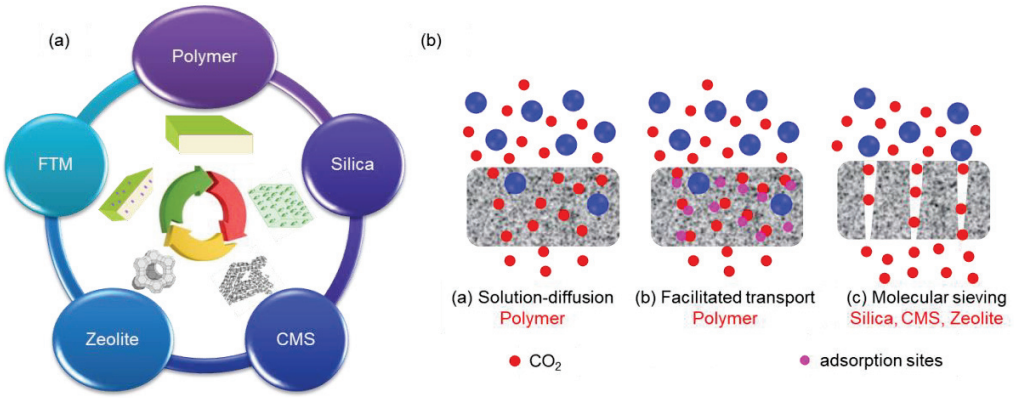

Fig. 1-6. (a) Materials used for CO_2 separation membranes (b) separation mechanism of various membranes.

Molecular sieving takes place when membrane pore size is wider enough to allow small molecules to permeate and large molecules experience blockage. Thereby, permselectivity

takes over from solution-diffusion to size sieving [43, 44]. Moreover, molecular sieving dominates when network pore size is effectively controlled for respective separation system such as CO_2/N_2, CO_2/CH_4, etc. Generally, inorganic materials such as silica, zeolite, and carbon molecular sieve (CMS) demonstrate excellent molecular sieving effect due to the narrow pore size distribution. On that account, membranes with high molecular sieving effect and strong CO_2 affinity could have strong effect on enhanced CO_2 transport of respective membranes.

1.3. Membranes used for CO_2 separation

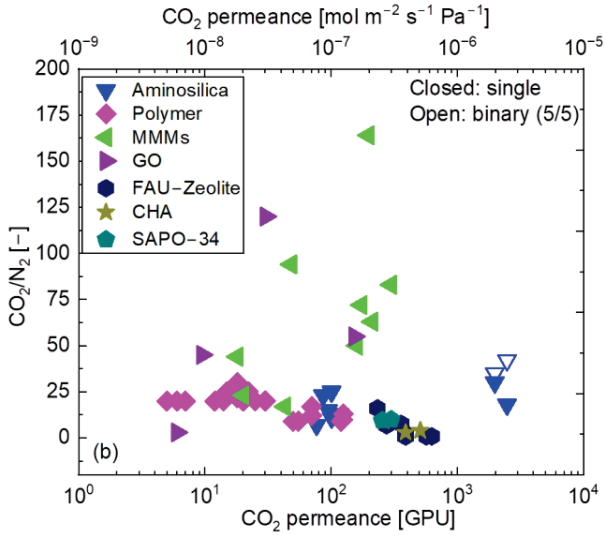

Fig. 1-7. Trade-off relationship between CO_2 permeance and CO_2/N_2 selectivity for various membrane materials.

Up to now, few of materials with high selectivity (<100) have been utilized to fabricate membranes for target applications. However, high selectivity of these membranes corresponds to the decrease permeability, which is not effective for industrial applications.

Fig. 1-7 shows the CO_2 separation performance of various membrane materials. The following section describes the various materials that have been investigated for CO_2 separation membranes.

1.3.1. Polymeric membranes

Polymers are widely utilized membrane materials for gas separation applications due to their easy processability with asymmetric structures. Most commonly used polymers are polyethersulfone (PES), Polyimide (PI), polysulfone (PSf), and cellulose acetate (CA) [45-48]. Fig. 1-8 shows the solution casting process for polymeric membranes [49].

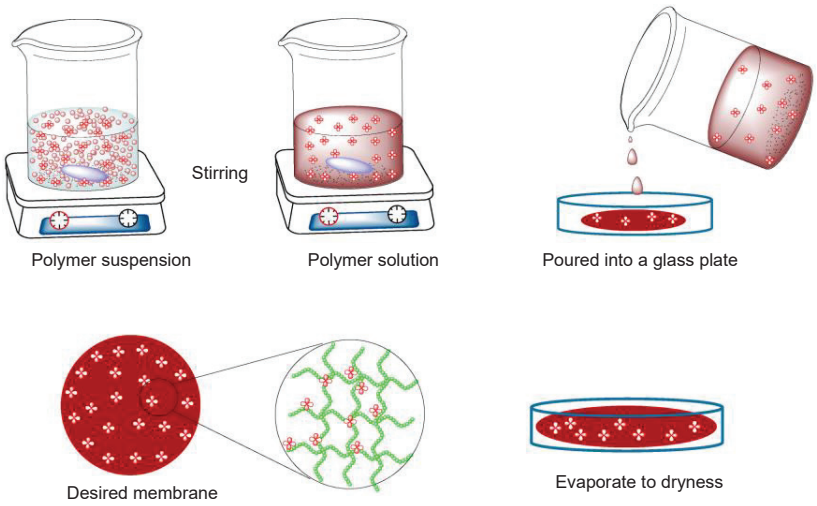

Fig. 1-8. Schematic illustration of solution casting process for polymeric membranes [49].

Polyimides were extensively utilized which further divided into commercially available Matrimid® and hexafluoro aromatic contained polymers. Fluoropolymers (6FDA) showed favorable chemical/thermal stability, and resultant membrane exhibited excellent CO_2

permeability attributed to the large volume provided by CF_3 groups [50]. Several types of polymers were utilized to fabricate CO_2 separation membranes as shown in Table 1-4. Recently, various studies reported the incorporation of ethylene oxide (EO) to tailor the polymers suitable for CO_2 separation. These copolymers with hard and soft segments provided mechanical strength and preferentially adsorbed CO_2, respectively [51,52].

Poly (amide-b-ethylene oxide) refer to Pebax® showed CO_2 permeability of 50-500 Barrer with CO_2/N_2 selectivity of 40-69, which is far below the desired CO_2 permeability of 1000-10000 Barrer. Polyethylene glycol (PEG) was blended with Pebax® to fabricate dense polymeric membranes and obtained structure showed CO_2/N_2 selectivity of 75. This improved permeability was attributed to the plasticize structure of PEG which offers free volume to permeating species inside a designed membrane matrix. However, currently available membranes offer the permeability below Robeson upper bound [53-57]. Current studies are focusing on the development of polymers with high diffusivity and high CO_2 permeability such as thermally rearranged polymers (TR-polymers) [58-60], fluoropolymers (AF polymers) [61-63], and polymers of intrinsic microporosity (PIM) [64-66]. Husna et al. [67] reported that blended polymer membranes possessed high resistance against plasticization and CO_2 permeability which surpassed the Robeson 2008 upper bound. Despite this, because of the low gas separation performance of the existing polymeric materials coupled with poor chemical/thermal stabilities and plasticization, their use in gas separation applications is still limited.

Table 1-4. CO_2 separation performance of variety of polymeric membranes.

Polymeric membranes	CO_2/N_2	Measurement Temp. [ºC]	Separation P_{CO2} [Barrer]	CO_2/N_2 selectivity	Ref.
Polysulfone	Single gas	RT	0.71	1.61	[68]
Polysulfone	Single gas	25	6	38	[69]
Matrimid® 9725	Single gas	25	6.2	27.5	[70]
Matrimid® 9725	50/50	35	4	23	[71]
6FDA-TMPDA	10/90	35	400	17	[72]
Pebax® MH-1657	10/90	25	480	48	[73]

Barrer: 10^{-10} cm^3 (STP) cm cm^{-2} s^{-1}; RT: room temperature

1.3.2. Facilitated transport membranes

Emerging membrane technology led to the redefinition of Robeson upper bound in 2008 and CO_2/N_2 was added to further excelling the membrane gas separation performance since drawbacks associated with polymeric membranes, which always showed CO_2 permeability (50-500 Barrer) below Robeson upper bound, were identified in 1991 Robeson upper bound value as shown in Fig. 1-9a [74-76]. Facilitated transport membranes comprise of carriers (metal ions, amines, carboxylate groups etc.) with a special affinity towards a target gas have been extensively utilized for CO_2 separation applications. Moreover, this interaction between CO_2 polar molecules and carrier agents also controls the rate of transport. Fig. 1-9b shows the CO_2 permeance via amine-functionalized facilitated transport membrane wherein, CO_2 permeation occurs by following reversible reaction with amine

groups which shows strong affinity for CO_2 permeating molecules and paired gas (H_2, CH_4, N_2) experience solution-diffusion mechanism by following dissolution and diffusion inside the membrane matrix [77, 78].

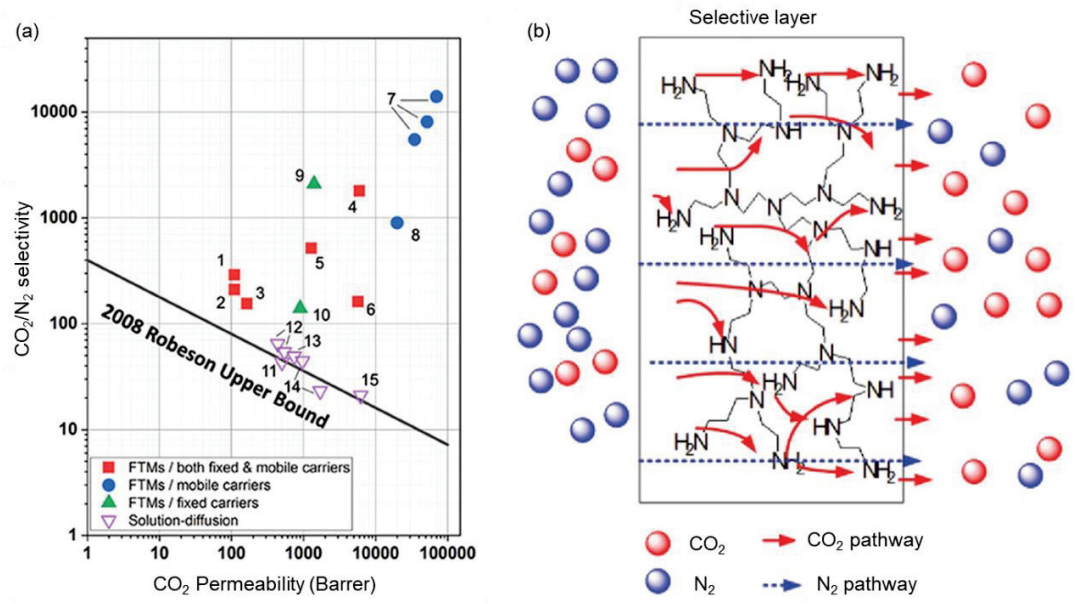

Fig. 1-9. (a) Robeson upper bound 2008 for CO_2/N_2 selectivity and (b) CO_2 permeation mechanism in facilitated transport membranes [76, 77].

Table 1-5 summarizes CO_2 separation performance of various facilitated transport membranes. Polymer membranes functionalized with amines, carboxylate, and/or metal ions complex provided significantly improved CO_2 separation performance. Extensive work has been done on various high density amine contained polymers to facilitate CO_2 separation such as polyethylenimine (PEI), polyvinylamine (PVam), and polyacrylamide (PAAm) [79]. For example, a hollow fiber membrane prepared with commonly used poly (vinyl alcohol) PVA and mixed with polyethylenimine (PEI). These composite membranes

showed excellent CO_2/N_2 separation selectivity of 300 at low pressure of 1 bar [77]. Polyvinylamine (PVam) membranes demonstrates suitable CO_2 separation performance with high CO_2/X selectivity (X= H_2, N_2, CH_4). However, crystallinity and saturation of career molecules restrict their application to fabricate CO_2 separation membranes. Hagg et al. reported the poly (vinyl alcohol) PVA and PVam blended facilitated transport membranes and obtained thin film showed suppressed crystallinity as well as the increased water retention [80, 81]. These membranes are of great interest and have wide room to explore this technology. To further excelling the development of facilitated transport membranes, these membranes are under European project of nanostructured membranes against global warming (NanoGloWa) [82].

Table 1-5. CO_2 separation performance of various facilitated transport membranes.

FTM membranes	CO_2 partial pressure [bar]	Measurement Temp. [ºC]	CO_2 Perm. [GPU]	CO_2/N_2 selectivity [-]	Ref.
PEI-PVA/PES	-	100	419	300	[77]
PVAm-PVA	2	25	212	174	[80]
PVAm	0.11	35	1827	500	[83]
PVAm-PIP	0.17	22	6500	277	[84]
PVAm-EDA	0.2	25	607	106	[85]
PVAm-MC	0.6	25	1180	410	[86]
PVAm/PDA	0.17	25	1887	83.1	[87]

PEI, polyethylenimine; **PVA**, poly(vinyl alcohol); **PES**, polyethersulphone; **PVAm**, polyvinylamine; **PIP**, piperazine; **PVA**, polyvinyl alcohol; **EDA**, ehtanediamine; **MC**, carbamate; **PDA**, polydopamine.

1.3.3. Mixed matrix membranes (MMMs)

Mixed matrix membranes (MMMs) are considered prominent candidates with high CO_2 separation performance and initially were developed while introducing 5A into the polymeric network structure. The incorporated filler (inorganic material) as disperse phase and polymers as continuous phase have been able to design selective membranes with superior gas separation performance. Additionally, hybrid structure could have strong resistance against harsh conditions of high pressure, temperature, and stability of polymer structure [88-91]. Therefore, MMMs with addition of inorganic fillers showed promising results as summarized in Table 1-6. Recently, various studies reported the MMMs with organic fillers, synthesis of polymers and fillers, filler's modification, and cross-linked fillers and polymers. Organic fillers which shows strong adherence with polymers compared to inorganic fillers have been investigated widely. For instance, membrane fabricated with PVam and COF, showed excellent CO_2 permeability of 396 at feed pressure of 0.15 MPa [92].

A self-assembly method was employed to prepared ZIF-8 and poly (sodium 4-styrenesulfonate) mixed matrix hybrid membranes on PAN substrate [93]. Another MMMs was designed by mixing MOFs (Cd-6 F) with 6FDA-ODA polymer matrix and resultant network structure showed interaction between amines ($-NH_2$) of polymer (6FDA-ODA) and COO from Cd-6 F, which enhanced CO_2 separation efficiency of these membranes.

Similarly, modification method to increase the compatibility between polymer and filler was found promising alternative wherein polar groups with strong CO_2 interaction were introduced such as $–NH_2$, COOH, etc. [94]. In an attempt to obtain high CO_2 solubility selectivity, UiO-66 surface was functionalized with amines ($-NH_2$) and COOH, and resultant membrane showed dramatically improved CO_2/N_2 separation performance [95]. Khan et al. [96] reported a mixed matrix membrane by mixing polymer with intrinsic microporosity (PIM-1) and potassium dodecahydrododecaborate ($K_2B_{12}H_{12}$) as shown in Fig. 1-10. Koros et al. [97, 98] proposed various possible approaches of material selection and mixing method in order to improve the compatibility and CO_2 separation performance of mixed matrix membranes.

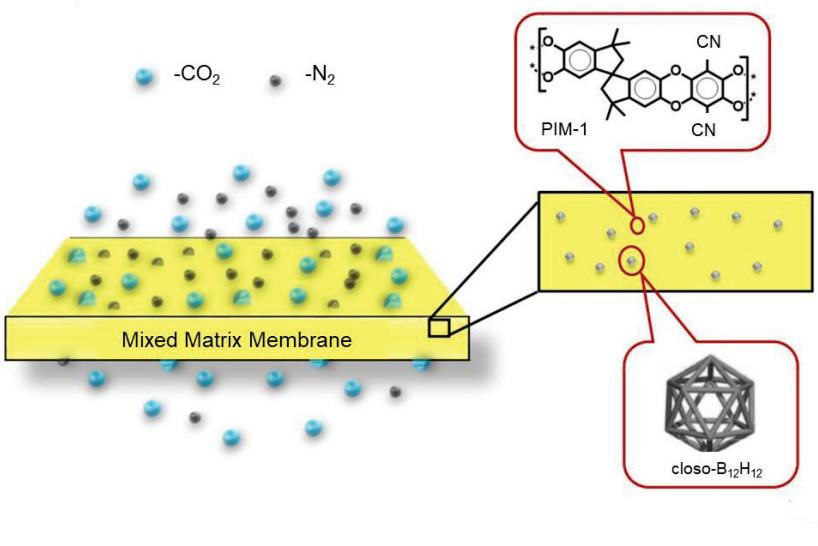

Fig. 1-10. CO_2/N_2 separation mechanism inside a mixed matrix membranes (MMMs) [96].

Table 1-6. CO_2 separation performance of mixed matrix membranes (MMMs).

MMMs	CO_2 partial pressure	Measurement Temp. [ºC]	CO_2 Perm. [GPU]	CO_2/N_2 selectivity	Ref.
PVAm/COF	0.6	25	396	-	[92]
PEIE-HT	0.17	25	5693	268	[99]
PEIE-HT	2.25	25	450	29	[99]
rGO-PBOI	1	25	1784	17.7	[100]
PES/ZIF-8	-	35	200	-	[101]
PEBA/MOF-801	0.5	20	22.4	66	[102]

COF, covalent organic framework; **PEIE**, polyethyleneimine epichlorohydrin; **HT**, hydrotalcite; **rGO**, reduced graphene oxide; **PBOI**, polybenzoxazole-co-imide; **PES**, poly (ether sulfone); **ZIF-8**, zeolitic imidazolate framework 8; **PEBA**, polyether-block-amide

1.3.4. Inorganic microporous membranes

Microporous membranes have been used extensively in gas separation applications due to high microporosity and surface area. Table 1-7 summarizes the advantages and disadvantages of inorganic microporous materials used for membranes fabrication.

Table 1-7. Summarizes the advantages and disadvantages of microporous inorganic materials that will be discussed in this section.

Membrane Material	Advantages	Disadvantages
CMS	Micropores achieved after pyrolysis of polymers, high molecular sieving effect, easy synthesis [103]	High brittleness, high cost [104]
Zeolite	Uniform pore size, pore size control, high adsorption [105]	Scale up difficulty, reproducibility [106]
Silica (SiO_2)	High chemical-Thermal stability, tunable pore size [107]	Dense structure, hydrophilic structure, small pore size [108]

1.3.4.1. CMS membranes

Carbon molecular sieves (CMS) possess attractive characteristics of easy synthesis, molecular sieve, suitable than polymers, and high permeance. Generally, separation thin layer is achieved after pyrolysis of employed monomer at high temperature (773.15K – 1273.15K) as shown in Fig. 1-11 [109]. CMS membrane technology is relatively new; however, various studies reported the chemical and thermal stability of CMS membranes under harsh conditions. Carbonized polymers were reported by Koresh and Sofer back in 1983, they concluded that resultant carbon membranes showed superior permeability compared to those of polymer membranes. Moreover, promising characteristic of tunable

micropore and ultramicropore make them attractive for next generation gas separation (GS) membranes [110]. Variety of polymers such as poly (acrylonitrile) [111], phenolic resins [112], cellulose [113], poly (furfuryl aclcohol) [114], polyimides (PI) [115], and poly (phthalazinone ether sulfone ketone) [116] have been utilized to fabricate carbon membranes.

Further, it was revealed that appropriate selection of polymer could have strong influence on pore size of obtained membranes. Hence, polymers with rigid structure and high carbon density would be of great interest to achieve high separation performance. Polyimides (PI) offers appealing characteristic of high chemical/thermal stability, rigid organic chain, and wide room for pore size tuning. Koros et al. reported several polyimides mixed with 6FDA to fabricate highly permeable CMS gas separation membranes [117]. Pinnau et al. fabricated PIM-6FDA membranes functionalized with hydroxyl (OH) and carbonized at 803.15 K under N_2 atmosphere. The resultant membranes showed CO_2 permeance of 41110 Barrer and selectivity of 20 [118, 119]. Hu et al. [120] prepared CMS membrane by mixing polymimides with different diamines and concluded that increased fraction free volume (FFV) resulted in higher CO_2 permeance (3000 Barrer) due to the pendent chain flexibility. The major disadvantage that hinders their commercialization is their brittleness and the cost which is 1 to 3 orders of magnitude greater per unit area than polymeric membranes [123, 122].

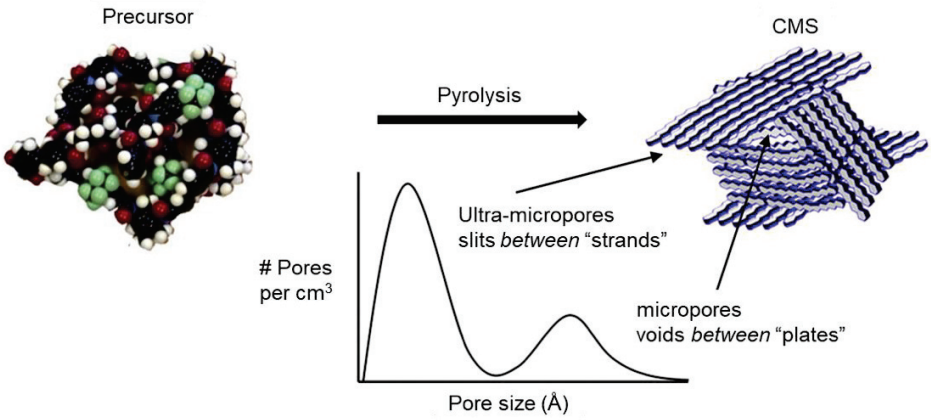

Fig. 1-11. Formation of micropores in a CMS membrane from pyrolysis of parent precursor [109].

1.3.4.2. Zeolite membranes

Zeolite materials offer appealing characteristics which includes uniform pore size (0.3-1 nm), chemical/thermal stability, and unique chemical composition which makes them attractive candidate for various applications such as gas separation, purification, and catalyst. By adjusting the Si/Al ratio, it is possible to prepare zeolite membrane for desired applications [123, 124]. SAPO-17 thin film membranes prepared on mullite tube instead of alumina, showed CO_2 permeance of 3300 GPU [125]. Lok et al. [126] introduced new type of zeolite referred as "SAPO-34" which exhibited pore size ranging from 0.3-0.8 nm and scale up from 2-25 cm on porous stainless tube. This eight membered ring structure (diameter: 9) exhibit moderate hydrophobicity and high chemical and thermal stability. Fig. 1-12 shows the SAPO-34 membrane used for CO_2 separation [127]. Li et al. [128] prepared a SAPO-34 zeolite membrane which showed CO_2 permeance of 1.6×10^{-7} mol m^{-2} s^{-1} Pa^{-1}

at 297 K. Carreon et al. [129] reported zeolite membrane with CO_2 permeance of 2×10^{-6} mol m^{-2} s^{-1} Pa^{-1} at 295 K. Li et al. [130] fabricated a zeolite membrane which demonstrated CO_2 permeance of 1.2×10^{-6} mol m^{-2} s^{-1} Pa^{-1} and CO_2/N_2 selectivity of 32 at 295 K. Various studies reported the hydrothermal stability of these zeolite membrane over 100 ºC. Amine functionalized zeolite membranes showed drastic increase in CO_2 permeance of 2.1×10^{-6} mol m^{-2} s^{-1} Pa^{-1} and CO_2/N_2 selectivity of 39 [131]. Makertihartha et al. [132] synthesized zeolite membrane on silica support and resultant membrane showed CO_2 permeance of 2.01×10^{-6} mol m^{-2} s^{-1} Pa^{-1} with CO_2/N_2 selectivity of 53.

However, defect free film formation and scale up remained challenge in using zeolite membranes due to its high brittleness. Generally, zeolite membranes fabricated via two commonly used methods: (1) Pure zeolite membranes deposited on alumina, silica, and stainless steel substrate. (2) Incorporation of zeolite in polymer structure via solvent evaporation, phase inversion, solution casting, and dip coating. For later approach, it was revealed that incorporation of zeolite into polymer structure could offer significant results to fabricate CO_2 separation membranes [127]. Messaoud et al. [133] prepared a zeolite based polymer (polyetherimide) membrane and simultaneously studied the effect of various solvents on membrane separation performance. It was concluded that 5% addition of SAPO-34 resulted in CO_2 permeance of 4.41×10^{-10} mol m^{-2} s^{-1} Pa^{-1}. Zhao et al. [134] prepared zeolite/Pebax1657 using solvent evaporation and explained that inclusive zeolite into polymer structure dramatically improved CO_2 permeability as compared to pure membrane.

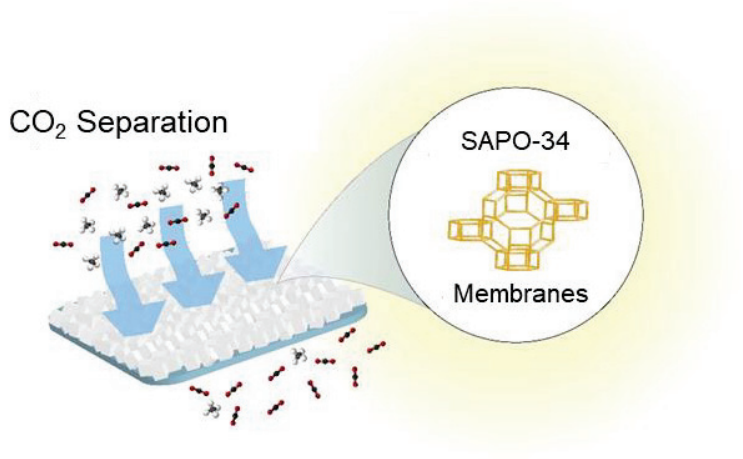

Fig. 1-12. Zeolite (SAPO-34) CO_2 separation membranes [127].

1.4. Silica membranes

Polymeric and zeolite membranes have intensive long history and widely employed in liquid and gas separation applications. Microporous silica membranes, which are relatively new, are being explored since 1980's. Silica structure offers promising characteristics such as high thermal stability (~1000 ºC), stability of amorphous phase at high temperature, network pore size tunability, and high molecular sieving effect [135-137]. These particular properties make silica attractive candidate for membrane fabrication over mostly used metal oxide TiO_2 and ZrO_2, where pore size enlarge as a result of crystalline formed after certain temperature of 600 ºC [138]. Fig. 1-13 shows the molecular permeation inside a silica matrix typical silica structure obtained via molecular dynamic simulation (MD simulation) [139].

However, flexibility of silica network structure provides the possibility to tune the network pore size (>1nm) in accordance with the separation system. Further investigation

also revealed that silica structure shows less resistance against water vapors under humid conditions since excessive amount of hydroxyl groups (OH) present in the silica network structure interact with water vapors which consequently degraded the performance of silica membrane [140]. To overcome the issues associate with conventional silica membranes, many studies reported the effective strategies to avoid the densification effect caused by silanol groups (OH) as well as the enlarged silica pore size which will be discussed in later sections.

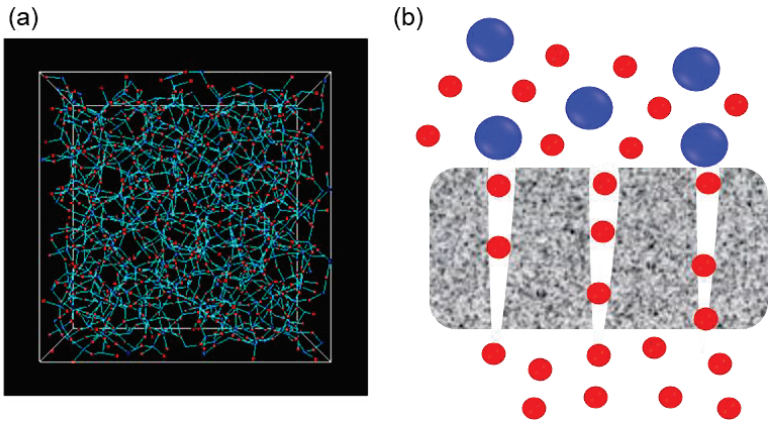

Fig. 1-13. (a) MD snapshot of amorphous silica network structure [139] and (b) permeation mechanism of inorganic silica membranes.

1.4.1. Fabrication of silica membranes via sol-gel method

Fig. 1-14 shows the sol-gel process which has been extensively employed for membrane fabrication because of easy processability and convenience with pore size controllability. Generally, respective monomers (metal alkoxide/inorganic salt) undergo hydrolysis with a simultaneous condensation reaction which corresponds to the polymeric or colloidal sol-gel. The formation of

polymeric or colloidal sol-gel strongly depends on various preparation conditions such as concentration of alkoxide, catalysts, temperature, solvent, etc. For example, colloidal sol route involves the addition of base and/or higher water ratio which results in faster hydrolysis reaction with excessive amount of hydroxyl (OH) groups and molecules can permeate through interparticle pore obtained via colloidal sol-gel route. Moreover, colloidal particles, which are considered membrane pores, are difficult to control within subnano range [141, 142].

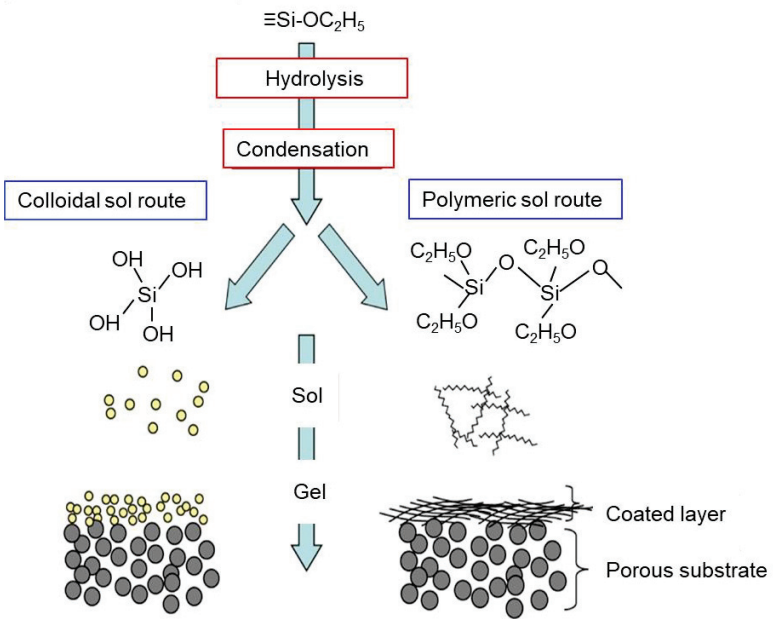

Fig. 1-14. Diagram of sol-gel preparation procedures.

Castricum et al. [143] reported the effect of water ratio on particle size distribution, they concluded that considerable amount of added water is suitable to control the colloid sol size since sol size was increased rapidly as water ratio increased due to the faster hydrolysis rates. Yu et al. [144] prepared a sol by using acid and base as a catalysts, respectively, and results were in favor of acidic conditions with stable sol size for certain period of time. Generally, sol size within subnano range (separation

layer) is required for thin film formation to avoid the granular network structure. Therefore, polymeric sol route offers desired sol size suitable to coat top separation layer which demonstrate the separation ability. Polymeric sols obtained via partial hydrolysis due to the low reaction rates and resultant linear network structure shows pore size smaller than 1 nm and these reactions kinetic in polymeric sol route are accomplished by acid and/or dropping small amount of water into the solution [145].

In order to prevent the penetration of sol into the porous substrate, a layer by layer coating is required before depositing the top separation layer to avoid any miscellaneous factors involved in undesired thin film formation. Fig. 1-15 shows the morphology of top separation layer where a clear thin layer with certain thickness can be observed. Most commonly, α-Al_2O_3 porous support, which is obtained via extrusion or slip casting with pore size larger than 1 μm, is utilized for deposition of top separation layer via sol-gel method. Firstly, γ-Al_2O_3 particles used to reduce the pore size of porous support to several nanometers. Secondly, SiO_2-ZrO_2 sol is deposited on particle layer to further reduce the pore size. Finally, top separation layer, which possess the ability of molecular separation, is coated on SiO_2-ZrO_2 intermediate layer via sol-gel method [146-148].

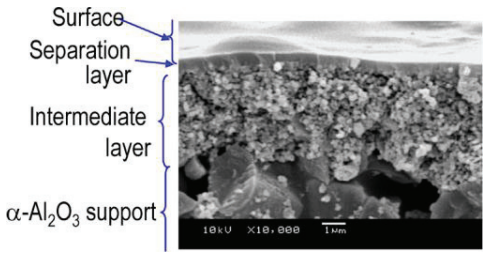

Fig. 1-15. Cross section image of top separation layer of inorganic silica membrane [138].

1.4.2. Strategies to design silica network structure for CO_2 separation

The desirable characteristics of CO_2 separation membranes include high chemical and thermal stability under harsh conditions such as high temperature and pressure. For instance, polymer membranes which offers promising CO_2/N_2 separation efficiency but, on the other hand, polymer structure undergo plasticization effect at high pressure [149]. Alternatively, inorganic amorphous silica is a potential membrane material with high chemical-thermal stability and tunable pore size. Moreover, silica membranes are easy to synthesis with ultramicropores (<7Å) by commonly used facile sol-gel method [150]. This ultramicroporous structure, however, is not suitable for CO_2 and N_2 permeance as discussed above. The design of network pore structure of microporous silica for CO_2/N_2 separation is challenging due to the close resemblance of kinetic diameters of CO_2 (3.3 Å) and N_2 (3.6 Å). Table 1-8 summarizes the strategies that were employed to design silica network structure suitable for CO_2 separation membranes.

Table 1-8. Various approaches to design CO_2 selective silica membranes.

	Approach	Ref.
Pore size control	Template method	[151-153]
	Spacer method	[154-158]
	Ion doping	[159-166]
Affinity control by amines incorporation	Co-condensation	[167-172]
	Surface grafting	[173-177]
Affinity control by controlled Si-OH	Calcination parameters/ post treatment	[165, 178-180]

1.4.2.1. Pore size Control

1.4.2.1.1. Pore size control via template method

A typical conventional tetraethoxysilane (TEOS) network structure is not suitable for a gas (CO_2/N_2) which requires pore size larger than He and H_2. Therefore, it was made possible to tune silica network structure by utilizing the non-hydrolyzed silsesquioxane ($RSiO_{1.5}$), which resulted in loose network formation compared to those prepared with pure silica (TEOS). These organic chains (silsesquioxane) were further distinguished into pendent-type, where terminal organic chain attached to the Si atom ($Si-CH_2$). Various studies reported the sol-gel derived organic/inorganic synthesis due to its mild conditions such as low temperature which allows organic groups to keep present in the structure and

these organic chains could control the pore size as well as the affinity to permeating gases [151].

Fig. 1-16 shows the TEOS network structure co-polymerized with pendent-type alkoxysilane (methyltriethoxysilane). The optimized silica network structure includes the film coating on porous support which was then fired in an air atmosphere and subsequent removal of methyl groups at certain temperature resulted in the formation of enlarged pore size which showed CO_2 permeance of ~10^{-7} mol m^{-2} s^{-1} Pa^{-1} and CO_2/CH_4 selectivity of 70 [152]. Another similar study reported silica (TEOS) membranes functionalized with series of organic alkoxysilanes. The resultant membranes demonstrated dramatically improved H_2 and CO_2 permeance as a result of template removal at 600 ºC [153].

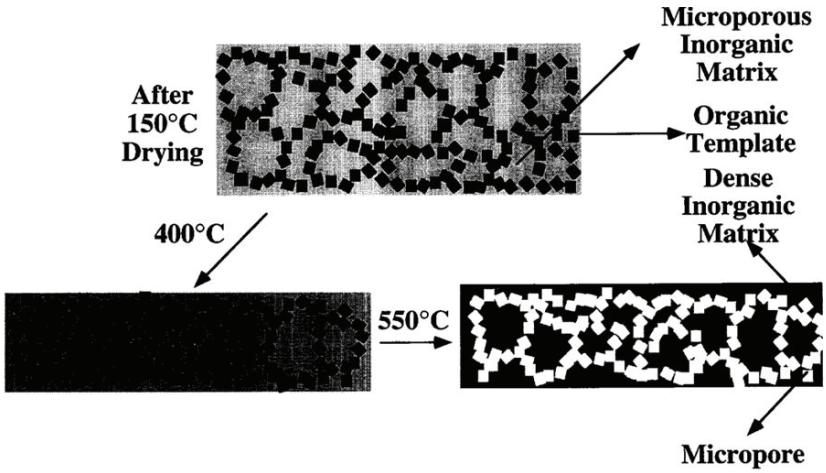

Fig. 1-16. Schematic illustration of pore size control for pendent-type organic-inorganic silica network structure [152].

1.4.2.1.2. Pore size control via spacer method

For the first time, sol-gel derived bridged-type organosilica membranes were reported in 2008 by utilizing BTESE and bis (triethoxysilyl) methane (BTESM, Si-CH_2-Si) organosilica network structures. These membranes outperformed pure silica while showing high pervaporation performance at 150 ºC. Later, many studies reported the gas permeation properties of bridged-type organosilica membranes and results were significant in terms of improved gas permeance and hydrothermal stability [154]. Fig. 1-17 shows the sol-gel derive pure silica and bridged type organosilica network structures [155]. Castricum et al. [156] tailored the network structures of organosilica membranes consist of short (C_1, C_2) and long chain (C_3, C_6, C_8) organic linking units and concluded that membranes with short chain exhibited rigid structure which resulted in high permeation properties.

On the contrary, long chain or aromatic/phenyl membranes showed lower permeation properties due to the steric hindrance of flexible organic chain which occupied enough channel space and restricted molecules movement inside the pore wall. Ren et al. [157] investigated sol-gel derived BTESE and bis (triethoxysilyl) octane (BTESO, Si-C_8H_{16}-Si) organosilica membranes which showed CO_2 permeance of 7.66×10^{-7} and 6.63×10^{-7} mol m^{-2} s^{-1} Pa^{-1} with selectivity of 36.1 and 12.6 at 40 ºC, respectively. Further these membranes were applied under wet conditions and CO_2 permeance for BTESE membrane significantly decreased due to the micropores filled with water vapors which restricted CO_2 diffusivity and simultaneous factor of less hydrophilicity of BTESE structure. On the contrary, CO_2 permeance of BTESO membrane was less affected under

wet conditions due to the existence of long organic chain which significantly improved the hydrophobicity of silica network structure.

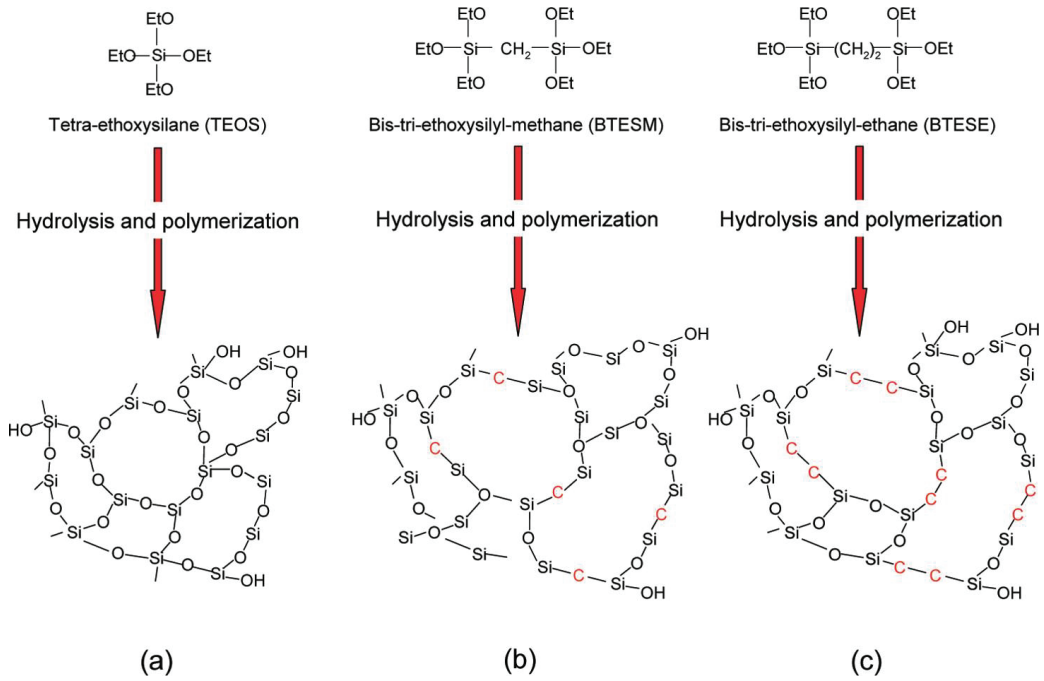

Fig. 1-17. Sol-gel derived silica and organosilica network structures obtained via spacer technique [155].

Fig. 1-18 shows the variety of pendent- and bridged-type organosilica structures and some of them widely used and commercialized for industrial applications. These organosilica structures were further divided into Si-1, Si-2, and Si-3 depending on the number of silicon atoms present in a molecule and alkoxy groups were ethoxy and in some cases methoxy which were responsible for network pore formation upon their subsequent loss [158].

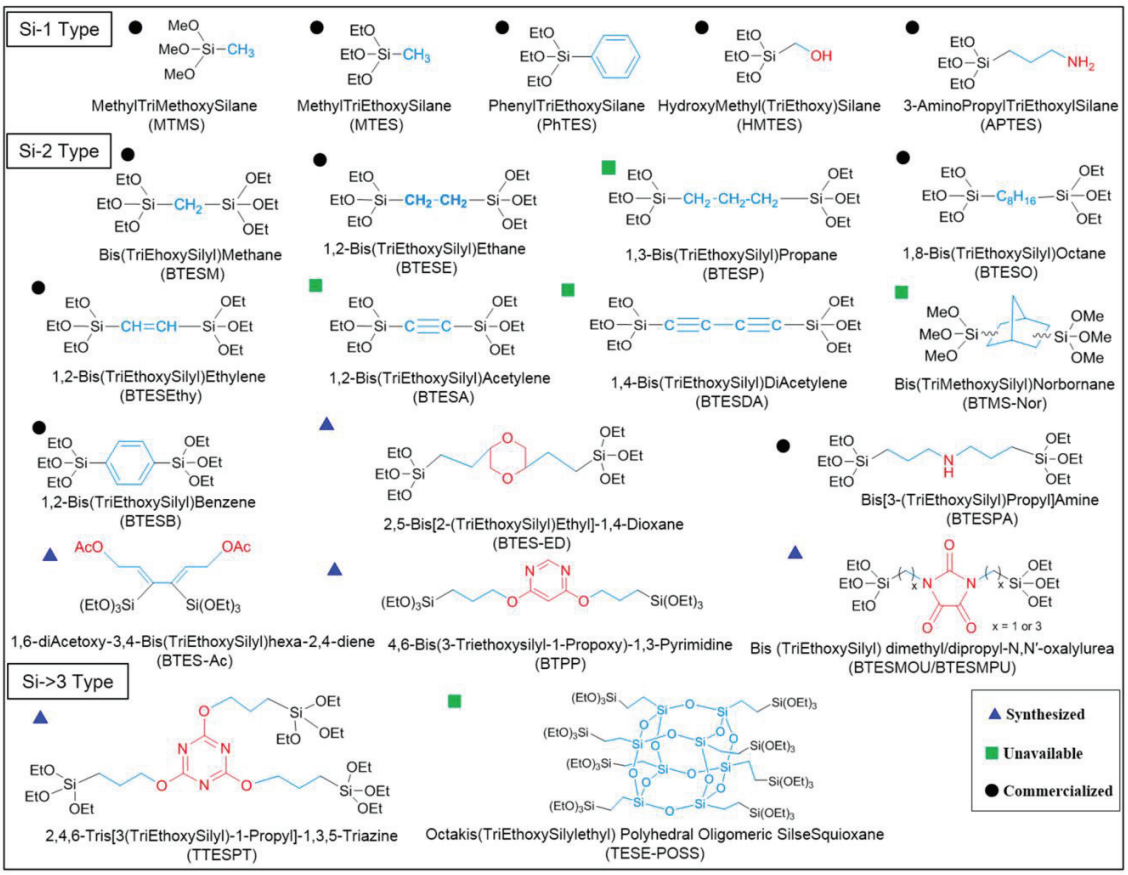

Fig. 1-18. Variety of pendent- and bridged-type organoalkoxysilane precursors used for membrane fabrication [158].

1.4.2.1.3. Pore size control via ion doping

The flexibility of silica (TEOS) network structure led to the possibility of network pore size tuning via incorporation of various cations and/or anions. Boffa et al. [159] investigated the niobia doped silica membranes for CO_2 separation from gas mixtures as shown in Fig. 1-19. However, the resultant membrane showed decrease CO_2 performance which was attributed to the strong interaction between CO_2 and membrane pore walls.

Similarly, Yoshida et al. [160] reported the zirconia doped silica membrane and permeation properties decreased with increasing doped zirconia concentration. Same group investigated sol-gel derived micropours silica membranes and resultant network structure showed CO_2 permeance of 7×10^{-7} mol m^{-2} s^{-1} Pa^{-1} with CO_2/N_2 permselectivity of 36 at 50 ºC [161].

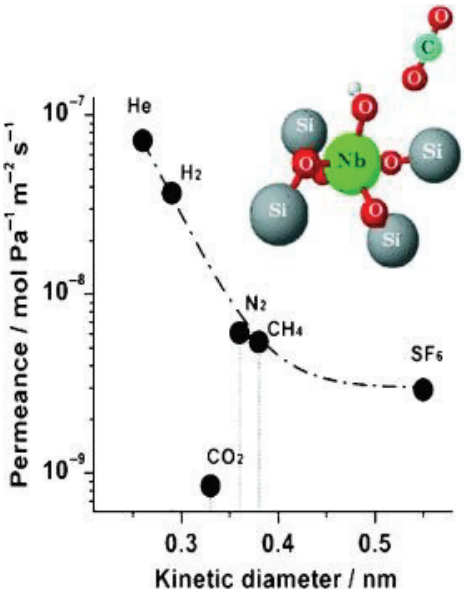

Fig. 1-19. CO_2 permeation properties of niobia doped silica membranes [159].

Another strategy that was introduced recently and showed excellent results in terms of controlled silica network pore size and higher hydrothermal stability. Since silica network structure consists of abundant silanol groups (Si-OH) groups which correspond to the increased condensation reaction and simultaneously degrade the membrane performance under humid environment. Therefore, elimination of these hydrophilic groups (Si-OH) could have improved silica network structure and gas permeation properties. Generally, this approach involves the incorporation of fluoride ions (F^-) into the silica network structure

which replaced the hydrophilic Si-OH groups by Si-F bonds. During sol-gel process, these hydrophobic Si-F groups perturbed Si-O-Si bond angle and membranes showed loose network formation with improved gas permeation as well as hydrothermal stability [162-166].

For instance, a tetraethoxyfluorosilane (TEFS) network structure, which consists of inherent Si-F groups, showed H_2 permeance of 10^{-6} mol m^{-2} s^{-1} Pa^{-1} which is superior to that of conventional silica (TEOS) membranes. Subsequently, membrane applied under humid environment (steam partial pressure: 90 kPa, 500 ºC) demonstrated excellent hydrothermal stability. These results were attributed to the existence of Si-F groups which significantly improved hydrothermal stability of silica network structure [165].

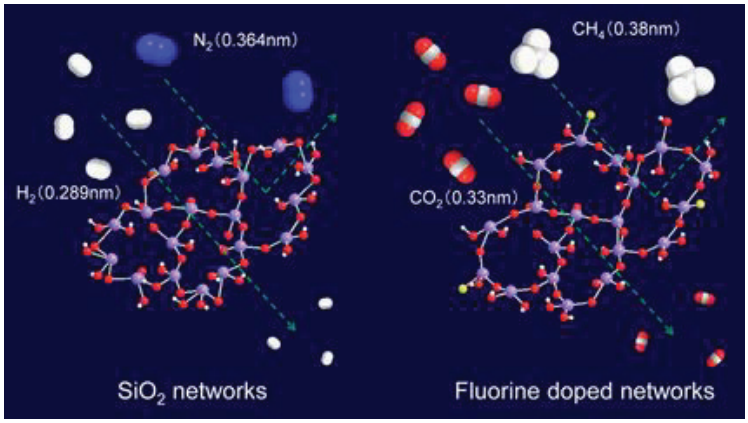

Fig. 1-20. Network pore structure of fluorine-induced microporous silica [163].

Fig. 1-20 shows the network structure of fluorine (NH_4F) induced microporous silica. F-SiO_2 membrane (F/Si = 1/9) showed CO_2 permeance of 4.1×10^{-7} mol m^{-2} s^{-1} Pa^{-1} and CO_2/CH_4 selectivity of 300 at 35 ºC [163]. Overall, gas permeation properties of these fluorine induced silica membranes improved as the fluorine concentration increased, which

indicates that fluorine effectively controlled network pore size of conventional silica (TEOS) which was affected by Si-F groups. Nonetheless, these membranes have not been explored for CO_2/N_2 separation system.

1.4.2.2. Affinity control by amine incorporation

1.4.2.2.1. Co-condensation with amine based Si precursors

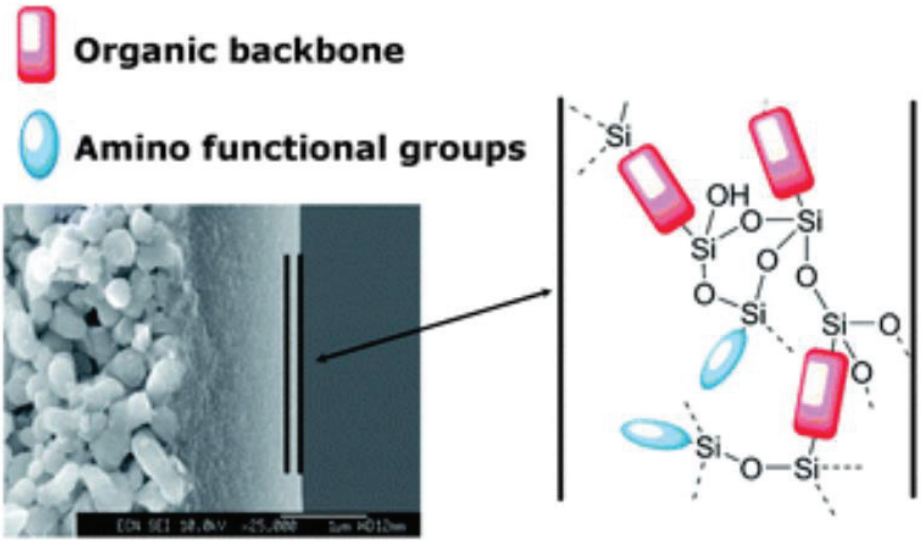

Fig. 1-21. Surface morphology of amine-contained silica membrane [167].

Fig. 1-21 shows the SEM image of amine functionalized silica surface [167]. These functional groups (amines), which possess strong CO_2 affinity, have been extensively utilized for gas separation applications and categorized as primary ($-NH_2$), secondary (-NH-), and tertiary (-N-) amines in accordance with the CO_2 affinity of the respective amines. Commonly used primary amine (3-aminopropyltrethoxysilane, APTES), which contains

hydrophobic organic chain, not only enhanced CO_2 permeation properties of employed silica membranes but simultaneously significantly improved hydrophobicity of network structure. Hence, surface functionalization of silica with CO_2-philic sites (amines) was found promising strategy to change the chemical and physical properties of respective materials, and this objective was achieved via co-condensation strategy in which two precursor with different nature were mixed to optimize the CO_2 selective silica membranes.

Xoremitakis et al. [168] fabricated amine contained sol-gel derived silica membranes with APTES and triethoxysilyl (TEOS), and membrane showed CO_2/N_2 selectivity of 80 at 25 ºC. Another study reported by same group revealed that functional groups ($-NH_2$) present in silica structure have significant effect on CO_2 permeation properties. The employed amine silica membrane showed CO_2/N_2 separation factor of 100-200 under relative humidity of 0-40% [169]. Paradis et al. [167] studied variety of functional groups to fabricate microporous silica membranes and concluded that shielding of CO_2 adsorption sites had drastic effects on controlled CO_2 affinity of respective membranes. Suzuki et al. [170] prepared amine-silica membranes with various APTES ratios (0-100%) and membrane with 20% APTES concentration showed optimum CO_2 permeation flux of 2.3×10^{-7} mol m^{-2} s^{-1} Pa^{-1} and CO_2/CH_4 separation factor of 40.

Guo et al. [171] fabricated the CO_2 selective hybrid organosilica membranes as shown in Fig. 1-22. The obtained bis (triethoxysilyl) acetylene (BTESA) and (3-aminopropyl) trethoxysilane (APTES) membranes demonstrated CO_2 permeance of 2550-3230 GPU and CO_2/N_2 selectivity ranging from 31-42. These significant results were attributed to the controlled pore size which drastically improved molecular sieving effect and improved CO_2

affinity resulted from co-polymerized APTES structure which contains CO_2 philic sites (amines, NH_2). Yu et al. [172] reported the co-condensation of 4,6-bis(3-(triethoxysilyl)-1-propoxy)-1,3-pyrimidine (BTPP) with TEOS and BTESE silica precursors. The tailored ultramicroporous network structure showed CO_2 permeance of ~2000 GPU with CO_2/N_2 selectivity of 20.

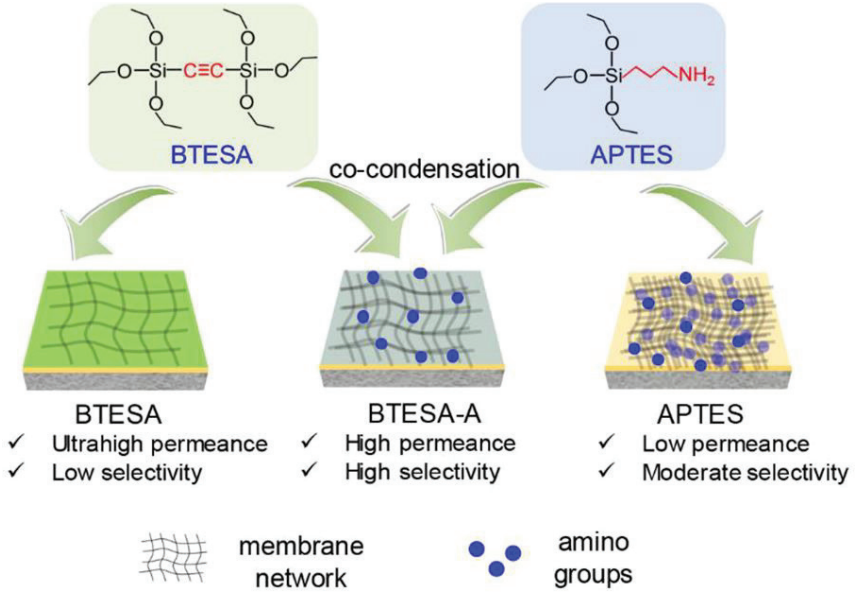

Fig. 1-22. CO_2 selective silica membranes obtained via co-condensation reaction [171].

1.4.2.2.2. Surface grafting with amine based Si precursors

Amine functionalized silica membranes attracted much attention and numerous studies reported the CO_2 separation efficiency of amine grafted silica membranes. Incorporation of these functional groups (amines) via post synthesis method has been reported extensively in an attempt to improve CO_2 affinity of microporous silica membranes. Ostwal et al. [173] reported amine modified silica membrane as shown in Fig. 1-23.

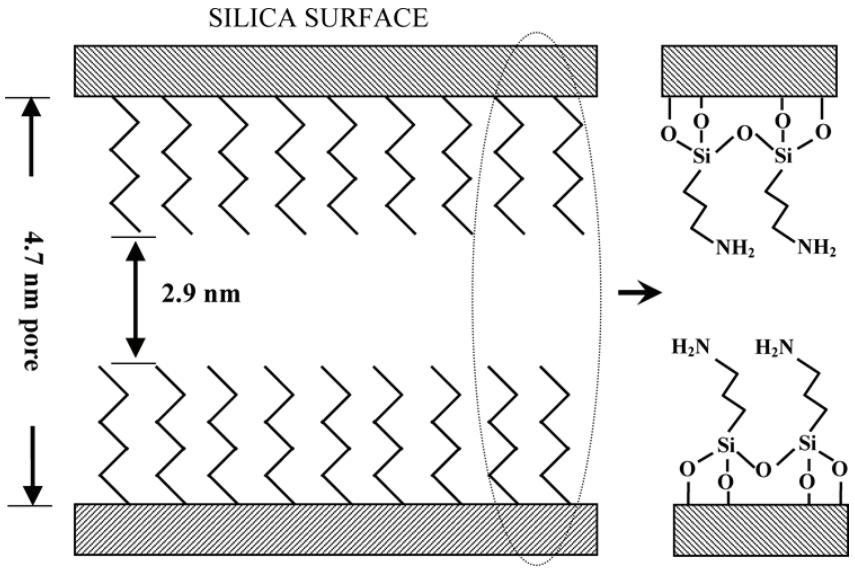

Fig. 1-23. Surface grafting of inorganic silica with amine based Si precursor [173].

These membranes showed excellent CO_2 separation performance by comparison with unmodified silica which exhibited Knudsen behavior as well as surface diffusion for large gases such as CO_2, CH_4, etc. Sing et al. [174] reported gas permeation results of organosilane membranes which showed superior CO_2 selectivity with those of untreated silica membranes. Sakamoto et al. [175] reported sol–gel derived amine functionalized mesoporous silica membrane which exhibited CO_2 permeance of 1×10^{-9} mol m^{-2} s^{-1} Pa^{-1} with CO_2/N_2 selectivity of 800. Kim et al. [176] fabricated CO_2 selective silica membranes and resultant membrane showed CO_2 permeance of 100 GPU at 35 ºC in single system with CO_2/N_2 and CO_2/CH_4 selectivity of 17 and 12, respectively. Further, membrane performance was evaluated in binary (CO_2/CH_4 = 50/50) separation system at 35 ºC, and CO_2 permeance was obtained as 57 GPU with CO_2/CH_4 selectivity of 9. These results were ascribed to the enhanced CO_2 adsorption properties of respective silica surface resultant

from amine grafted molecules. Miyamoto et al. [177] investigated the CO_2 separation performance under dry and wet conditions for amine loaded silica membranes. The respective membranes showed excellent CO_2/N_2 selectivity in either dry or wet system.

1.4.2.3. Affinity control by controlled Si-OH density

1.4.2.3.1. Calcination parameters/post synthesis

Generally, sol-gel derived silica network pore size range from 0.3 to 0.4 nm which was confirmed by positron annihilation spectroscopy (PALS), indicating silica pore size smaller for CO_2/N_2 permeation. Since silica is rich in flexible Si-OH groups which correspond to the creation of Si-O-Si bonds followed by condensation reaction. Hence, controlled Si-OH density of silica network structure by changing the calcination temperature could have significant effect to design CO_2 selective silica membranes. de Vos et al. [178] fabricated silica membranes and resultant membranes showed decreased permeation properties followed by increased densification effect as temperature changed from 400 ºC to 600 ºC. Kanezashi et al. [179] reported silica membranes calcined at 700 ºC and high molecular sieving effect as well as hydrothermal stability was confirmed which was attributed to the decreased silanol density and increased siloxane bonds.

Moreover, studies explained the loose network formation as a result of template removal at high calcination temperature. The removal of organic template during calcination process left voids through which molecules permeate with less resistance [152]. Cao et al. [180] investigated the effect of heat treatment temperature on templated microporous silica

network structure. A dense network structure was obtained at 150 ºC and subsequent template removal resulted in improved gas permeation properties which attributed to the increase pore size resultant from pyrolysis of organic ligand.

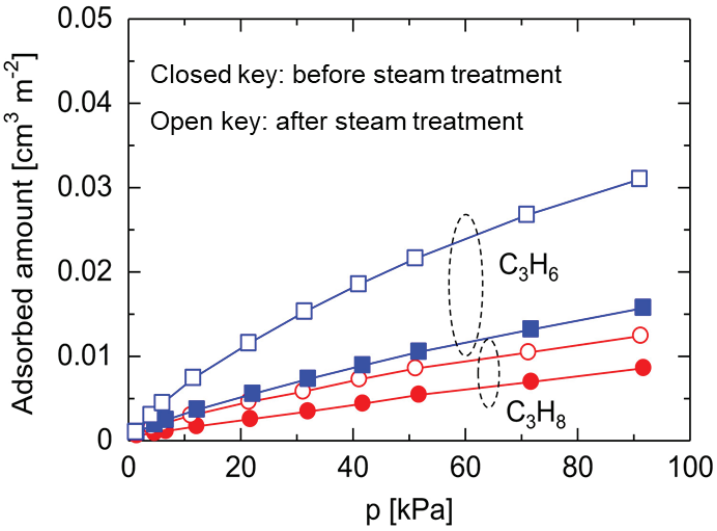

Fig. 1-24. C_3H_6/C_3H_8 adsorption isotherms at 25 ºC before/after steam treatment for TEFS powder calcined at 350 ºC under air atmosphere [165].

Kanezashi et al. [165] prepared a TEFS membrane to evaluate the propylene/propane (C_3H_6/C_3H_8) separation performance which shares similar adsorption properties with CO_2 molecules. TEFS is a silica precursor with inherited Si-F bonds and demonstrate similar amorphous structure and gas permeation properties with pure silica. Since existence of hydrophilic Si-OH groups can effectively control the preferential adsorption of permeating molecules. Therefore, this effect was investigated under humid environment to enhance the C_3H_6 adsorption sites (Si-OH) resultant from consequent reaction between Si-F groups and steam particles. Adsorbed C_3H_6 amount for TEFS gels calcined at 350 ºC drastically

increased after steam exposure as shown in Fig. 1-24. After steam exposure, the selected TEFS membrane showed excellent C_3H_6 permeance of 2.2×10^{-7} mol mol m^{-2} s^{-1} Pa^{-1} with C_3H_6/C_3H_8 selectivity of 42 at 35 ºC.

1.5. Scope of this thesis

Overall objective of this work is to tailor the network pore structure of microporous organic and inorganic silica membranes via fluorine doping and gas permeation properties. From conventional silica (TEOS) to organosilica (pendent/bridged), various monomers were selected to tune the pore size suitable for CO_2/N_2 separation. Following points were considered while fabricating fluorine induced CO_2 selective microporous silica membranes.

1. Effect of fluorine doping exert on network pore structure of conventional silica and pendent-/bridged-type organosilica membranes
2. Pore size controllability for CO_2/N_2 separation
3. Affinity control for CO_2 molecules

This dissertation consists of 5 chapters, as follow;

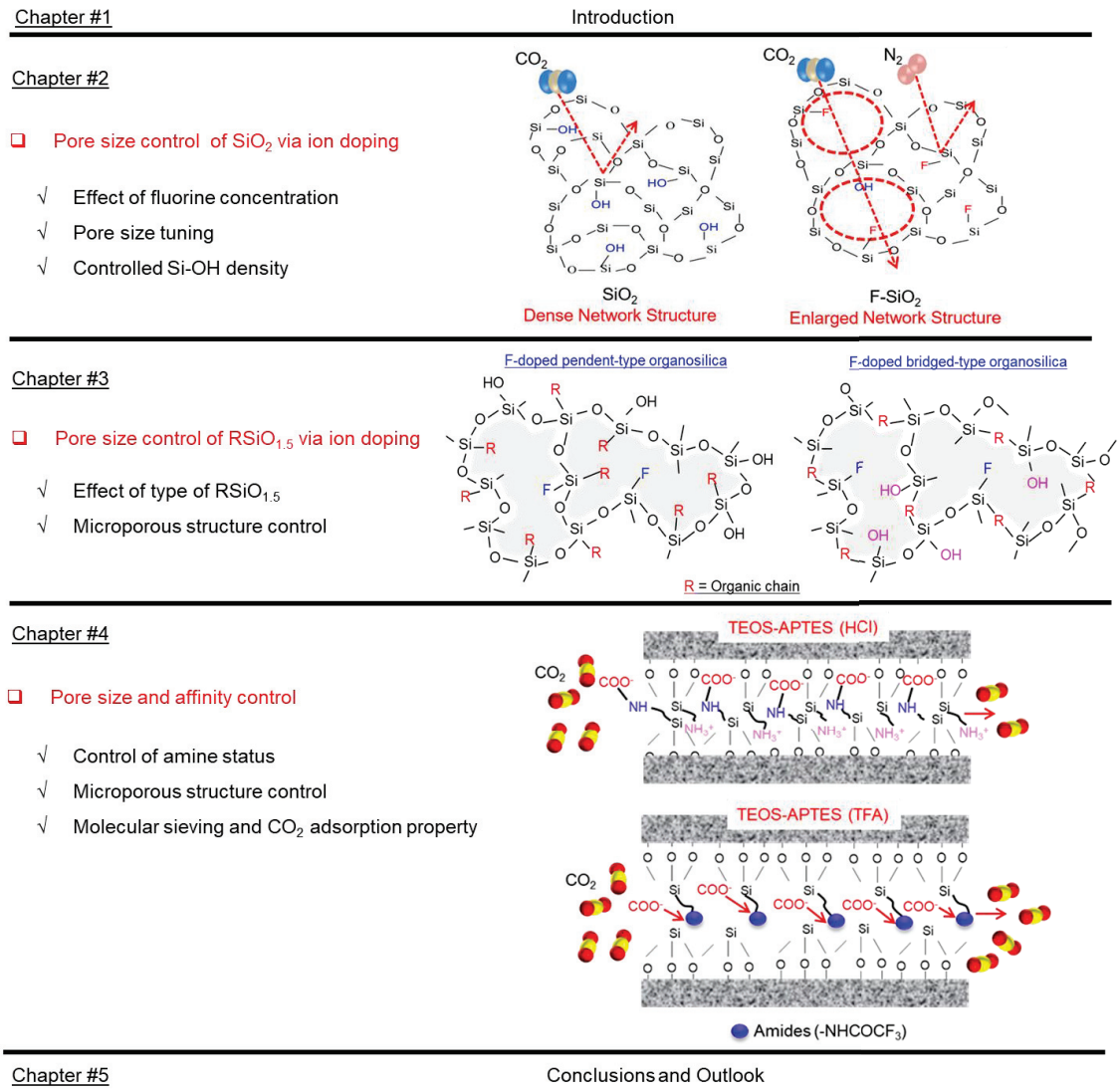

Fig. 1-25. Overview of this project.

Chapter 1 is **"General introduction"**, explaining the background of CO_2 separation and objective of this study

Chapter 2 is **"Tailoring the structure of a sub-nano silica network via fluorine doping to enhance CO_2 separation and evaluating CO_2 separation performance under dry or wet conditions".** The amorphous nature of a silica network structure offers an attractive opportunity for excellent separation of small molecules such as He and H_2. CO_2 separation systems are restricted, however, by the density of amorphous silica structures. Hence, the objective of this work was to tailor the network pore size of conventional tetraethoxysilane (TEOS)-derived silica membranes via fluorine (NH_4F) doping. Fluorine doping can precisely enlarge the network pore size in a subnano range by reducing the Si-OH groups in the network structure, while CO_2 adsorption properties are decreased as doped fluorine concentration increases. A fluorine-doped silica membrane (F/Si=0.1/9.9) showed a CO_2/N_2 permeance ratio that reached as high as 50 with CO_2 permeance of 1.6×10^{-7} mol mol m^{-2} s^{-1} Pa^{-1} at 50 ºC. In a wet system (200-300 ^{o}C, H_2O partial pressure of 3 kPa), fluorine-doped silica membranes were quite stable, irrespective of the doped fluorine concentration. Under steam with a high partial pressure (300 ºC, H_2O partial pressure of 30 kPa), the hydrothermal stability of silica membranes was increased with increases in the fluorine concentration.

Chapter 3 is **"Network pore engineering of fluorine induced microporous pendent/bridged type organosilica membranes".** The effect of fluorine was evaluated on pendant-type [methytriethoxysilane (MTES), propyltrimethoxysilane (PTMS)] and

bridged-type [1,2-bis(triethoxysilyl)methane (BTESM) bis(triethoxysilyl)propane (BTESP)] organosilica structures with similar carbon numbers (C_1 & C_3). The gas-permeation properties of F-doped pendant network structures revealed values for pore size, H_2/N_2 selectivity, and E_p (H_2) that were comparable to those of pristine organosilica membranes. This could be ascribed to the pendant side chains, which might have hindered the effectiveness of fluorine in pendant-type organosilica structures. The F-doped bridged-type organosilica (BTESM & BTESP) membranes, on the other hand, exhibited a looser network formation as the fluorine concentration increased.

Chapter 4 is **"Catalytic effect of trifluoroacetic acid on the CO_2 transport properties of organic-inorganic hybrid silica membranes".** Developing silica membranes that are highly selective for CO_2 has always been a challenge due to the small sizes of the pores and less amount of CO_2 philic sites in a typical silica network structure. Herein, we describe the fabrication of silica (tetraethoxysilane) membranes functionalized with 3-aminopropyltriethoxysilyl (APTES) and trifluoroacetic acid (TFA). An interaction generated among primary (NH_2) amines and TFA was identified, which was then also revealed by the reversible nature of CO_2 adsorption/desorption — an opposite trend from observations when using another catalyst (HCl). The resultant TEOS-APTES (TFA) membranes demonstrated CO_2 permeance of 3.8×10^{-7} mol m^{-2} s^{-1} Pa^{-1} and CO_2/N_2 selectivity of 35 at 50 ºC via the effect of surface diffusion. This is attributed to the increased microporosity and structural variations affected by TFA, which enhanced molecular sieving and controls the CO_2-philic sites (-$NHCOCF_3$) via interaction with amines. Finally, TEOS-APTES (TFA) membranes showed excellent hydrothermal stability

irrespective of the single/binary separation system. This novel approach would be effective for the energy-efficient fabrication of highly CO_2-permeable membranes.

Chapter 5 is **"Conclusions and outlooks".**

References

1. J. P. Ciferno, T. E. Fout, A.P. Jones, J. T. Murphy, Capturing carbon from existing coal-fired power plants. Chem. Eng. Pr. 105 (2009) 33.

2. Y. Cai, C. Y. Sam, T. Chang, Nexus between clean energy consumption, economic growth, and CO_2 emissions. J. Clean. Prod. 182 (2018) 1001-1011.

3. A. Basile, A. Gugliuzza, A. D. O. L. F. O. Iulianelli, P. Morrone, Membrane technology for carbon dioxide (CO_2) capture in power plants. Adv. Membr. Sci. Technol. Sus. Energy. Env. App. (2011) 113-159.

4. F. Russo, F. Galiano, A. Iulianelli, A. Basile, A. Figoli, Biopolymers for sustainable membranes in CO_2 separation: A review. Fuel Proc. Technol. 213 (2021) 106643.

5. A. Brunetti, F. Scura, G. Barbieri, E. Drioli, Membrane technologies for CO_2 separation. J. Membr. Sci. 359 (2010) 115-125.

6. A. K. Datta, P. K. Sen, Optimization of membrane unit for removing carbon dioxide from natural gas. J. Membr. Sci. 283 (2006) 291-300.

7. C. A. Scholes, G. W. Stevens, S. E. Kentish, Membrane gas separation applications in natural gas processing. Fuel 96 (2012) 15-28.

8. A. D. Ebner, J. A. Ritter, State-of-the-art adsorption, and membrane separation processes for carbon dioxide production from carbon dioxide emitting industries. Sep. Sci. Technol. 44 (2009) 1273-1421.

9. H. Kopnina, European renewable energy. Applying circular economy thinking to policy-making. Vis. Sus. (2017).

10. R.S. Haszeldine, Carbon capture and storage: how green can black be? Sci. 325 (2009) 1647-1652.

11. P.C. Sahoo, M. Kumar, S.K. Puri, S.S.V. Ramakumar, Enzyme inspired complexes for industrial CO_2 capture: opportunities and challenges, J. CO_2 Util. 24 (2018) 419-429.

12. H. Herzog, What future for carbon capture and sequestration? Env. Sci. Technol. Colum. 35 (2001) 148A.

13. C. M. White, B. R. Strazisar, E. J. Granite, J. S. Hoffman, H. W. Pennline, Separation and capture of CO_2 from large stationary sources and sequestration in geological formations—coalbeds and deep saline aquifers. J. Air Waste Manag. Assoc. 53 (2003) 645-715.

14. E. Favre, Carbon dioxide recovery from post-combustion processes: can gas permeation membranes compete with absorption? J. Membr. Sci. 294 (2007) 50-59.

15. A. A. Olajire, CO_2 capture and separation technologies for end-of-pipe applications–A review. Energy 35 (2010) 2610-2628.

16. B. Metz, O. Davidson, H. C. De Coninck, M. Loos, L. Meyer, IPCC special report on carbon dioxide capture and storage. Cambridge: Cambridge University Press. 2005.

17. L. Zheng, L. (Ed.) Oxy-fuel combustion for power generation and carbon dioxide (CO_2) capture. Elsevier 2011.

18. M. A. Habib, H. M. Badr, S. F. Ahmed, R, Ben-Mansour, K. Mezghani, S. Imashuku, A. F. Ghoneim, A review of recent developments in carbon capture utilizing oxy-fuel combustion in conventional and ion transport membrane systems. Int. J. Ener. Res. 35 (2011) 741-764.

19. C. A. Scholes, K. H. Smith, S. E. Kentish, G. W. Stevens, CO_2 capture from pre combustion processes—Strategies for membrane gas separation. Int. J. Green. Gas Cont. 4 (2010) 739-755.

20. D. Jansen, M. Gazzani, G. Manzolini, E. van Dijk, M. Carbo, Pre-combustion CO_2 capture. Int. J. Green. Gas Cont. 40 (2015)167-187.

21. M. Wang, A. Lawal, P. Stephenson, J. Sidders, C. Ramshaw, Post-combustion CO_2 capture with chemical absorption: A state-of-the-art review. Chem. Eng. Res. Des. 89 (2011) 1609-1624.

22. M. Wang, A. S. Joel, C. Ramshaw, D. Eimer, N. M. Musa, Process intensification for post-combustion CO_2 capture with chemical absorption: A critical review. App. Ener. 158 (2015) 275-291.

23. Y. Wang, L. Zhao, A. Otto, M. Robinius, D. Stolten, A review of post-combustion CO_2 capture technologies from coal-fired power plants. Ener. Proc. 114 (2017) 650-665.

24. X. Yu, C. O. Catanescu, R. Bird, S. Satagopan, Z. J. Baum, Q. A. Zhou, Trends in research and development for CO_2 capture and sequestration. ACS Omega 8., (2023) 11643-11664

25. W. J. Choi, J. B. Seo, S. Y. Jang, J. H. Jung, K. J. Oh, Removal characteristics of CO_2 using aqueous MEA/AMP solutions in the absorption and regeneration process. J. Env. Sci. 21 (2009) 907-913.

26. K. Damen, M. van Troost, A. Faaij, W. Turkenburg, A comparison of electricity and hydrogen production systems with CO_2 capture and storage. Part A: Review and selection of promising conversion and capture technologies. Prog. Ener. Comb. Sci. 32 (2006) 215-246.

27. Z. L. Ooi, P. Y. Tan, L. S. Tan, S. P. Yeap, Amine-based solvent for CO_2 absorption and its impact on carbon steel corrosion: A perspective review. Chinese J. Chem. Eng. 28 (2020) 1357-1367.

28. S. Ma'mun, V. Y. Dindore, H. F. Svendsen, Kinetics of the reaction of carbon dioxide with aqueous solutions of 2-((2-aminoethyl) amino) ethanol. Ind. Eng. Chem. Res. 46 (2007) 385-394.

29. A. L. Kohl, R. Nielsen, Gas purification. Elsevier 1997.

30. J. P. Ciferno, T. E. Fout, A. P. Jones, J. T. Murphy, Capturing carbon from existing coal-fired power plants. Chem. Eng. Prog. 105 (2009) 33.

31. R. T. J. Porter, M. Fairweather, C. Kolster, N. Mac Dowell, N. Shah, R. M. Woolley, Cost and performance of some carbon capture technology options for producing different quality CO_2 product streams. Int. J. Green. Gas Cont. 57 (2017) 185-195.

32. R. M. Bohloul, A. Vatani, S. M. Peyghambarzadeh, Experimental and theoretical study of CO_2 solubility in N-methyl- 2-pyrrolidone (NMP). Fluid Phase Equilib. 365 (2014) 106-111.

33. W. Chen, M. Chen, M. Yang, E. Zou, H. Li, C. Jia, C. Sun, Q. Ma, G. Chen, H. Qin, A new approach to the upgrading of the traditional propylene carbonate washing process with significantly higher CO_2 absorption capacity and selectivity. Appl. Ener. 240 (2019) 265-275.

34. T. N. Borhani, M. Wang, Role of solvents in CO_2 capture processes: The review of selection and design methods. Ren. Sust. Ener. Rev. 114 (2019) 109299.

35. C. Zhou, S. Yu, K. Ma, B. Liang, S. Tang, C. Liu, H. Yue, Amine-functionalized mesoporous monolithic adsorbents for post combustion carbon dioxide capture. Chem. Eng. J. 413 (2021) 127675.

36. L. Giraldo, D. P. Vargas, J. C. Moreno-Piraján, Study of CO_2 Adsorption on Chemically Modified Activated Carbon With Nitric Acid and Ammonium Aqueous. Fron. Chem. 8 (2020) 1.

37. S. Acevedo, L. Giraldo, J. C. Moreno-Piraján, Adsorption of CO_2 on Activated Carbons Prepared by Chemical Activation with Cupric Nitrate. ACS Omega 5 (2020) 10423-10432.

38. A. E. Creamer, B. Gao, Carbon-based adsorbents for postcombustion CO_2 capture: a critical review. Env. Sci. Technol. 50 (2016) 7276-7289.

39. C. E. Powell, G. G. Qiao, Polymeric CO_2/N_2 gas separation membranes for the capture of carbon dioxide from power plant flue gases. J. Membr. Sci. 279 (2006) 1-49.

40. R. W. Baker, Membrane technology and applications. John Wiley & Sons 2012

41. J. Xu, H. Wu, Z. Wang, Z. Qiao, S. Zhao, J. Wang, Recent advances on the membrane processes for CO_2 separation. Chinese J. Chem. Eng. 26 (2018) 2280-2291.

42. S. T. Oyama, M. Yamada, T. Sugawara, A. Takagaki, R. Kikuchi, Review on mechanisms of gas permeation through inorganic membranes. J. Jpn Petro. Inst. 54 (2011) 298-309.

43. C. Ma, M. Wang, Z. Wang, M. Gao, J. Wang, Recent progress on thin film composite membranes for CO_2 separation. J. CO_2 Util. 42 (2020) 101296.

44. N. Norahim, P. Yaisanga, K. Faungnawakij, T. Charinpanitkul, C. Klaysom, Recent membrane developments for CO_2 separation and capture. Chem. Eng. Technol. 41 (2018) 211-223.

45. P. Bernardo, E. Drioli, G. Golemme, Membrane gas separation: A review/state of the art. Ind. Eng. Chem. Res. 48 (2009) 4638-4663.

46. R. W. Baker, Future directions of membrane gas separation technology. Ind. Eng. Chem. Res. 41 (2002) 1393-1411.

47. W. J. Koros, G. K. Fleming, Membrane-based gas separation. J. Membr. Sci. 83 (1993) 1-80.

48. S. Roy, N. R. Singha, Polymeric nanocomposite membranes for next generation pervaporation process: strategies, challenges and future prospects. Membranes 7 (2017) 53.

49. D. Shekhawat, D. R. Luebke, H. W. Pennline, A review of carbon dioxide selective membranes. US Depart. Ener. (2003) 9-11.

50. W. Yave, A. Car, K. V. Peinemann, M. Q. Shaikh, K. Rätzke, F. Faupel, Gas permeability and free volume in poly (amide-b-ethylene oxide)/polyethylene glycol blend membranes. J. Membr. Sci. 339 (2009) 177-183.

51. M. Czyperek, P. Zapp, H. J. Bouwmeester, M. Modigell, K. Ebert, I. Voigt D. Stöver, Gas separation membranes for zero-emission fossil power plants: MEM-BRAIN. J. Membr. Sci. 359 (2010) 149-159.

52. R. T. Adams, S. J. Lee, T. H. Bae, J. K. Ward, J. R. Johnson, C. W. Jones, W. J. Koros, CO_2-CH_4 permeation in high zeolite 4A loading mixed matrix membranes. J. Membr. Sci. 367 (2011) 197-203.

53. H. Wu, X. Li, Y. Li, S. Wang, R. Guo, Z. Jiang, X. Lu, Facilitated transport mixed matrix membranes incorporated with amine functionalized MCM-41 for enhanced gas separation properties. J. Membr. Sci. 465 (2014) 78-90.

54. G. Dong, J. Hou, J. Wang, Y. Zhang, V. Chen, J. Liu, Enhanced CO_2/N_2 separation by porous reduced graphene oxide/Pebax mixed matrix membranes. J. Membr. Sci. 520 (2016) 860-868.

55. A. Car, C. Stropnik, W. Yave, K. V. Peinemann, PEG modified poly (amide-b ethylene oxide) membranes for CO_2 separation. J. Membr. Sci. 307 (2008) 88-95.

56. L. Zhao, E. Riensche, L. Blum, D. Stolten, Multi-stage gas separation membrane processes used in post-combustion capture: Energetic and economic analyses. J. Membr. Sci. 359 (2010) 160-172.

57. P. M. Budd, B. S. Ghanem, S. Makhseed, N. B. McKeown, K. J. Msayib, C. E. Tattershall, Polymers of intrinsic microporosity (PIMs): robust, solution-processable, organic nanoporous materials. Chem. Comm. (2004) 230-231.

58. N. B. McKeown, P. M Budd, Polymers of intrinsic microporosity (PIMs): Organic materials for membrane separations, heterogeneous catalysis and hydrogen storage. Chem. Soc. Rev. 35 (2006) 675-683.

59. N. Du, H. B. Park, G. P. Robertson, M. M. Dal-Cin, T. Visser, L. Scoles, M. D. Guiver, Polymer nanosieve membranes for CO_2-capture applications. Nat. Mater. 10 (2011) 372-375.

60. A. Y. Alentiev, V. P. Shantarovich, T. C. Merkel, V. I. Bondar, B. D. Freeman, Y. P. Yampolskii, Gas and vapor sorption, permeation, and diffusion in glassy amorphous Teflon AF1600. Macromol. 35 (2002) 9513-9522.

61. I. Pinnau, L. G. Toy, Gas and vapor transport properties of amorphous perfluorinated copolymer membranes based on 2, 2-bistrifluoromethyl-4, 5-difluoro-1, 3-dioxole/tetrafluoroethylene. J. Membr. Sci. 109 (1996) 125-133.

62. V. Arcella, P. Colaianna, P. Maccone, A. Sanguineti, A. Gordano, G. Clarizia, E. Drioli, A study on a perfluoropolymer purification and its application to membrane formation. J. Membr. Sci. 163 (1999) 203-209.

63. S. H. Han, J. E. Lee, K. J. Lee, H. B. Park, Y. M. Lee, Highly gas permeable and microporous polybenzimidazole membrane by thermal rearrangement. J. Membr. Sci. 357 (2010) 143-151.

64. D. F. Sanders, Z. P. Smith, C. P. Ribeiro Jr, R. Guo, J. E. McGrath, D. R. Paul, B. D. Freeman, Gas permeability, diffusivity, and free volume of thermally rearranged polymers

based on 3, 3′-dihydroxy-4, 4′-diamino-biphenyl (HAB) and 2, 2′-bis-(3, 4 dicarboxyphenyl) hexafluoropropane dianhydride (6FDA). J. Membr. Sci. 409 (2012) 232 241.

65. S. H. Han, N. Misdan, S. Kim, C. M. Doherty, A. J. Hill, Y. M. Lee, Thermally rearranged (TR) polybenzoxazole: Effects of diverse imidization routes on physical properties and gas transport behaviors. Macromol. 43 (2010) 7657-7667.

66. A. Husna, I. Hossain, O. Choi, S. M. Lee, T. H. Kim, Efficient CO_2 separation using a PIM-PI-functionalized UiO-66 MOF incorporated mixed matrix membrane in a PIM-PI-1 polymer. Macromol. Mater. Eng. 306 (2021) 2100298.

67. A. D. Kiadehi, A. Rahimpour, M. Jahanshahi, A. A. Ghoreyshi, Novel carbon nano fibers (CNF)/polysulfone (PSf) mixed matrix membranes for gas separation. J. Ind. Eng. Chem. 22 (2015) 199-207.

68. M. Sarfraz, M. Ba-Shammakh, Synergistic effect of adding graphene oxide and ZIF 301 to polysulfone to develop high performance mixed matrix membranes for selective carbon dioxide separation from post combustion flue gas. J. Membr. Sci. 514 (2016) 35-43.

69. A. L. Khan, C. Klaysom, A. Gahlaut, A. U. Khan, I. F. Vankelecom, Mixed matrix membranes comprising of matrimid and -SO_3H functionalized mesoporous MCM-41 for gas separation. J. Membr. Sci. 447 (2013) 73-79.

70. M. W. Anjum, B. Bueken, D. De Vos, I. F. Vankelecom, MIL-125 (Ti) based mixed matrix membranes for CO_2 separation from CH_4 and N_2. J. Membr. Sci. 502 (2016) 21-28.

71. C. A. Scholes, G. Q. Chen, G. W. Stevens, S. E. Kentish, Nitric oxide and carbon monoxide permeation through glassy polymeric membranes for carbon dioxide separation. Chem. Eng. Res. Des. 89 (2011) 1730-1736.

72. R. T. Adams, J. S. Lee, T. H. Bae, J. K. Ward, J. R. Johnson, C. W. Jones, W. J. Koros, CO_2-CH_4 permeation in high zeolite 4A loading mixed matrix membranes. J. Membr. Sci. 367 (2011) 197-203.

73. L. M. Robeson, Correlation of separation factor versus permeability for polymeric membranes. J. Membr. Sci. 62 (1991) 165-185.

74. L. M. Robeson, The upper bound revisited. J. Membr. Sci. 320 (2008) 390-400.

75. A. Klemm, Y. Y. Lee, H. Mao, B. Gurkan, Facilitated transport membranes with ionic liquids for CO_2 separations. Front. Chem. 8 (2020) 637.

76. M. S. Abd Rahaman, L. Zhang, L. H. Cheng, X. H. Xu, H. L. Chen, Capturing carbon dioxide from air using a fixed carrier facilitated transport membrane. RSC Adv. 2 (2012) 9165-9172.

77. R. Rea, M. G. De Angelis, M. G. Baschetti, Models for facilitated transport membranes: A review. Membranes 9 (2019) 26.

78. M. Wang, Z. Wang, S. Zhao, J. Wang, S. Wang, Recent advances on mixed matrix membranes for CO_2 separation. Chinese J. Chem. Eng. 25 (2017) 1581-1597.

79. L. Deng, M. B. Hagg, Fabrication and evaluation of a blend facilitated transport membrane for CO_2/CH_4 separation. Ind. Eng. Chem. Res. 54 (2015) 11139-11150.

80. May-Britt, H. Ä. G. G., Kim, T. J., & Li, B. (2005).

81. http://www.nanoglowa.com/

82. T. J. Kim, H. Vrålstad, M. Sandru, M. B. Hägg, Separation performance of PVAm composite membrane for CO_2 capture at various pH levels. J. Membr. Sci. 428 (2013) 218-224.

83. Z. Qiao, Z. Wang, C. Zhang, S. Yuan, Y. Zhu, J. Wang, S. Wang, PVAm–PIP/PS composite membrane with high performance for CO_2/N_2 separation. AIChE J. 59 (2013) 215-228.

84. S. Yuan, Z. Wang, Z. Qiao, M. Wang, J. Wang, S. Wang, Improvement of CO_2/N_2 separation characteristics of polyvinylamine by modifying with ethylenediamine. J. Membr. Sci. 378 (2011) 425-437.

85. Z. Qiao, Z. Wang, S. Zhao, S. Yuan, J. Wang, S. Wang, High adsorption performance polymers modified by small molecules containing functional groups for CO_2 separation. RSC Adv. 3 (2013) 50-54.

86. P. Li, Z. Wang, W. Li, Y. Liu, J. Wang, S. Wang, High-performance multilayer composite membranes with mussel-inspired polydopamine as a versatile molecular bridge for CO_2 separation. ACS App. Mater. Int. 7 (2015) 15481-15493.

87. Q. Hu, E. Marand, S. Dhingra, D. Fritsch, J. Wen, G. Wilkes, Poly(amideimide)/TiO_2 nano-composite gas separation membranes: fabrication and characterization. J. Membr. Sci. 135 (1997) 65.

88. C. J. Cornelius, E. Marand, Hybrid silica-polyimide composite membranes: Gas transport properties. J. Membr. Sci. 202 (2002) 97-118.

89. R. Mahajan, R. Burns, M. Schaeffer, W. J. Koros, Challenges in forming successful mixed matrix membranes with rigid polymeric materials. J. App. Poly. Sci. 86 (2002) 881-890.

90. D. R. Paul, D. R. Kemp, The diffusion time lag in polymer membranes containing adsorptive fillers. J. Poly. Sci. 41 (1973) 79-93.

91. X. Cao, Z. Qiao, Z. Wang, S. Zhao, P. Li, J. Wang, S. Wang, Enhanced performance of mixed matrix membrane by incorporating a highly compatible covalent organic framework into poly (vinylamine) for hydrogen purification. Inter. J. Hyd. Ener. 41 (2016) 9167-9174.

92. R. Zhang, S. Ji, N. Wang, L. Wang, G. Zhang, J. R. Li, Coordination-driven in situ self-assembly strategy for the preparation of metal-organic framework hybrid membranes. Ang. Chem. Int. Ed. 53 (2014) 9775-9779.

93. R. Lin, L. Ge, L. Hou, E. Strounina, V. Rudolph, Z. Zhu, Mixed matrix membranes with strengthened MOFs/polymer interfacial interaction and improved membrane performance. ACS App. Mater. Int. 6 (2014) 5609-5618.

94. P. D. Sutrisna, J. Hou, M.Y. Ulkifli, H. Li, Y. Zhang, W. Liang, V. Chen, Surface functionalized UiO-66/Pebax-based ultrathin composite hollow fiber gas separation membranes. J. Mater. Chem. A 6 (2018) 918-931.

95. M. M. Khan, S. Shishatskiy, V. Filiz, Mixed matrix membranes of boron icosahedron and polymers of intrinsic microporosity (PIM-1) for gas separation. Membranes 8 (2018) 1.

96. C. M. Zimmerman, A. Singh, W. J. Koros, Tailoring mixed matrix composite membranes for gas separations. J. Membr. Sci. 137 (1997) 145-154.

97. R. Mahajan, W. J. Koros, Factors controlling successful formation of mixed-matrix gas separation materials. Ind. Eng. Chem. Res. 39 (2000) 2692-2696.

98. J. Liao, Z. Wang, C. Gao, S. Li, Z. Qiao, M. Wang, S. Wang, Fabrication of high performance facilitated transport membranes for CO_2 separation. Chem. Sci. 5 (2014) 2843-2849.

99. S. Kim, J. Hou, Y. Wang, R. Ou, G. P. Simon, J. G. Seong, H. Wang, Highly permeable thermally rearranged polymer composite membranes with a graphene oxide scaffold for gas separation. J. Mater. Chem. A. 6 (2018) 7668-7674.

100. S. C. Hess, R. N. Grass, W. J. Stark, MOF channels within porous polymer film: Flexible, self-supporting ZIF-8 poly (ether sulfone) composite membrane. Chem. Mater. 28 (2016) 7638-7644.

101. J. Sun, Q. Li, G. Chen, J. Duan, G. Liu, W. Jin, MOF-801 incorporated PEBA mixed matrix composite membranes for CO_2 capture. Sep. Purif. Technol. 217 (2019) 229-239.

102. S. Fu, E. S. Sanders, S. Kulkarni, Y. H. Chu, G. B. Wenz, W. J. Koros, The significance of entropic selectivity in carbon molecular sieve membranes derived from 6FDA/DETDA: DABA (3:2) polyimide. J. Membr. Sci. 539 (2017) 329-343.

103. P. Bernardo, E. Drioli, G. Golemme, Membrane gas separation: A review/state of the art. Ind. Eng. Chem. Res. 48 (2009) 4638-4663.

104. J. Hou, P. Liu, M. Jiang, L. Yu, L. Li, Z. Tang, Olefin/paraffin separation through membranes: From mechanisms to critical materials. J. Mater. Chem. A. 7 (2019) 23489-23511.

105. J. Gascon, F. Kapteijn, B. Zornoza, V. Sebastian, C. Casado, J. Coronas, Practical approach to zeolitic membranes and coatings: State of the art, opportunities, barriers, and future perspectives. Chem. Mater. 24 (2012) 2829-2844.

106. M. Kanezashi, T. Fujita, M. Asaeda, Nickel-doped silica membranes for separation of helium from organic gas mixtures. Sep. Sci. Technol. 40 (2005) 225-238.

107. M. Kanezashi, M. Asaeda, Hydrogen permeation characteristics and stability of Ni doped silica membranes in steam at high temperature. J. Membr. Sci. 271 (2006) 86-93.

108. M. Rungta, G. B. Wenz, C. Zhang, L. Xu, W. Qiu, J. S. Adams, W. J. Koros, Carbon molecular sieve structure development and membrane performance relationships. Carbon 115 (2017) 237-248.

109. J. E. Koresh, A. Sofer, Molecular sieve carbon permselective membrane. Part I. Presentation of a new device for gas mixture separation. Sep. Sci. Technol. 18 (1983) 723-734.

110. M. Hou, W. Qi, L. Li, R. Xu, J. Xue, Y. Zhang, T. Wang, Carbon molecular sieve membrane with tunable microstructure for CO_2 separation: Effect of multiscale structures of polyimide precursors. J. Membr. Sci. 635 (2021) 119541.

111. L. I. B. David, A. F. Ismail, Influence of the thermastabilization process and soak time during pyrolysis process on the polyacrylonitrile carbon membranes for O_2/N_2 separation. J. Membr. Sci. 213 (2003) 285-291.

112. W. Zhou, M. Yoshino, H. Kita, K. I. Okamoto, Carbon molecular sieve membranes derived from phenolic resin with a pendant sulfonic acid group. Ind. Eng. Chem. Res. 40 (2001) 4801-4807.

113. C. Song, T. Wang, X. Wang, J. Qiu, Y. Cao, Preparation and gas separation properties of poly (furfuryl alcohol)-based C/CMS composite membranes. Sep. Purif. Technol. 58 (2008) 412-418.

114. Z. Wang, H. Ren, S. Zhang, F. Zhang, J. Jin, Carbon molecular sieve membranes derived from Tröger's base-based microporous polyimide for gas separation. ChemSusChem 11 (2018) 916-923.

115. B. Zhang, T. Wang, S. Zhang, J. Qiu, X. Jian, Preparation and characterization of carbon membranes made from poly (phthalazinone ether sulfone ketone). Carbon 44 (2006) 2764-2769.

116. C. Staudt-Bickel, W. J. Koros, Olefin/paraffin gas separations with 6FDA-based polyimide membranes. J. Membr. Sci. 170 (2000) 205-214.

117. X. Ma, R. Swaidan, B. Teng, H. Tan, O. Salinas, E. Litwiller, I. Pinnau, Carbon molecular sieve gas separation membranes based on an intrinsically microporous polyimide precursor. Carbon 62 (2013) 88-96.

118. O. Salinas, X. Ma, E. Litwiller, I. Pinnau, High-performance carbon molecular sieve membranes for ethylene/ethane separation derived from an intrinsically microporous polyimide. J. Membr. Sci. 500 (2016) 115-123.

119. C. P. Hu, C. K. Polintan, L. L. Tayo, S. C. Chou, H. A. Tsai, W. S. Hung, J. Y. Lai, The gas separation performance adjustment of carbon molecular sieve membrane depending on the chain rigidity and free volume characteristic of the polymeric precursor. Carbon 143 (2019) 343-351.

120. S. M. Saufi, A. F. Ismail, Fabrication of carbon membranes for gas separation—a review. Carbon 42 (2004) 241-259.

121. J. E. Koresh, A. Soffer, The carbon molecular sieve membranes. General properties and the permeability of CH_4/H_2 mixture. Sep. Sci. Technol. 22 (1987) 973-982.

122. S. Li, J. Li, M. Dong, S. Fan, T. Zhao, J. Wang, W. Fan, Strategies to control zeolite particle morphology. Chem. Soc. Rev. 48 (2019) 885-907.

123. F. Collins, A. Rozhkovskaya, J. G. Outram, G. J. Millar, A critical review of waste resources, synthesis, and applications for Zeolite LTA. Micro. Meso. Mater. 291 (2020) 109667.

124. S. Zhong, N. Bu, R. Zhou, W. Jin, M. Yu, S. Li, Aluminophosphate-17 and silicoaluminophosphate-17 membranes for CO_2 separations. J. Membr. Sci. 520 (2016) 507-514.

125. B. M. Lok, C. A. Messina, R. L. Patton, R. T. Gajek, T. R. Cannan, E. M. Flanigen, Silicoaluminophosphate molecular sieves: Another new class of microporous crystalline inorganic solids. J. Am. Chem. Soc. 106 (1984) 6092-6093.

126. M. Usman, Recent progress of SAPO-34 zeolite membranes for CO_2 separation: A review. Membranes 12 (2022) 507.

127. S. Li, J. L. Falconer, R. D. Noble, SAPO-34 membranes for CO_2/CH_4 separation. J. Membr. Sci. 241 (2004) 121-135.

128. M. A. Carreon, S. Li, J. L. Falconer, R. D. Noble, Alumina-supported SAPO-34 membranes for CO_2/CH_4 separation. J. Am. Chem. Soc. 130 (2008) 5412-5413.

129. S. Li, C. Q. Fan, High-flux SAPO-34 membrane for CO_2/N_2 separation. Ind. Eng. Chem. Res. 49 (2010) 4399-4404.

130. S. R. Venna, M. A. Carreon, Amino-functionalized SAPO-34 membranes for CO_2/CH_4 and CO_2/N_2 separation. Lang. 27 (2011) 2888-2894.

131. I. G. B. N. Makertihartha, K. S. Kencana, T. R. Dwiputra, K. Khoiruddin, R. R. Mukti, I. G. Wenten, Silica supported SAPO-34 membranes for CO_2/N_2 separation. Micro. Meso. Mater. 298 (2020) 110068.

132. S. B. Messaoud, A. Takagaki, T. Sugawara, R. Kikuchi, S. T. Oyama, Mixed matrix membranes using SAPO-34/polyetherimide for carbon dioxide/methane separation. Sep. Purif. Technol. 148 (2015) 38-48.

133. D. Zhao, J. Ren, H. Li, K. Hua, M. Deng, Poly (amide-6-b-ethylene oxide)/SAPO-34 mixed matrix membrane for CO_2 separation. J. Ener. Chem. 23 (2014) 227-234.

134. M. Kanezashi, T. Fujita, M. Asaeda, Nickel-doped silica membranes for separation of helium from organic gas mixtures. Sep. Sci. Technol. 40 (2005) 225-238.

135. M. Kanezashi, K. Yada, T. Yoshioka, T. Tsuru, Organic-inorganic hybrid silica membranes with controlled silica network size: Preparation and gas permeation characteristics. J. Membr. Sci. 348 (2010) 310-318.

136. T. Tsuru, R. Igi, M. Kanezashi, T. Yoshioka, S. Fujisaki, Y. Iwamoto, Permeation properties of hydrogen and water vapor through porous silica membranes at high temperatures. AIChE J. 57 (2011) 618-629.

137. T. Tsuru, Silica-based membranes with molecular-net-sieving properties: Development and applications. J. Chem. Eng. Jpn. 51 (2018) 713-725.

138. T. Yoshioka, A. Nakata, K. L. Tung, M. Kanezashi, T. Tsuru, Molecular dynamic simulation study of solid vibration permeation in microporous amorphous silica network voids. Membranes 9 (2019) 132.

139. H. R. Lee, M. Kanezashi, Y. Shimomura, T. Yoshioka, T. Tsuru, Evaluation and fabrication of pore-size-tuned silica membranes with tetraethoxydimethyl disiloxane for gas separation. AIChE J. 57 (2011) 2755-2765.

140. M. Kanezashi, M. Kawano, T. Yoshioka, T. Tsuru, Organic-inorganic hybrid silica membranes with controlled silica network size for propylene/propane separation. Ind. Eng. Chem. Res. 51 (2012) 944-953.

141. M. Kanezashi, T. Shioda, T. Gunji, T. Tsuru, Gas permeation properties of silica membranes with uniform pore sizes derived from polyhedral oligomeric silsesquioxane. AIChE J. 58 (2012) 1733-1743.

142. H. L. Castricum, A. Sah, R. Kreiter, D. H. Blank, J. F. Vente, J. E. ten Elshof, Hydrothermally stable molecular separation membranes from organically linked silica. J. Mater. Chem. 18 (2008) 2150-2158.

143. X. Yu, L. Meng, T. Niimi, H. Nagasawa, M. Kanezashi, T. Yoshioka, T. Tsuru, Network engineering of a BTESE membrane for improved gas performance via a novel pH-swing method. J. Membr. Sci. 511 (2016) 219-227.

144. N. Moriyama, H. Nagasawa, M. Kanezashi, T. Tsuru, Improved performance of organosilica membranes for steam recovery at moderate-to-high temperatures via the use of a hydrothermally stable intermediate layer. J. Membr. Sci. 620 (2021) 118895.

145. R. M. De Vos, H. Verweij, High-selectivity, high-flux silica membranes for gas separation. Sci. 279 (1998) 1710-1711.

146. Y. S. Lin, I. Kumakiri, B. N. Nair, H. Alsyouri, Microporous inorganic membranes. Sep. Purif. Meth. 31 (2002) 229-379.

147. N. W. Ockwig, T. M. Nenoff, Membranes for hydrogen separation. Chem. Rev. 107 (2007) 4078-4110.

148. X. Ren, K. Nishimoto, M. Kanezashi, H. Nagasawa, T. Yoshioka, T. Tsuru, CO_2 permeation through hybrid organosilica membranes in the presence of water vapor. Ind. Eng. Chem. Res. 53 (2014) 6113-6120.

149. L. Yu, M. Kanezashi, H. Nagasawa, M. Guo, N. Moriyama, K. Ito, T. Tsuru, Tailoring ultramicroporosity to maximize CO_2 transport within pyrimidine-bridged organosilica membranes. ACS Appl. Mater. Inter. 11 (2019) 7164-7173.

150. G. Li, M. Kanezashi, T. Tsuru, Preparation of organic-inorganic hybrid silica membranes using organoalkoxysilanes: The effect of pendant groups. J. Membr. Sci. 379 (2011) 287-295.

151. N. K. Raman, C. J. Brinker, Organic “template” approach to molecular sieving silica membranes. J. Membr. Sci. 105 (1995) 273-279.

152. K. Kusakabe, S. Sakamoto, T. Saie, S. Morooka, Pore structure of silica membranes formed by a sol-gel technique using tetraethoxysilane and alkyltriethoxysilanes. Sep. Purif. Technol. 16 (1999) 139-146.

153. H. L. Castricum, R. Kreiter, H. M. van Veen, D. H. Blank, J. F. Vente, J. E. ten Elshof, High-performance hybrid pervaporation membranes with superior hydrothermal and acid stability. J. Membr. Sci. 324 (2008) 111-118.

154. M. Kanezashi, M. Kawano, T. Yoshioka, T. Tsuru, Organic–inorganic hybrid silica membranes with controlled silica network size for propylene/propane separation. Ind. Eng. Chem. Res. 51 (2012) 944-953.

155. H. L. Castricum, G. G. Paradis, M. C. Mittelmeijer-Hazeleger, R. Kreiter, R., J. F. Vente, J. E. ten Elshof, Tailoring the separation behavior of hybrid organosilica membranes by adjusting the structure of the organic bridging group. Adv. Fun. Mater. 21 (2011) 2319-2329.

156. X. Ren, K. Nishimoto, M. Kanezashi, H. Nagasawa, T. Yoshioka, T. Tsuru, CO_2 permeation through hybrid organosilica membranes in the presence of water vapor. Ind. Eng. Chem. Res. 53 (2014) 6113-6120.

157. X. Ren, T. Tsuru, Organosilica-based membranes in gas and liquid-phase separation. Membranes 9 (2019) 107.

158. V. Boffa, J. E. ten Elshof, A. V. Petukhov, D. H. Blank, Microporous niobia–silica membrane with very low CO_2 permeability. ChemSusChem: Chem. Sus. Ener. Mater. 1 (2008) 437-443.

159. K. Yoshida, Y. Hirano, H. Fujii, T. Tsuru, M. Asaeda, Hydrothermal stability and performance of silica-zirconia membranes for hydrogen separation in hydrothermal conditions. J. Chem. Eng. Jpn. 34 (2001) 523-530.

160. T. Yoshioka, E. Nakanishi, T. Tsuru, M. Asaeda, Experimental studies of gas permeation through microporous silica membranes. AIChE J. 47 (2001) 2052-2063.

161. M. Takenaka, H. Nagasawa, T. Tsuru, M. Kanezashi, Hydrocarbon permeation properties through microporous fluorine-doped organosilica membranes with controlled pore sizes. J. Membr. Sci. 619 (2021) 118787.

162. M. Kanezashi, T. Matsutani, T. Wakihara, H. Tawarayama, H. Nagasawa, T. Yoshioka, T. Tsuru, Tailoring the subnano silica structure via fluorine doping for development of highly permeable CO_2 separation membranes. ChemNanoMat 2 (2016) 264-267.

163. M. Kanezashi, T. Matsutani, T. Wakihara, H. Nagasawa, T. Okubo, T. Tsuru, Preparation and gas permeation properties of fluorine–silica membranes with controlled amorphous silica structures: Effect of fluorine source and calcination temperature on network size. ACS App. Mater. Int. 9 (2017) 24625-24633.

164. M. Kanezashi, T. Matsutani, H. Nagasawa, T. Tsuru, Fluorine-induced microporous silica membranes: Dramatic improvement in hydrothermal stability and pore size controllability for highly permeable propylene/propane separation. J. Membr. Sci. 549 (2018) 111-119.

165. M. Kanezashi, N. Hataoka, R. Ikram, H. Nagasawa, T. Tsuru, Hydrothermal stability of fluorine-induced microporous silica membranes: Effect of steam treatment conditions. AIChE J. 67 (2021) e17292.

166. G. G. Paradis, R. Kreiter, M. M. van Tuel, A. Nijmeijer, J. F. Vente, Amino functionalized microporous hybrid silica membranes. J. Mater. Chem. 22 (2012) 7258-7264.

167. G. Xomeritakis, C. Y. Tsai, Y. B. Jiang, C. J. Brinker, Tubular ceramic-supported sol gel silica-based membranes for flue gas carbon dioxide capture and sequestration. J. Membr. Sci. 341 (2009) 30-36.

168. G. Xomeritakis, C. Y. Tsai, C. J. Brinker, Microporous sol–gel derived aminosilicate membrane for enhanced carbon dioxide separation. Sep. Purif. Technol. 42 (2005) 249-257.

169. S. Suzuki, S. B. Messaoud, A. Takagaki, T. Sugawara, R. Kikuchi, S. T. Oyama, Development of inorganic–organic hybrid membranes for carbon dioxide/methane separation. J. Membr. Sci. 471 (2014) 402-411.

170. M. Guo, M. Kanezashi, H. Nagasawa, L. Yu, J. Ohshita, T. Tsuru, Amino-decorated organosilica membranes for highly permeable CO_2 capture. J. Membr. Sci. 611 (2020) 118328.

171. L. Yu, M. Kanezashi, H. Nagasawa, M. Guo, N. Moriyama, K. Ito, T. Tsuru, Tailoring ultramicroporosity to maximize CO_2 transport within pyrimidine-bridged organosilica membranes. ACS App. Mater. Int. 11 (2019) 7164-7173.

172. M. Ostwal, R. P. Singh, S. F. Dec, M. T. Lusk, J. D. Way, 3 Aminopropyltriethoxysilane functionalized inorganic membranes for high temperature CO_2/N_2 separation. J. Membr. Sci. 369 (2011) 139-147.

173. R. P. Singh, J. D. Way, K. C. McCarley, Development of a model surface flow membrane by modification of porous vycor glass with a fluorosilane. Ind. Eng. Chem. Res. 43 (2004) 3033-3040.

174. Y. Sakamoto, K. Nagata, K. Yogo, K. Yamada, Preparation and CO_2 separation properties of amine-modified mesoporous silica membranes. Micro. Meso. Mater. 101 (2007) 303-311.

175. K. S. Jang, H. J. Kim, J. R. Johnson, W. G. Kim, W. J. Koros, C. W. Jones, S. Nair, Modified mesoporous silica gas separation membranes on polymeric hollow fibers. Chem. Mater. 23 (2011) 3025-3028.

176. M. Miyamoto, A. Takayama, S. Uemiya, K. Yogo, Gas permeation properties of amine loaded mesoporous silica membranes for CO_2 separation. Des. Water Treat. 34 (2011) 266-271.

177. R. M. De Vos, H. Verweij, Improved performance of silica membranes for gas separation. J. Membr. Sci. 143 (1998) 37-51.

178. M. Kanezashi, T. Sasaki, H. Tawarayama, T. Yoshioka, T. Tsuru, Hydrogen permeation properties and hydrothermal stability of sol-gel derived amorphous silica membranes fabricated at high temperatures. J. Am. Ceram. Soc. 96 (2013) 2950-2957.

179. G. Cao, Y. Lu, L. Delattre, C. J. Brinker, G. P. López, Amorphous silica molecular sieving membranes by sol-gel processing. Adv. Mater. 8 (1996) 588-591.

Chapter 2

Tailoring the structure of sub-nano silica network via fluorine doping to enhance CO_2 separation and evaluating CO_2 separation performance under dry or wet conditions

2.1. Introduction

The surge in CO_2 emissions is creating immense environmental issues, and this impurity gas (CO_2) must be removed from mixtures of light gases such as CO_2/H_2, CO_2/N_2, and CO_2/CH_4. Thus far, processes for the separation/capture of CO_2 from mixtures have depended on absorption, pressure swing absorption, and membrane separation. Among all these alternatives, the membrane-based CO_2 separation/capture process is more advantageous for reasons that include membrane mechanical simplicity, energy efficiency, easy fabrication, and suitability to small- and medium-scale separation procedures [1-8]. Hence, various types of membranes such as polymeric [9], carbon molecular sieve [10], zeolite [11, 12], graphene oxide [13], metal-organic frameworks (MOFs) [14], and silica [15-17] have been designed for CO_2 separation.

In industrial processing, however, membranes selective for CO_2 must possess high levels of chemical and thermal stability under severe conditions of elevated temperatures and pressures. For example, polymeric membranes have shown CO_2/N_2 selectivity of 40 and CO_2/CH_4 selectivity approximating 100, but the weak physicochemical properties of polymer structures restrict their applications [18]. In this context, since the 1980s silica

structures have garnered a considerable amount of interest due to the promise of robust physicochemical stability (up to 800 ºC).

More specifically, commonly used tetraethoxysilane (TEOS) is considered one of the most promising Si precursors for the fabrication of silica membranes via chemical vapor deposition (CVD) and sol-gel methods [19]. For example, silica membranes prepared via sol-gel methods have shown H_2 permeance of 5.5×10^{-7} mol m^{-2} s^{-1} Pa^{-1} with a H_2/N_2 permeation ratio of more than 100 at 750 ºC [20]. This excellent membrane performance, however, is associated with the sol-gel derived silica network pore structure (average pore size: 0.34 nm) that is suitable for permeation by small molecules (He, H_2), but is not appropriate for larger gases such as CO_2 (0.33 nm) and N_2 (0.36 nm) [21, 22]. In addition, conventional silica membranes fail to maintain their stability against an atmosphere (moist) whereby water molecules may interact with the membrane surface and generate Si-OH groups and an excessive amount of silanol density (Si-OH). The generation of Si-OH in the silica structure leads to structural rearrangements (densification) and simultaneously to an enlargement of grain boundaries. The hydrothermal instability of conventional silica degrades membrane performance [21-23].

Hence, a reduction in the Si-OH density to improve the hydrophobic properties of the silica structure is considered an effective approach with the dual benefits of improved hydrothermal stability and the ability to tune the network pore size. For instance, the introduction of hydrophobic functional organic groups coupled with two Si atoms (Si-R-Si) effectively controlled the silica network pore size and allowed H_2 permeance of a sol-gel-derived organosilica 1,2-bis (triethoxysilyl) methane (BTESM, Si-CH_2-Si) membrane on

the order of 10^{-6} mol m^{-2} s^{-1} Pa^{-1}, which is one order of magnitude higher than those of pure silica (10^{-7} mol m^{-2} s^{-1} Pa^{-1}) membranes [24]. These organic units shield the Si atoms in dry systems and prevent the regeneration of silanol groups that is followed by the decomposition of siloxane due to interactions with water. Over the past few years, several studies have evaluated the hydrothermal stability of organosilica 1,2-bis(triethoxysilyl)ethane (BTESE, Si-C_2H_4-Si) membranes in PV applications/humid gas separation and confirmed that organosilica membranes show superior stability [25,26]. In a similar manner, Igi et al. [27] developed metal-doped silica membranes and observed that small crystals of cations may be dispersed into the silica matrix, which stabilizes the network structure over a time period of 60 h and promises H_2 permeance on the order of 10^{-7} mol m^{-2} s^{-1} Pa^{-1} with H_2/N_2 selectivity of (250-270). Kanezashi et al. [28] reported the achievement of hydrothermal stability in Ni-doped silica membranes with stable He permeance (10^{-6} mol m^{-2} s^{-1} Pa^{-1}) even under very high levels of steam partial pressure and temperature (500 ºC, partial pressure of steam: 90-400 kPa).

Another substitute for the above-mentioned strategies is to induce Si-F bonds into the silica matrix via the addition of NH_4F into silica sols. During the sol-gel polymerization process, highly reactive fluorine resulted in the formation of Si-F bonds, which replaced the silanol groups [19]. The formation of Si-F bonds in the silica matrix affected the Si-O-Si bond angle, which resulted in the formation of a loose network structure. For instance, a tetraethoxyfluorosilane (TEFS) membrane showed H_2 permeance on the order of 10^{-6} mol m^{-2} s^{-1} Pa^{-1}, which is superior to conventional silica membranes, and was quite stable under a steam atmosphere (500 ^{o}C, partial pressure of steam: 30-90 kPa), because a high

concentration of Si-F bonds decreases Si-OH density and improves the hydrothermal stability and permeation properties of silica membranes [29]. However, F-doped SiO_2 membranes have never been applied to a CO_2/N_2 separation system.

Therefore, a strategy for anion (NH_4F) doping into a silica matrix was applied to fabricate highly permeable membranes for CO_2/N_2 separation. NH_4F and TEOS were used as doping agent and Si precursor, respectively. The physiochemical structure of fluorine-doped silica gels/films was characterized via Fourier transform infrared spectroscopy (FT-IR), N_2 and CO_2 adsorption/desorption isotherms, XPS spectra, and XRD patterns. H_2O adsorption isotherms were carried out for hydrophobicity/hydrophilicity analysis. Furthermore, activation energies (E_p) of gas permeation were used to evaluate the effect that fluorine exerts on the pore structure of a silica network. In subsequent experiments, the CO_2/N_2 separation performance of all prepared membranes was compared based on E_p (CO_2) and E_p (N_2) to further examine the CO_2 separation potential of fluorine-doped silica membranes. Finally, membranes were applied in a humid environment to examine the hydrothermal stability of the network structure.

2.2. Experimental section

2.2.1. Sol/gel preparation

A sol-gel method was employed to prepare fluorine doped and undoped silica sols via hydrolysis/polymerization process [30-37] and final composition ratio (mole) of TEOS:H_2O:HNO_3 (1/200/0.1) was maintained. To the ethanol solution, we simultaneously added water, a catalyst (HNO_3), and a Si precursor under vigorous stirring at 500 rpm for

40-60 minutes at room temperature. The final precursor concentration was fixed with weight % of 0.5, and the fluorine concentrations (F/Si) were 1-20 mol%. Under and air atmosphere, slow drying process was employed to prepare the F-doped silica gel at the temperature of 40 ºC and then gel was ground in a mortar. For analysis (XPS, XRD, N_2, H_2/CO_2 adsorption), the powder was calcined at 350 °C under an air atmosphere.

2.2.2. Characterization of F-doped silica sols/gels

A DLS analyzer (Malvan Zetasizer Nano ZS) was used for F-doped silica sol sizes. KBr plate wsa used to evaluate the Fourier transform infrared (FT-IR) spectrum of F-doped and undoped samples in the range of 400-4,000 cm^{-1} using a FT-IR spectrometer (FT/IR-4100, Jasco, Japan). To examine the fluorine status in the silica matrix, X-ray photoelectron spectroscopy (XPS) (XPS, Shimadzu, Japan) analyses were performed and each sample was vacuumed prior to measurement. Adsorption behavior of all gels was assessed by utilizing a BELMAX (BELJAPAN INC.) and prior to start the measurements, all samples were pretreated for 12 h at 200 °C to remove the adsorbed water. Similarly, H_2O and CO_2 adsorption isotherms were carried out at ambient temperature (25 °C) to evaluate the hydrophobicity/hydrophilicity and CO_2 adoption properties, respectively.

2.2.3 Membrane fabrication

Porous alumina tubes with 60% porosity and pore size of 1.2 μm were supplied from Nikkato Ltd., Japan and were used to fabricate the fluorine-doped silica membranes. The tubes were coated by alumina particles (0.2 and 2 μm) diluted with a SiO_2-ZrO_2 sol (5-10

wt%) by following the calcination at 550 ºC for 30 min to achieve a smooth particle layer. Next, an intermediate layer (average pore size of 1-2 nm) was formed by depositing the sol (SiO_2-ZrO_2) with reduced concentration (0.5-1 wt% diluted with H_2O). Finally, a top separation thin layer was coated on the intermediate layer with F-doped and undoped silica sol by following the calcination at 350 ºC in an air environment. A defect-free top separation layer was achieved with 5-6 coats and ramping rate of calcination temperature was controlled at 10 ºC min^{-1}.

2.2.4. Membrane performance evaluation

Using the experimental apparatus shown in Fig. 2-1, we conducted single gas (He, H_2, CO_2, N_2, CH_4, CF_4, and SF_6) permeation measurements at 50-300 ºC. Each gas was fed from the outer surface of the membrane, and the permeate side pressure was maintained at an atmospheric level. To desorb water from the membrane surface, each membrane was kept overnight at 200 ºC under an inert environment. A film flow meter (SF-U, Horiba Ltd., Japan) was used to measure gas permeate flow. The binary separation performance was examined using a vacuum pump attached to the permeate side to control the upstream and downstream pressures at 100 kPa and 10-12 kPa, respectively. The composition of the gas mixture (CO_2/N_2) was evaluated using gas chromatography (GC-14B, Shimadzu, Japan) and a TCD detector (column: Unibeads 1S80/100, GL Science, Japan; column temperature: 75 ºC). In order to evaluate the hydrothermal stability under steam at low partial pressure (H_2O partial pressure = 3 kPa), each gas (He, N_2, CO_2) was fed to the membrane cell after passing through a water evaporator at ambient temperature. Gas permeation properties under a wet system were evaluated at temperatures ranging from 50 to 300 ºC. Finally, the

F-doped membranes were exposed to a steam atmosphere under a higher partial pressure of steam (300 ºC, 30 kPa) for 1 h using an apparatus reported elsewhere [29,38].

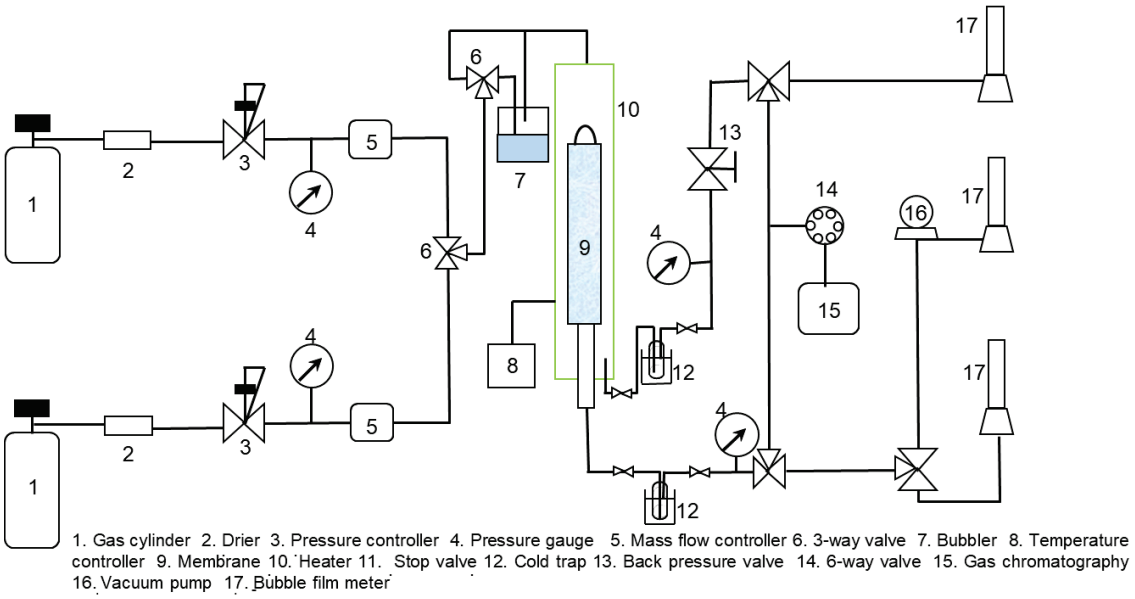

Fig. 2-1. Schematic illustration of the experimental apparatus used for single/binary gas permeation measurement.

The binary separation performance was examined under upstream and downstream pressure controlled at 100 kPa and 10-12 kPa, respectively, and a vacuum pump was attached to the permeate side. The composition of the gas mixture (CO_2/N_2) was evaluated using gas chromatography (GC-14B, Shimadzu, Japan) and a TCD detector (column: Unibeads 1S80/100, GL Science, Japan; column temperature: 75 ºC).

In order to evaluate the hydrothermal stability under steam at low partial pressure (H_2O partial pressure = 3 kPa), each gas (He, N_2, CO_2) was fed to the membrane cell after passing through a water evaporator at ambient temperature. Gas permeation properties under a wet system were evaluated at temperatures ranging from 50-300 ºC. Finally, the F-

doped membranes were exposed to a steam atmosphere under a higher partial pressure of steam (300 ºC, 30 kPa) for 1 hour using an apparatus reported elsewhere [29, 38].

2.3. Results and discussion

2.3.1. Physico-chemical properties of F-doped silica gel/powder

Fig. 2-2a indicates the FT-IR spectra of fluorine-doped silica films calcined at 350 ºC under an air atmosphere. Irrespective of the fluorine concentration, the asymmetric vibrations of Si-O-Si ranged from 980 to 1,100 cm^{-1} and were detected in all samples, which include complete hydrolysis and polymerization reactions. A small shoulder peak of Si-F was detected at around 940 cm^{-1} in F-doped samples and increased as fluorine concentration was increased from 1 to 20%. As a result, the existence of these Si-F groups into the silica structure affected the Si-O-Si bond angle, which led to a shift in the Si-O-Si peak to a higher wave number (blue shift) [39].

Fig. 2-2b depicts the Si-OH/Si-O-Si peak area ratios for fluorine-doped and undoped silica films. The Si-OH/Si-O-Si peak area ratio for the pure silica sample was higher than those of the F-doped silica samples. The Si-OH/Si-O-Si peak area ratio was decreased largely by lower concentrations of fluorine (F/Si = 0.1/9.9, 0.3/9.7, 0.5/9.5) and was somewhat independent of doped-fluorine concentrations above 10 mol% (F/Si=1/9). These results suggest that when Si-F groups replaced silanol groups (Si-OH), small concentration of fluorine significantly decreased the Si-OH density.

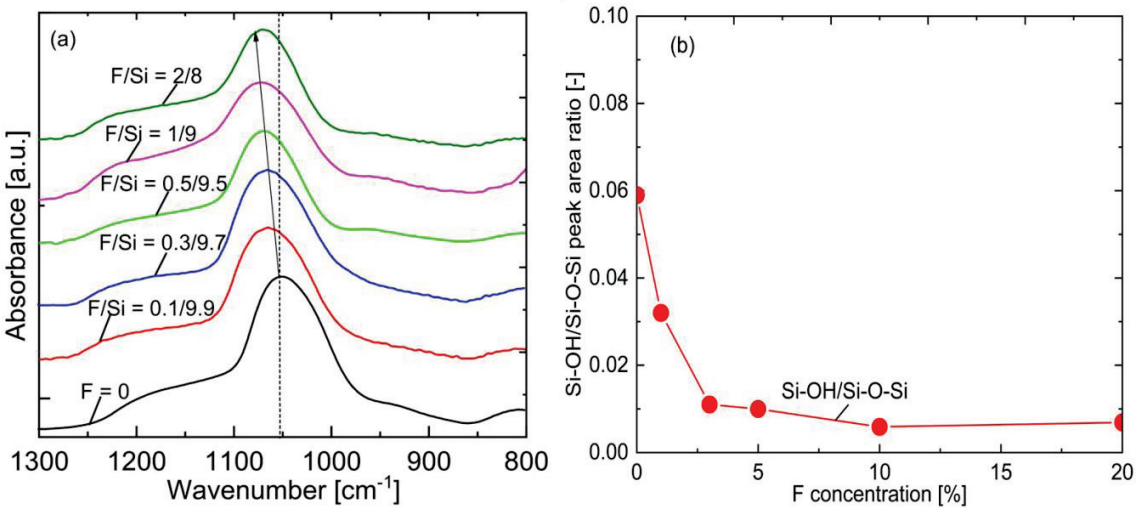

Fig. 2-2. FTIR spectra (a) and peak area ratios (b) for F-SiO_2 films (F/Si = 0/10-2/8) calcined at 350 ºC in an air atmosphere.

Fig. 2-3 shows the XRD patterns for fluorine-doped (F = 0-20%) and undoped silica gels calcined at 350 ºC under an air atmosphere. All samples demonstrated an amorphous structure with a single peak irrespective of the fluorine concentration. This peak was shifted to a lower degree of 2θ and this trend was more prominent in samples with higher fluorine concentrations, which indicates an enlargement of the *d*-spacing. The change in the bond angle (Si-O-Si) indicated via FT-IR increased with increases in the fluorine concentration. Thus, the FT-IR and XRD results depict the effectiveness of fluorine by showing the formation of a loose network structure with decreased silanol (Si-OH) density [19,38,40-42].

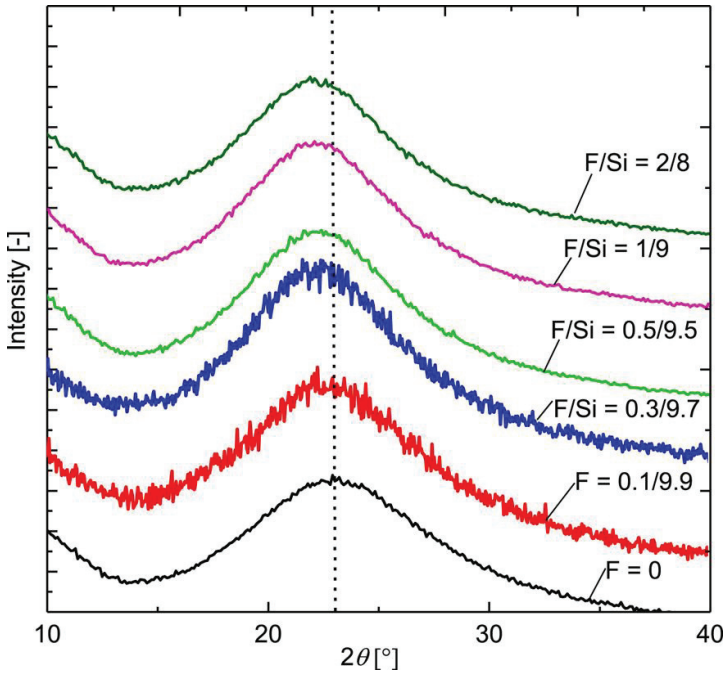

Fig. 2-3. XRD patterns for fluorine-doped (F/Si = 0/10-2/8) and undoped silica gels calcined at 350 ºC in an air atmosphere.

Fig. 2-4a shows the water adsorption isotherms at 25 ºC for F-doped (F/Si = 0.1/9.9, F/Si = 0.3/9.7, and F/Si = 0.5/9.5) and undoped (F = 0) silica gels. Conventional silica reaches the upper limits of absorbed water due to hydrophilic characteristics that make it attractive to water vapors. After fluorine doping, however, H_2O adsorption properties was dependent on the concentration of fluorine doping since doped fluorine can dramatically reduce Si–OH density. For example, high levels of silanol (Si-OH) in a gel (F/Si = 0.1/9.9) leads to higher amounts of adsorbed water: F/Si = 0.3/9.7 and 0.5/9.5. Kanezashi et al. [40] reported similar results and concluded that despite being hydrophobic due to the organic liking units, a sample of fluorine containing 1,2-bis(triethoxysilyl)methane (BTESM, Si CH_2-Si) showed a reasonably lower amount of absorbed water by comparison with pure BTESM.

Fig. 2-4b illustrates the CO_2 adsorption isotherms at 25 ºC for F-doped and undoped silica gels. Higher CO_2 uptake was observed for pure silica (TEOS) gel by comparison with F-doped silica gels, since silica interacts with CO_2 due to polar characteristics. F-doped silica gels, however, showed that fluorine effectively controls the hydrophobic/ hydrophilic characteristics of conventional silica with decreases in CO_2 adsorption as the content of fluorine increases. For instance, the gel with an F/Si ratio of 0.1/9.9 contained a higher amount of silanol groups compared with other samples (F/Si = 0.3/9.7 & 0.5/9.5), which resulted in higher levels of CO_2 adsorption. This trend for CO_2 adsorption was consistent with that of Si–OH density; i.e., F-doped silica with less Si-OH showed a lower amount of CO_2 adsorption.

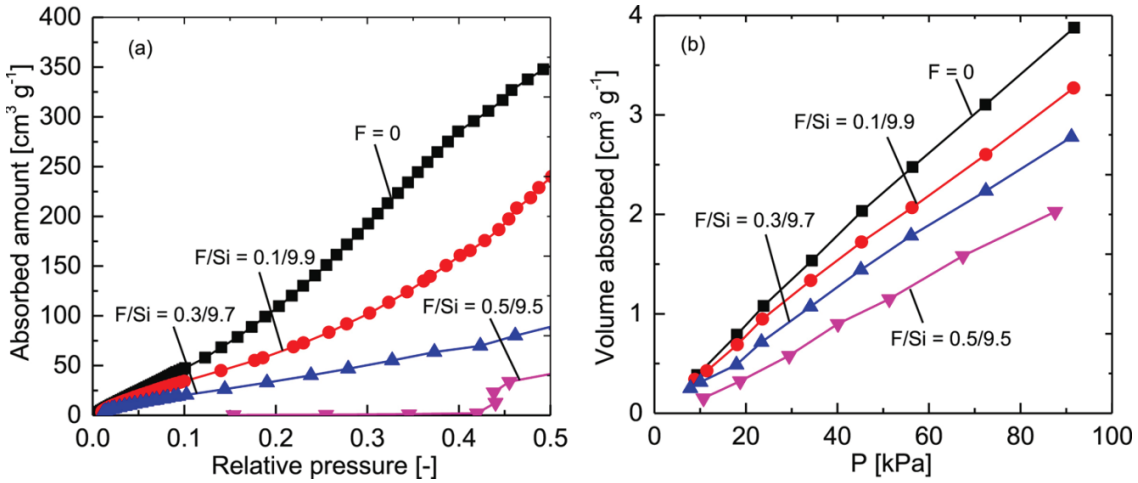

Fig. 2-4. H_2O adsorption (a) CO_2 adsorption (b) isotherms for fluorine-doped and undoped silica gels calcined at 350 ºC in an air atmosphere.

2.3.2. Network pore size evaluation of fluorine-doped and undoped silica membranes

Fig. 2-5 shows the typical SEM images of the cross-sectional morphologies of fluorine doped SiO_2 membranes (F/Si = 0.1/9.9, 0.3/9.7, 0.5/9.5). Since it is difficult to distinguish between the layers, however, a continuous defect-free separation layer was formed on the intermediate layer, irrespective of the concentration of doped fluorine. This thin layer formation is common to the fabrication of membranes with high levels of permeance and molecular sieving properties.

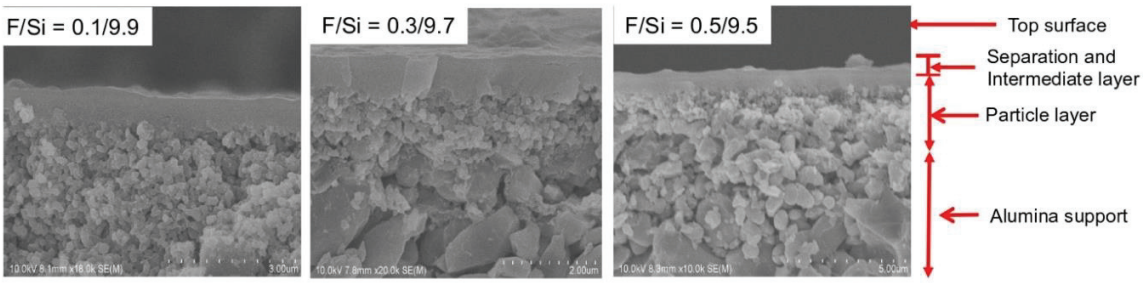

Fig. 2-5. SEM images of cross-sectional morphologies of F-SiO_2 (F/Si = 0.1/9.9, 0.3/9.7, 0.5/9.5) membranes calcined at 350 ºC under an air atmosphere.

Fig. 2-6 shows gas permeance results and permeance ratios at 50 ºC as a function of fluorine concentration for fluorine-doped and undoped silica membranes calcined at 350 ºC under an air atmosphere. Since conventional silica exhibits a dense network structure, H_2 permeance of 1.1×10^{-7} mol m^{-2} s^{-1} Pa^{-1} with permselectivity of $H_2/N_2 = 64$ was observed. On the contrary, F-induced membranes displayed improved gas permeation with decreased permselectivity followed by the loose network formation. For instance, a membrane (F/Si = 0.1/9.9) showed H_2 permeance of 4.0×10^{-7} mol m^{-2} s^{-1} Pa^{-1} with H_2/N_2 selectivity of 58

by comparison with another membrane with an F/Si ratio of 2/8, which recorded H_2 permeance of 9.6×10^{-6} mol m^{-2} s^{-1} Pa^{-1} with H_2/N_2 selectivity of 31. It should be noted that the fixed coating times and calcination conditions returned similar results for each membrane, which confirms the reproducibility of F-SiO_2 membranes, irrespective of fluorine concentration.

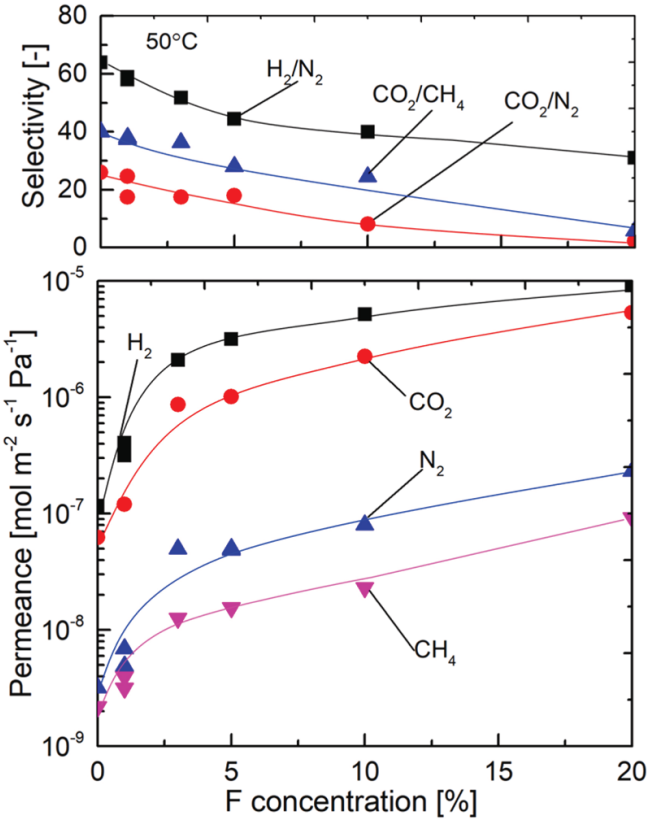

Fig. 2-6. Gas permeance and permeance ratio at 50 ºC as a function of fluorine concentration for fluorine-doped and undoped silica membranes calcined at 350 ºC in an air atmosphere.

These results indicate that the presence of Si-F groups into a silica matrix form a loose network, which results in improved permeation properties. Several studies have reported the controllability of network pore size via fluorine incorporation, and it was thus emphasized that fluorine effectiveness is independent irrespective of the silica precursor. For example, study results reported by our group explain how fluorine effectively controls the network pore sizes for both pure silica (SiO_2) and bridged-type organosilica structures 1,2-bis (triethoxysilyl) methane (BTESM, Si-CH_2-Si) and 1,2-bis (triethoxysilyl) propane (BTESP, Si-C_3H_6-Si). F-doped bridged-type organosilica membranes show a loose network structure by comparison with F-SiO_2 membranes using the same doped-fluorine concentration due to the existence of a nonhydrolyzed organic chain [38,40,41].

Fig. 2-7 shows the temperature dependence (50-200 ºC) of He permeance for fluorine-doped silica membranes. The temperature dependence of He permeance was evaluated to discuss how fluorine impacts the silica network pore structure since most He permeates the network pores and is unaffected by the presence of pinholes.

The permeance of He for fluorine-doped silica membranes slightly increases as temperature increases, which suggests an activated diffusion mechanism, but the slope of temperature dependence was decreased as the doped-fluorine concentration increased. The permeance of He for fluorine-doped silica membranes (F/Si = 2/8) was somewhat independent of temperature. Permeance was increased with increases in the fluorine concentration, irrespective of temperature (50-200 ºC), which further demonstrated how significantly fluorine controls the network pore size of conventional silica (TEOS).

The activation energy of He permeation was calculated using equation (2-1) [42].

$$P = \frac{k_0}{\sqrt{MRT}} exp\left[-\frac{E_p}{RT}\right] \quad (2\text{-}1)$$

In equation (2-1), P is the gas permeance k_0 is the permeation constant, M is the molecular weight of gas [kg mol^{-1}], R is the gas constant [J mol^{-1} K^{-1}], T is the absolute temperature [K], and E_p is the activation energy of permeation [kJ mol^{-1}].

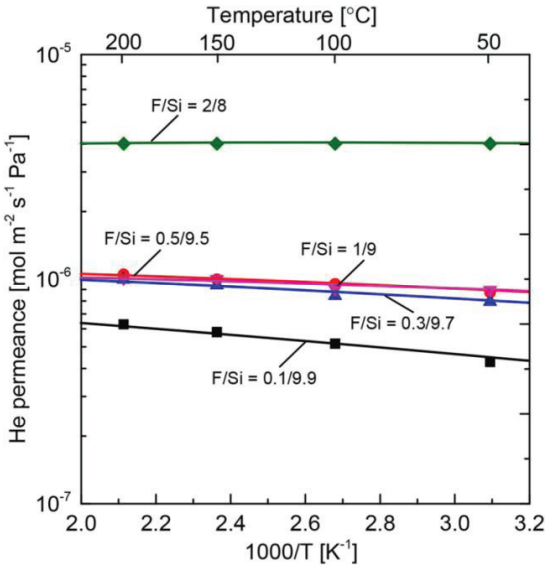

Fig. 2-7. Temperature dependence of He permeance at 50-200 ºC for fluorine-doped silica membranes calcined at 350 ºC in an air atmosphere.

Table 2-1 summarizes the activation energy of He permeation (E_p (He)) for F-SiO_2 membranes with different amount of incorporated fluorine. A decreased E_p (He) was observed as the amount of incorporated fluorine was increased, indicating that molecules can permeate micropores with less resistance due to the enlargement of pores in a network. The activation energy for He permeation in amorphous SiO_2 membranes is approximately

~10 kJ mol^{-1}, depending on the calcination temperatures [24,29,43]. This value of activation energy is clearly larger than that of F-SiO_2 membranes, which is consistent with the enlargement of the network pore size via F doping.

Table 2-1. E_p (He) for F-SiO_2 membranes with different fluorine concentrations.

Membranes	E_P (He) kJ mol^{-1}
F/Si = 0.1/9.9	4.8
F/Si = 0.3/9.7	3.6
F/Si = 0.5/9.5	3.1
F/Si = 1/9	2.79
F/Si = 2/8	1.6

2.3.3. Evaluation of binary (CO_2/N_2) separation for fluorine-doped silica membranes

Fig. 2-8 shows the temperature dependence of CO_2 and N_2 permeance in single and binary separation for fluorine-doped silica membranes. In a single-permeation system, the permeance of CO_2 was increased with decreased temperature, which showed a surface-diffusion property. This trend was independent of the concentration of doped fluorine in SiO_2. It should be noted that CO_2 is an adsorptive gas, and the obtained trend suggests that adsorption played a crucial role in the CO_2 permeation properties. The permeance of N_2 for a fluorine-doped silica membrane (F/Si = 0.1/9.9) was slightly increased as the temperature

increased, showing an activated permeation mechanism. The permeance of N_2 for fluorine-doped silica membranes (F/Si = 0.3/9.7, 0.5/9.5) was somewhat independent of permeation temperature. Accordingly, the CO_2/N_2 permselectivity was slightly increased with decreased temperature, irrespective of the fluorine concentration.

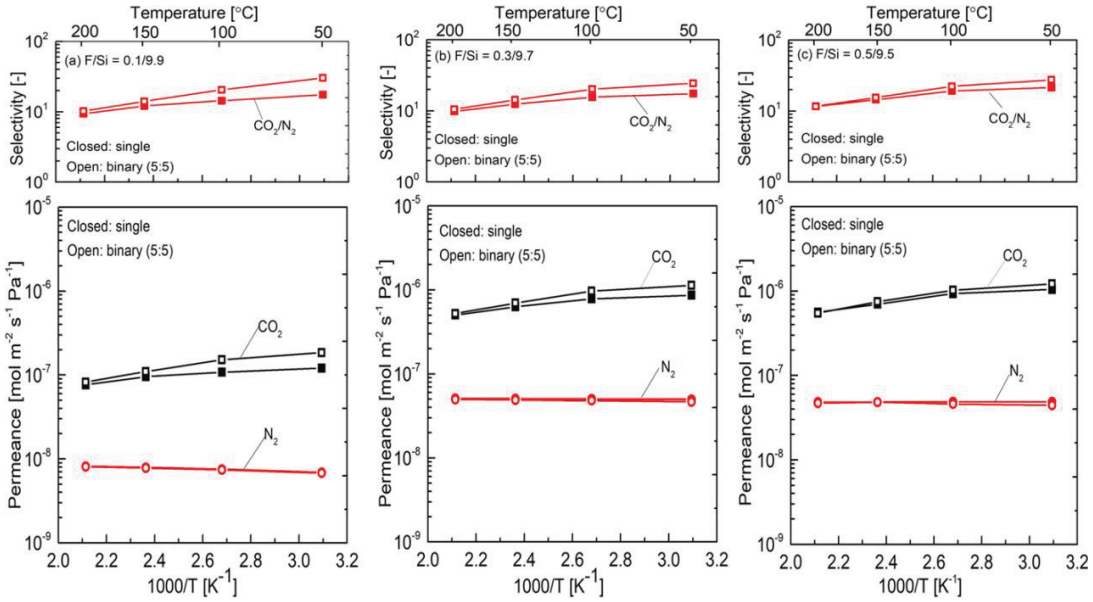

Fig. 2-8. Temperature-dependence of single and binary (CO_2/N_2 = 5/5) gas permeance at 50-200 ºC for fluorine-doped (F/Si = 0.1/9.9, 0.3/9.7, and 0.5/9.5) silica membranes calcined at 350 ºC in an air atmosphere.

In binary separation, all membranes showed a similar dependence on temperature with respect to CO_2 and N_2 permeance in a single permeation system. On the other hand, the deviation of CO_2 permeance between single permeation and binary separation was increased with decreased temperature, and this trend became more obvious in fluorine induced silica membranes (F/Si = 0.1/9.9) due to the increased CO_2 adsorptive effect, as

shown in Fig. 2-4b. For example, a fluorine-doped silica membrane (F/Si = 0.1/9.9) showed CO_2 permeance of 1.3 × 10^{-7} and 2.8 × 10^{-7} mol m^{-2} s^{-1} Pa^{-1} in single and binary separations at 50 ºC, respectively, and CO_2/N_2 selectivity in binary (5:5) separation was higher than that of single gas separation systems. It should be noted that there was no blocking of N_2 permeation by adsorbed CO_2 even at low temperature.

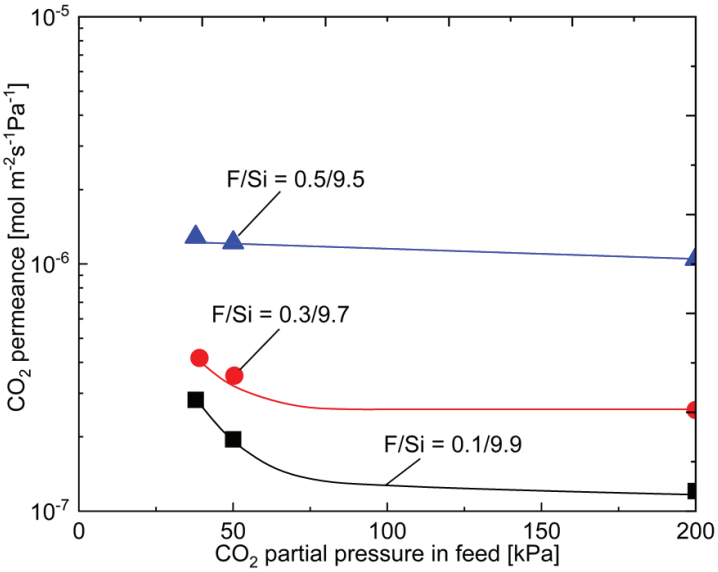

Fig. 2-9. Feed partial pressure dependence of CO_2 permeance at 50 ºC for fluorine-doped silica membranes (F/Si = 0.1/9.9, 0.3/9.7, 0.5/9.5) calcined at 350 ºC in an air atmosphere.

Fig. 2-9 shows the feed partial pressure dependence of CO_2 permeance at 50 ºC for fluorine-doped silica membranes (F/Si=0.1/9.9, 0.3/9.7, 0.5/9.5). The permeance of CO_2 increased as the feed partial pressure of CO_2 decreased in fluorine-doped silica membranes (F/Si=0.1/9.9, 0.3/ 9.7). On the contrary, the permeance of CO_2 in fluorine-induced silica membranes with F/Si = 0.5/9.5 was approximately independent of the partial pressure of

the CO_2 feed. These results suggested that the surface diffusion mechanism was more obvious with lower fluorine concentrations in SiO_2.

As shown in Fig. 2-4b, gels with a lower fluorine concentration (F/Si=0.1/9.9) showed reasonably higher CO_2 adsorption properties, which decreased as fluorine content increased from 0.3/9.7 to 0.5/9.5. That result demonstrated that hydrophobic fluorine apparently decreases the CO_2 adsorption properties of the silica surface as the fluorine concentration increases.

To further probe the CO_2 separation potential of fluorine-doped silica membranes, the relationship between the E_p of CO_2 and that of N_2 was calculated using equation (2-1). Fig. 2-10 shows the relationship between E_p (CO_2), E_p (N_2), and E_p (CO_2)-E_p (N_2) as a function of fluorine concentration. It should be noted that the apparent activation energy (activation energy of permeation), E_p, is the sum of the activation energy for diffusion and that of adsorption enthalpy ($E_p = E_d + \Delta H_{ad}$). The E_p of N_2 could be considered approximately equal to E_d, depending on the pore size of the permeating path and the molecular size, since N_2 has fewer adsorption properties [1]. The activation energy of N_2 permeation was clearly decreased with an increase in the fluorine concentration, which indicates a loose network formation for F-doped silica membranes.

The activation energy of CO_2 permeation was decreased from that of pure SiO_2 (0 mol%) with a 5 mol% concentration of fluorine but was slightly increased at higher fluorine concentrations. Here, if we assume the molecular size of CO_2 (0.33 nm) approximates that of N_2 (0.364 nm), the activation energy for the diffusion for both CO_2 and N_2 could be

assumed to be similar (E_d (CO_2) ≈ E_d (N_2)). Thus, the E_p (CO_2) – E_p (N_2) could be considered an expression of the adsorption enthalpy of CO_2 [1, 42], which indicates the CO_2 adsorption strength of membranes with different fluorine concentrations. E_p (CO_2) − E_p (N_2) was clearly increased with increases in the fluorine concentration, which indicated a small affinity for an increase in F-doping. Thus, we concluded that fluorine doping could be used to precisely enlarge the network pore size in a subnano range by reducing the concentration of Si-OH in the network structure. CO_2 adsorption was decreased with increases in the doping concentration of fluorine.

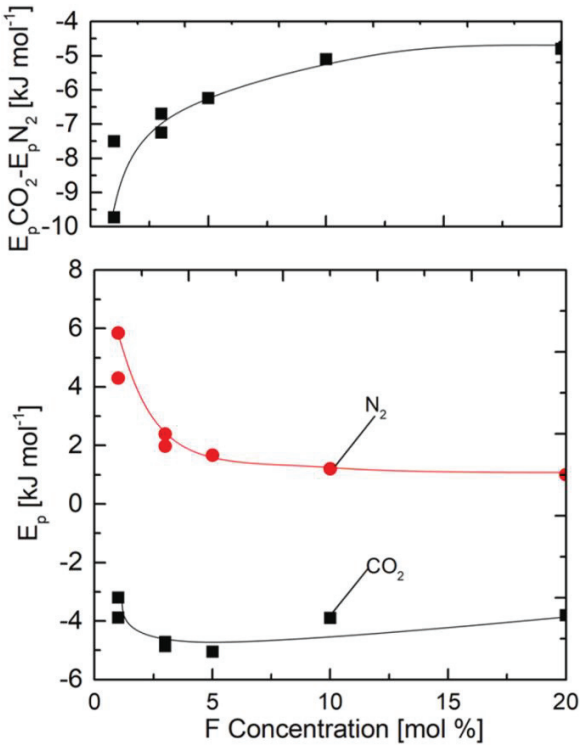

Fig. 2-10. Relationship between E_p (CO_2), E_p (N_2), and E_p (CO_2) − E_p (N_2) as a function of fluorine concentration.

Fig. 2-11 depicts the CO_2/N_2 selectivity at 50 ºC against CO_2 permeance for various fluorine concentrations of silica membranes. In the single-gas system (closed symbols), a conventional silica membrane exhibits a dense network structure with a lower CO_2 permeance of 6.2×10^{-8} mol m^{-2} s^{-1} Pa^{-1} and a moderate selectivity of 26.

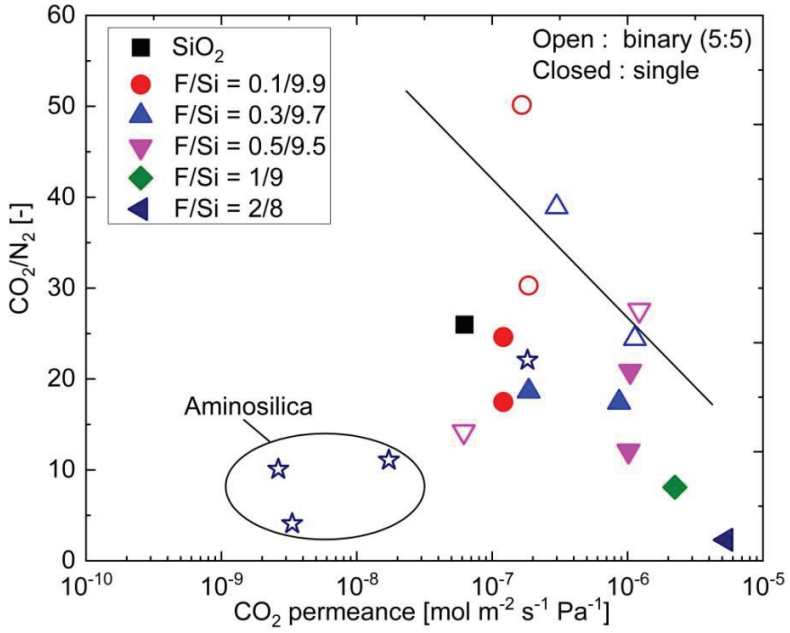

Fig. 2-11. CO_2/N_2 permeance ratio at 50 ºC as a function of CO_2 permeance in binary (CO_2/N_2 = 5/5) and single-permeation systems for pure silica and fluorine-doped (F/Si = 0.1/9.9, 0.3/9.7, 0.5/9.5, 1/9, 2/8) silica membranes calcined at 350 ºC under an air atmosphere. * The data of amine-contained SiO_2 membranes were taken from the reference [42].

Conversely, fluorine doping induced silica membranes to display a loose network structure with improved CO_2 permeance. In a binary system, on the other hand, membranes with an F/Si ratio of 0.1/9.9 showed a higher permeance ratio of 50 with CO_2 permeance of

1.6×10^{-7} mol m^{-2} s^{-1} Pa^{-1}. This could be associated with the fluorine-doped control of CO_2 permeation/adsorption properties. Since CO_2 is an adsorptive gas, this adsorptive effect was increased with decreases in the fluorine concentration, which resulted in improved selectivity. Thus, the simultaneous control of molecular sieving and adsorption properties could be a strategy to achieve high CO_2 selectivity with high CO_2 permeance.

2.3.4. Evaluating the hydrothermal stability of fluorine-doped SiO_2 membranes under steam conditions

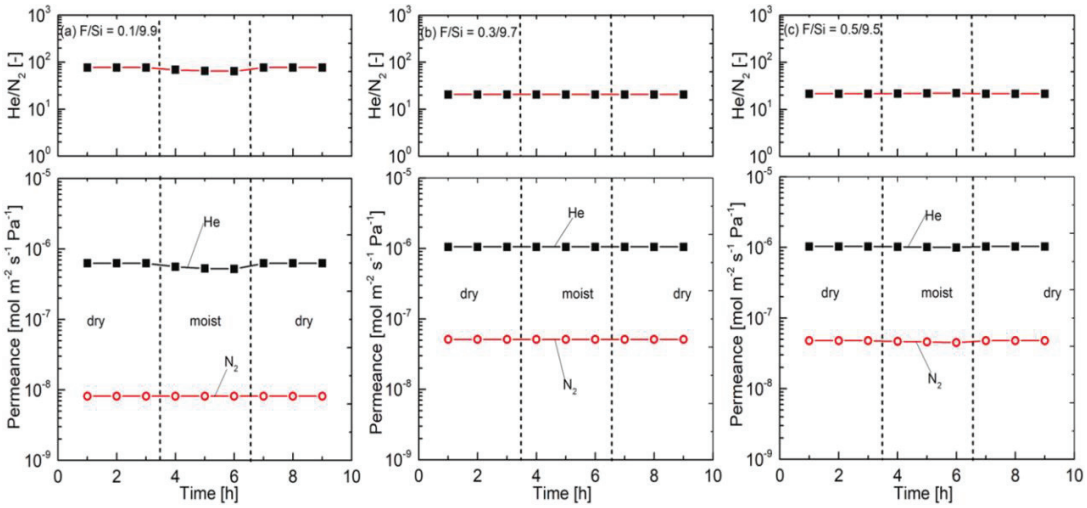

Fig. 2-12. Time course of He and N_2 permanence under both dry and wet (H_2O partial pressure: 3 kPa) systems at 200 ºC for F-SiO_2 membranes calcined at 350 ºC in an air atmosphere.

Hydrothermal stability for fluorine-doped silica membranes was evaluated by measuring the time courses of He and N_2 permeance in both dry and wet systems (H_2O partial pressure: 3 kPa). Fig. 2-12 shows the time courses of He and N_2 permanence under both dry

and wet atmospheres at 200 ºC for F-SiO_2 membranes. There were no changes in He and N_2 permeance, irrespective of fluorine concentration, neither before nor after exposure to a wet system. In addition, the values of permeance for He and N_2 in a wet system were similar to those in a dry system, and permeation blocking by adsorbed water molecules was not confirmed in these membranes.

Fig. 2-13 shows the molecular size dependence of single-gas permeance at 300 ºC for fluorine-doped silica membranes calcined at 350 ºC before/after steam treatment (300 ºC, H_2O partial pressure: 30 kPa) for 1 h. In steam with a low level of partial pressure (H_2O partial pressure: 3 kPa), a F-SiO_2 (F/Si = 0.1/9.9) membrane showed stable performance, as shown in Fig. 2-13a**.** Under steam with a high level of partial pressure, however, a F-SiO_2 membrane with the same makeup (F/Si = 0.1/9.9) showed drastic decreases in permeance, particularly for He and H_2. For example, the permeance of He was decreased by 20% of the initial value after an exposure of only 1h to steam with a high level of partial pressure.

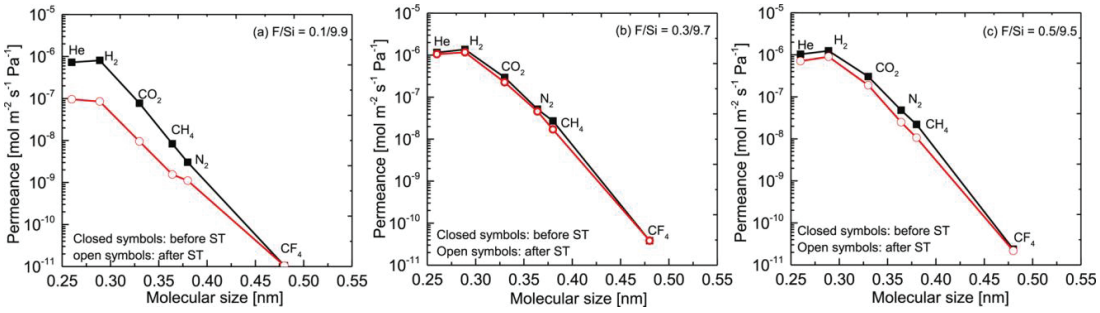

Fig. 2-13. Molecular size dependence for F-SiO_2 membranes (F/Si = 0.1/9.9, 0.3/9.7, 0.5/9.5) before/after steam treatment (300 ºC, partial pressure of steam: 30 kPa, 1h).

That significant decrease in permeance was probably caused by doping with a very low concentration of fluorine (F/Si = 0.1/9.9), which increased the frequency of interactions of the Si-OH rich silica structure with water vapor by increasing the silanol density and network rearrangements. On the contrary, when the fluorine content was increased, the hydrothermal stability was increased accordingly and both membranes (F/Si = 0.3/9.7 & 0.5/9.5) showed steady values of gas permeance under both dry and wet systems. Thus, the membrane performance evaluation in a wet system apparently depends on the hydrophobicity/hydrophilicity properties of the silica network structure.

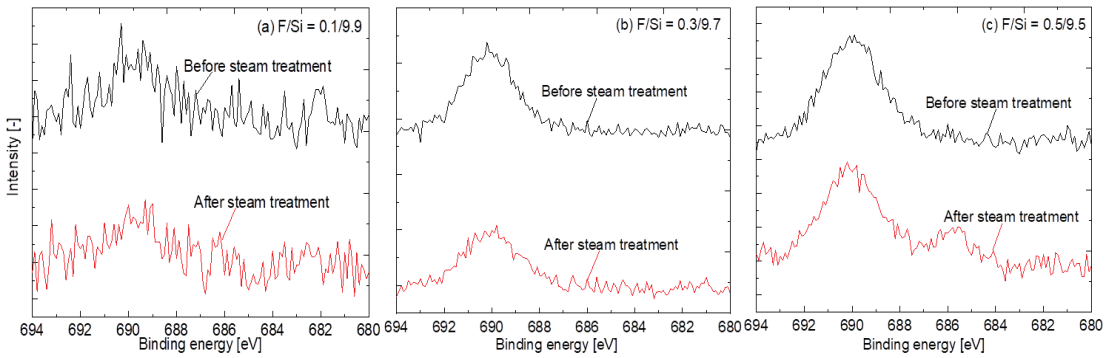

Fig. 2-14. F 1s peaks narrow spectra ranging from 680-694 eV before/after steam treatment (300 °C, partial pressure of steam: 30 kPa) for fluorine-doped (F/Si = 0.1/9.9, 0.3/9.7, 0.5/9.5) silica gels calcined at 350 ºC under an air atmosphere.

Fig. 2-14 shows the magnified F 1s spectra ranging from 680 to 694 eV for fluorine-containing silica gels. The results were obtained before/after steam treatment (300 ºC, steam partial pressure: 30 kPa, 1 h) for all fluorine-containing silica gels. An F 1s peak at around 688 eV was detected in all samples irrespective of the fluorine concentration;

however, in gels with F/Si ratios of 0.1/9.9, the physical appearance of the peak intensity was decreased due to the low amount of fluorine incorporated into the silica structure.

Table 2-2 summarizes the F/Si ratios for F-doped silica gels before/after steam treatment. It should be noted that the calculated F/Si ratios were approximately the same as those of the concentrations of doped fluorine. After steam treatment, the F/Si ratio was decreased, irrespective of fluorine concentration. The decreased fluorine concentration could be a result of the reaction between Si-F and water vapor during steam treatment [29, 44].

Table 2-2. Fluorine concentration before/after steam treatment for F-SiO_2 gels calcined at 350 ºC under an air atmosphere.

	Before ST	After ST
F/Si = 0.1/9.9	1.24/98.74	0.8/99.2
F/Si = 0.3/9.7	3.06/96.94	2.49/97.51
F/Si = 0.5/9.5	5.27/94.73	3.52/96.48

Fig. 2-15 shows the N_2 adsorption isotherms for fluorine-doped silica gels calcined at 350 ºC before/after steam treatment (300 ºC, steam partial pressure: 30 kPa, 1h). Both samples demonstrated type I isotherms with large levels of N_2 uptake under a low level of relative pressure, which indicates the microporous structure of gels. Table 2-3 summarizes the BET surface area and micropore volume for these samples. The adsorption properties increased with increases in the fluorine concentration, which demonstrates a strong dependency on the amount of fluorine incorporated into the silica matrix.

Following exposure to a steam atmosphere the gels showed similar results for the sample (F/Si = 0.3/9.7) shown in Table 2-3. On the contrary, the sample with a small amount of fluorine (0.1/9.9) underwent densification and exhibited decreases in the surface area and in the micropore volume, which demonstrated that the network structure was less resistive to water vapor and interacted with wet molecules, which resulted in the generation of Si-OH density and a subsequent promotion of condensation/densification. It should be noted that a similar trend was confirmed in the pore-size distribution of F-SiO_2 (F/Si = 0.1/9.9, 0.3/9.7) based on N_2 adsorption/desorption isotherms before/after steam treatment as shown in Fig 2-15.

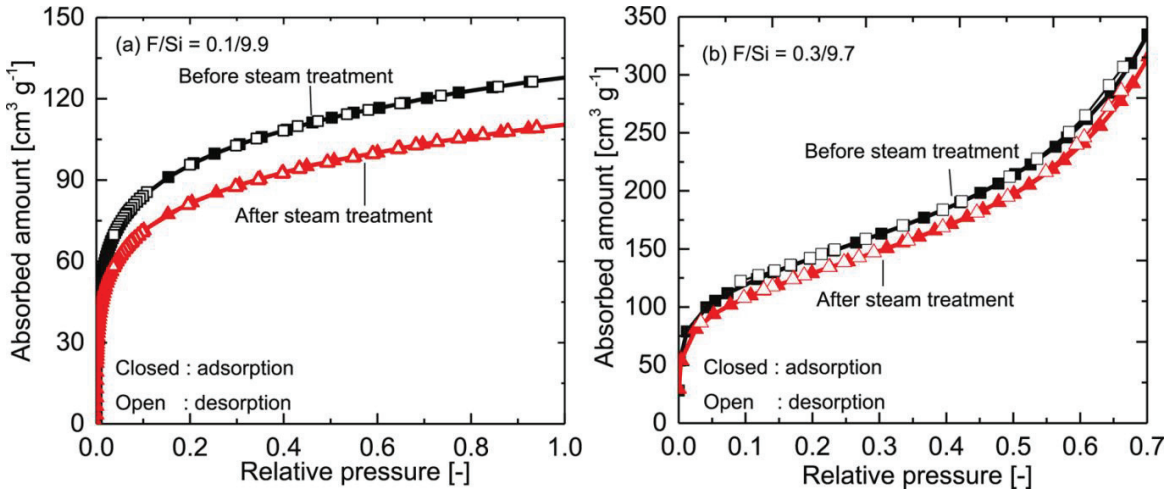

Fig. 2-15. N_2 adsorption isotherms at 77 K before/after steam treatment (300 ^{o}C, partial pressure of steam: 30 kPa, 1 h) for fluorine-doped (F/Si = 0.1/9.9, 0.3/9.7) silica gels calcined at 350 ºC in an air atmosphere.

Table 2-3. BET surface area and micropore volume of F-SiO_2 gels calcined at 350 ºC under an air atmosphere.

	S_{BET} surface area ($m^2.g^{-1}$)	Pore volume
F/Si = 0.1/9.9		
Before ST	335	0.23
After ST	285	0.20
F/Si = 0.3/9.7		
Before ST	512	0.59
After ST	462	0.55

Fig. 2-16 features the schematic images of the network pore structures of fluorine-doped silica membranes and the effect that steam treatment exerts on the network pore structure. It is evident that hydrothermal stability involves several factors such as membrane pore size, steam partial pressure, temperature, and exposure time [29]. Although fluorine tremendously improved the hydrothermal stability as reported in various studies [29, 38], results in the present study indicate that network stability is significantly affected by the amount of incorporated fluorine. For example, the network structure created by an F/Si ratio of 0.1/9.9 possesses a high level of silanol density and a smaller network pore size than networks doped with a higher concentration of fluorine. After steam exposure, Si-F

groups interacted with water vapor and the original concentration of Si-OH along with regenerated silanol groups resulted in network densification. On the contrary, network pore structures with a higher fluorine concentration showed less condensation/densification due to reduced silanol density, which resulted in improved hydrothermal stability.

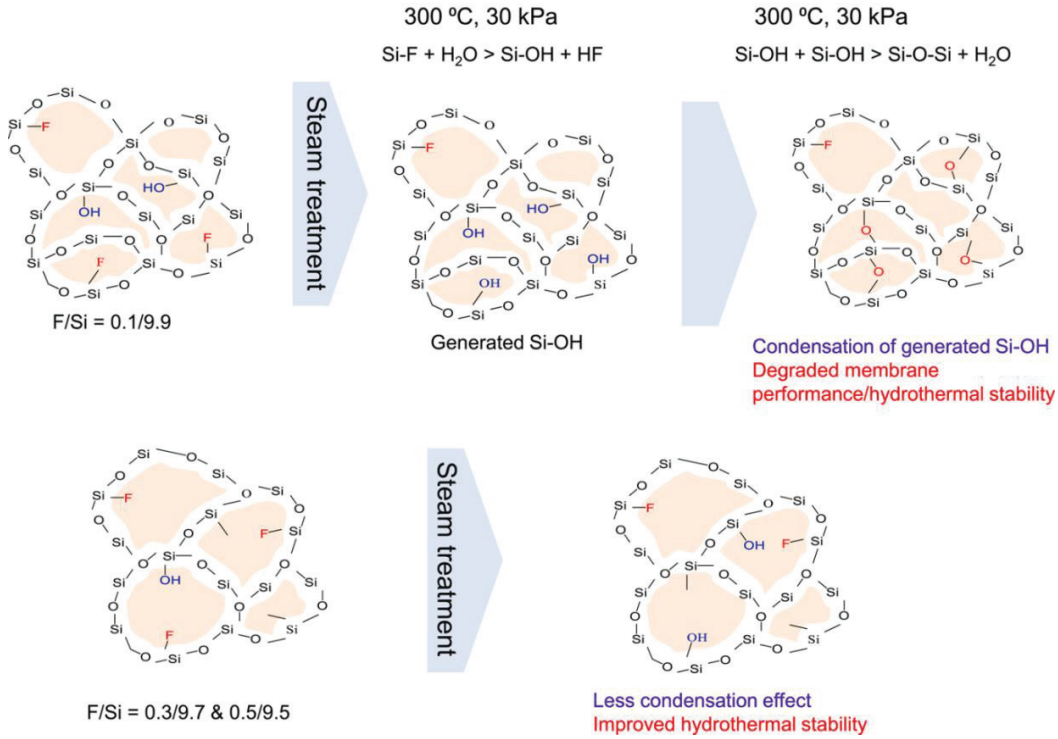

Fig. 2-16. Schematic illustration for F-SiO_2 network structures before/after steam treatment (30 kPa).

2.4. Conclusions

A strategy was proposed to control the network pore structure of conventional silica via fluorine doping to fabricate highly permeable membranes for CO_2 separation. Various fluorine concentrations (F/Si=0.1/9.9, 0.3/9.7, 0.5/9.5, 1/9, 2/8) were doped via a sol-gel

method to allow examination of the effect that fluorine exerts on a silica network structure. Physicochemical analysis revealed that fluorine effectively improved the hydrophobic/hydrophilic properties by eliminating the factors (Si-OH) involved in the formation of a dense silica structure.

Fluorine-doped silica membranes fabricated with different concentrations of fluorine showed consistent results according to structural characterization. For example, an F/Si ratio of 0.5/9.5 showed a loose network structure by comparison with smaller fluorine content (F/Si=0.1/9.9). Fluorine doping precisely enlarges the network pore size in a sub-nano range. Due to a reduction in Si-OH in a network structure, however, CO_2 adsorption is decreased as the concentration of doped fluorine increases. A fluorine-doped silica membrane with an F/Si ratio of 0.1/9.9 showed the highest permeance ratio of 50 with CO_2 permeance of 1.6×10^{-7} mol m^{-2} s^{-1} Pa^{-1} at 50 ºC.

In a wet system (200-300 ^{o}C, H_2O partial pressure: 3 kPa), fluorine-doped silica membranes were quite stable, irrespective of the concentration of the doped fluorine. Under steam with a high level of partial pressure (300 ^{o}C, H_2O partial pressure: 30 kPa), the concentration of doped fluorine strongly affected the hydrothermal stability. The F-SiO_2 membrane with an F/Si ratio of 0.1/9.9 showed drastic decreases for all examples of permeance. On the contrary, when fluorine content was increased, it was apparent that the change in pore size distribution accordingly suppressed the hydrothermal stability and the membranes with F/Si ratios of 0.3/9.7 & 0.5/9.5 showed steady values for gas permeance in both dry and wet systems.

References

1. L. Yu, M. Kanezashi, H. Nagasawa, J. Oshita, A. Naka, T. Tsuru, Pyrimidine-bridged organoalkoxysilane membrane for high-efficiency CO_2 transport via mild affinity. Sep. Purif. Technol. 178 (2017) 232-241.

2. A. M. W. Hillock, W. J. Koros, Cross-linkable polyimide membrane for natural gas purification and carbon dioxide plasticization reduction. Macro. 40 (2007) 583-587.

3. A. Car, C. Stropnik, W. Yave, K. V. Peinemann, Tailor-made polymeric membranes based on segmented block copolymers for CO_2 separation. Adv. Fun. Mater. 18 (2008) 2815-2823.

4. T. S. Chung, L.Y. Jiang, Y. Li, S. Kulprathipanja, Mixed matrix membranes (MMMs) comprising organic polymers with dispersed inorganic fillers for gas separation. Prog. Poly. Sci. 32 (2007) 483-507.

5. D. L. Gin, R. D. Noble, Designing the next generation of chemical separation membranes. Sci. 332 (2011) 674-676.

6. W. He, Z. Wang, W. Li, S. Li, Z. Bai, J. Wang, S. Wang, Cyclic tertiary amino group containing fixed carrier membranes for CO_2 separation. J. Membr. Sci. 476 (2015) 171-181.

7. H. Lin, B. D. Freeman, Materials selection guidelines for membranes that remove CO_2 from gas mixtures. J. Mol. Struc. 739 (2005) 57-74.

8. M. Ostwal, R. P. Singh, S. F. Dec, M. T. Lusk, J. D. Way, 3-aminopropyltriethoxysilane functionalized inorganic membranes for high temperature CO_2/N_2 separation. J. Membr. Sci. 369 (2011) 139-147.

9. D. E. Gottschlich, D. L. Roberts, G. J. Wijmans, C. M. Bell, R. W. Baker, Economic comparison of several membrane configurations for H_2/N_2 separation. Gas Sep. Purif. 3 (1989) 170-179.

10. W. Jiao, Y. Ban, Z. Shi, X. Jiang, Y. Li, W. Yang, Gas separation performance of supported carbon molecular sieve membranes based on soluble polybenzimidazole. J. Membr. Sci. 533 (2017) 1-10.

11. L. Yu, M. Grahn, P. Ye, J. Hedlund, Ultra-thin MFI membranes for olefin/nitrogen separation. J. Membr. Sci. 524 (2017) 428-435.

12. Y. Kuwahara, Y. Kamegawa, K. Mori, H. Yamashita, Fabrication of hydrophobic zeolites using triethoxyfluorosilane and their application as supports for TiO_2 photocatalysts. Chem. Comm. 39 (2008) 4783-4785.

13. H. P. Li, X. P. Shen, K. Han, G. Tang, Z. H. Zhang, Quantum chemistry study on the third-order nonlinear optical properties of spirobifluorene derivatives. Comp. The. Chem. 1023 (2013) 95-98.

14. Y. Peng, Y. Li, Y. Ban, H. Jin, W. Jiao, X. Liu, W. Yang, Metal-organic framework nanosheets as building blocks for molecular sieving membranes. Sci. 346 (2014) 1356-1359.

15. S. Chai, H. Du, Y. Zhao, Y. Lin, C. Kong, L. Chen, Fabrication of highly selective organosilica membrane for gas separation by mixing bis (triethoxysilyl) ethane with methyltriethoxysilane. Sep. Purif. Technol. 222 (2019) 162-167.

16. R. M. De Vos, W. F. Maier, H. Verweij, Hydrophobic silica membranes for gas separation. J. Membr. Sci. 158 (1999) 277-288.

17. J. Campaniello, C. W. Engelen, W. G. Haije, P. P. A. C. Pex, J. F. Vente, Long-term pervaporation performance of microporous methylated silica membranes. Chem. Comm. (2004) 834-835.

18. X. Ren, K. Nishimoto, M. Kanezashi, H. Nagasawa, T. Yoshioka, T. Tsuru, CO_2 permeation through hybrid organosilica membranes in the presence of water vapor. Ind. Eng. Chem. Res. 53 (2014) 6113-6120.

19. M. Kanezashi, T. Matsutani, T. Wakihara, H. Tawarayama, H. Nagasawa, T. Yoshioka, T. Tsuru, Tailoring the subnano silica structure via fluorine doping for development of highly permeable CO_2 separation membranes. ChemNanoMat. 2 (2016) 264-267.

20. X. Yu, H. Nagasawa, M. Kanezashi, T. Tsuru, Improved thermal and oxidation stability of bis (triethoxysilyl) ethane (BTESE)-derived membranes, and their gas-permeation properties. J. Mater. Chem. A 6 (2018) 23378-23387.

21. Y. S. Lin, I. Kumakiri, B. N. Nair, H. Alsyouri, Microporous inorganic membranes, Sep. Purif. Methods. 31 (2002) 229-379.

22. N. W. Ockwig, T. M. Nenoff, Membranes for hydrogen separation, Chem. Rev. 107 (2007) 4078-4110.

23. J. Dong, Y. S. Lin, M. Kanezashi, Z. Tang, Microporous inorganic membranes for high temperature hydrogen purification, J. Appl. Phys. 104 (2008) 121301-121317.

24. M. Kanezashi, Y. Yoneda, H. Nagasawa, T. Tsuru, Gas permeation properties for organosilica membranes with different Si/C ratios and evaluation of microporous structures. AIChE J. 63 (2017) 4491-4498.

25. N. Moriyama, H. Nagasawa, M. Kanezashi, T. Tsuru, Selective water vapor permeation from steam/non-condensable gas mixtures via organosilica membranes at moderate-to-high temperatures. J. Membr. Sci. 589 (2019) 117254.

26. H. L. Castricum, A. sah, R. Kreiter, D. H. A. Blank, J. F. Vente, J. E. ten Elshof, Hydrothermally stable molecular separation membranes from organically linked silica. J. Mater. Chem.18 (2008) 2150-2158.

27. R. Igi, T. Yoshioka, Y.H. Ikuhara, Y. Iwamoto, T. Tsuru, Characterization of Co doped silica for improved hydrothermal stability and application to hydrogen separation membranes at high temperatures. J. Am. Ceram. Soc. 91 (2008) 2975-2981.

28. M. Kanezashi, M. Asaeda, Stability of H_2-permselective Ni-doped silica membranes in steam at high temperature. J. Chem. Eng. J. 38 (2005) 908-912.

29. M. Kanezashi, N. Hataoka, I. Rana, H. Nagasawa, T. Tsuru, Hydrothermal stability of fluorine-induced microporous silica membranes: Effect of steam treatment conditions. AIChE J. 67 (2021) e 17292.

30. Q. Wei, F. Wang, Z.R. Nie, C.L. Song, Y.L. Wang, Q.Y. Li, Highly hydrothermally stable microporous silica membranes for hydrogen separation. J. Phys. Chem. B. 112 (2008) 9354-9359.

31. A. Darmawan, J. Motuzas, S. Smart, A. Julbe, J.C.D. da Costa, Binary iron cobalt oxide silica membrane for gas separation. J. Membr. Sci. 474 (2015) 32-38.

32. J. Yang, W. Fan, C.M. Bell, Effect of calcination atmosphere on microstructure and H_2/CO_2 separation of palladium-doped silica membranes. Sep. Purif. Technol. 210 (2010) 659-669.

33. H. Song, S. Zhao, J. Lei, C. Wang, H. Qi, Pd-doped organosilica membrane with enhanced gas permeability and hydrothermal stability for gas separation. J. Mater Sci. 51 (2016) 6275-6286.

34. D. L. Martens, J. Motuzas, S. Smart, J. C. Diniz da Costa, Structural investigation of cobalt oxide seeded silica xerogels under harsh hydrothermal condition. J. Sol-Gel Sci. Technol. 98 (2021) 470-477.

35. S. Smart, J. F. Vente, J. D. Da Costa, High temperature H_2/CO_2 separation using cobalt oxide silica membranes. Int. J. Hyd. Ener. 37 (2012) 12700-12707.

36. E. S. Mirza, B. Topuz, Nanoscale tailoring on thin bimetallic organo-oxide membranes for H_2/CO_2 separation. Sep. Purif. Technol. 280 (2022) 119801.

37. H. Qi, J. Han, N. Xu, Effect of calcination temperature on carbon dioxide separation properties of a novel microporous hybrid silica membrane. J. Membr. Sci. 382 (2011) 231-237.

38. I. Rana, H. Nagasawa, K. Yamamoto, T. Gunji, T. Tsuru, M. Kanezashi, Effect of fluorine doping on the network pore structure of non-porous organosilica bis (triethoxysilyl) propane (BTESP) membranes for use in molecular separation. J. Membr. Sci. (2021) 120083.

39. Y. H. Kim, M. S. Hwang, H. J. Kim, Infrared spectroscopy study of low-dielectric constant fluorine-incorporated and carbon-incorporated silicon oxide films. J. of App. Phy. 90 (2001) 3367-3370.

40. M. Kanezashi, M. Murata, H. Nagasawa, T. Tsuru, Fluorine doping of microporous organosilica membranes for pore size control and enhanced hydrophobic properties. ACS Omega 3 (2018) 8612-8620.

41. M. Takenaka, H. Nagasawa, T. Tsuru, M. Kanezashi, Hydrocarbon permeation properties through microporous fluorine-doped organosilica membranes with controlled pore sizes. J. Membr. Sci. 619 (2021) 118787.

42. L. Yu, M. Kanezashi, H. Nagasawa, J. Ohshita, A. Naka, T. Tsuru. Fabrication and microstructure tuning of a pyrimidine-bridged organoalkoxysilane membrane for CO_2 separation. Ind. Eng. Chem. Res. 56 (2017) 1316-1326.

43. M. Kanezashi, T. Sasaki, H. Tawarayama, H. Nagasawa, T. Yoshioka, K. Ito, T. Tsuru, Experimental and theoretical study on small gas permeation properties through amorphous silica membranes fabricated at different temperatures. J. Phys. Chem. C. 118 (2014) 20323-20331.

44. M. Kanezashi, T. Matsutani, H. Nagasawa, T. Tsuru, Fluorine-induced microporous silica membranes: Dramatic improvement in hydrothermal stability and pore size controllability for highly permeable propylene/propane separation. J. Membr. Sci. 549 (2018) 111-119.

Chapter 3

The effect of C/Si ratio and fluorine doping on the gas permeation properties of pendent-type and bridged-type organosilica membranes

3.1. Introduction

The separation of various gaseous molecules from industrial/natural waste has become a crucial issue, and inherent attractive characteristics such as low energy consumption and cost effectiveness have made membrane science the most promising approach to separation by comparison with cryogenic distillation or liquid/solid adsorption [1-3]. Various membrane materials (SiO_2, TiO_2, ZrO_2, Zeolite, etc.) have been introduced to develop the microporous thin layers required for different separation applications/systems [4-9]. Among all these materials, amorphous silica (average pore size: 0.34 nm) is considered the potential candidate with the higher chemical and thermal stability [10]. In the early 1990s, chemical vapor deposition (CVD) and sol-gel methods were employed to fabricate amorphous silica molecular sieve membranes, and both of these processes produced main-chain siloxane (Si-O-Si) and terminal silanol (Si-OH) bonding [11-16]. Silica-derived network structures appeared to be smaller (0.34 nm) and were applicable only to helium (He) and hydrogen (H_2) separation systems, but this type of structure was inappropriate when applied to molecules larger (CO_2: 0.33 nm and N_2: 0.36 nm) than helium (He: 0.26 nm) or hydrogen (H_2: 0.28 nm). Another drawback associated with traditional silica (TEOS) is its structural destabilization under humid conditions wherein H_2O molecules

interact with membrane surfaces, and consequently, silica network structures undergo densification that results in a drastic decrease in membrane performance [17-18].

To overcome the issues of hydrothermal stability and network pore size tuning of conventional silica, various studies have utilized the incorporation of two commonly known organic molecules, pendant-type alkoxysilane and organic bridged-type alkoxysilane, into inorganic silica (SiO_2) to fabricate sol-gel derived silica membranes with excellent molecular sieve properties and excellent hydrothermal stability. In general, a typical bridged-type alkoxysilane structure contains organic functional groups between two Si atoms (Si-R-Si, R is the functional group) such as 1,2-bis(triethoxysilyl) methane (BTESM, Si-C_1-Si), 1,2-bis(triethoxysilyl) ethane (BTESE, Si-C_2-Si), and bis(triethoxysilyl) propane (BTESP, Si-C_3-Si), while a pendant-type alkoxysilane network structure consists of organic functional groups directly bonded to the Si atom (R-Si-$O_{1.5}$): methyltriethoxysilane (MTES), phenyltriethoxysilane (PhTES), (trifluoropropyl)triethoxysilane (TFPTES), and ethylenetriethoxysilane (ETES).

To control the network stability and permeation properties of microporous organosilica (pendant- and bridged-type) membranes, two commonly used “spacer” and “template” methods were employed via an adjustment of the organic chain between two Si atoms (Si-R-Si) and/or the terminal organic (O-Si-R) chain [19,20]. Kanezashi et al. [21] reported a series of organosilica network structures consisting of various carbon numbers (C_1-C_8) and concluded that the network pore size regressed using the modified gas-translation model (mG-T), enlarged by an increase in the carbon number between two Si atoms. Despite the

enlarged pore sizes of some organosilica structures such as BTESP, bis(trimethoxysilyl)hexane (BTMSH), and bis(triethoxysilyl)octane (BTESO), the permeation properties were not as high as membranes with shorter organic linking units (BTESM, BTESE). Since the increased carbon numbers between two Si atoms occupied enough pore channel space via increased flexibility of a long chain to block the permeation of molecules, these membranes showed a low permeance. In a similar manner, membrane fabricated using pendant-type alkoxysilane, has demonstrated excellent water flux (4 kg m^2 h^{-1}) and stability over the time period of 18 months. The incorporation of -CH_3 groups into the silica matrix (SiO_2) improved the stability of siloxane bonds and reduced the number of hydroxyl groups (OH) [22]. However, microporous analysis of as-prepared pendant-type organosilica network structures demonstrated an inaccessibility to gas (N_2) due to an aggregation of pendant chains in silica pores, which resulted in a blocking effect [23]. Therefore, pore size controllability has remained elusive since the flexibility of the organic chains in a bridged-type organosilica network structure has proven ineffective for membrane fabrication. Similarly, increasing microporosity of pendant-type network structures through the decomposition of organic groups leads to the formation of additional pores [24].

To resolve these drawbacks (network pore size tuning and stability) associated with the conventional silica (TEOS) as well as the organosilica network structures (Si-R-Si), our group proposed an innovative strategy to tune the network pore size by introducing fluoride ions (ammonium fluoride (NH_4F) into the conventional silica and organosilica matrix. Fluorine-induced membranes have exhibited excellent hydrothermal stability and improved

permeation properties. Kanezashi et al. reported the effect of fluorine on conventional silica (TEOS) and bridged organosilica (BTESM) membranes and both membranes showed enlarged network pore size that was affected by Si-F and C-F bonds [25,26]. Fluorine-doped long-chain organosilica membranes with flexible organic linking units (BTESP, Si-C_3-Si) have demonstrated an enlarged pore size with permeation properties (H_2 permeance; 10^{-6} mol m^{-2} s^{-1} Pa^{-1}) that are at least one order of magnitude higher than those of undoped BTESP membranes (10^{-7} mol m^{-2} s^{-1} Pa^{-1}) [27]. To the best of our knowledge, no one has reported the effect of fluoride ions on pendant-type organosilica structures.

In the present study, we chose various mono-silicon pendant-type and bridged-type organosilica based on the carbon number adjacent to the Si atoms for fabrication of the organosilica membranes. Initially, we evaluated network pore sizes based on the gas permeation properties for all pendant groups (C_1-C_8). Next, we evaluated the effect of fluorine (NH_4F) doping on MTES and PTMS based on the gas permeation properties. The physiochemical properties of organosilica were examined via XRD, N_2 adsorption isotherms, and FT-IR. XPS measurement was conducted to observe the fluorine status of pendant-type organosilica structures.

3.2. Experimental section

3.2.1. F-doped and undoped sol-gel preparations

An organosilica sol was prepared via a process of hydrolysis/condensation using the sol-gel method [28-30] in an ethanol solution. It should be noted that, all chemicals were kindly supplied by TCI Co., Ltd. Tokyo, Japan. The reaction was catalyzed using nitric acid

(HNO_3) in the preparation of both fluorine-doped and undoped organosilica sols. After the addition of Si into an ethanol solution, the catalyst (HNO_3) and water (H_2O) were added dropwise with vigorous stirring at 500 r.p.m. to promote the hydrolysis/condensation at a reaction temperature of 25 ºC. The final molar composition of alkoxysilane/water/catalyst was maintained at 1/30/1, and ethanol (EtOH) was utilized to control the 0.5 wt% of Si. To prepare the fluorine-doped pendant/bridged organosilica sols, the fluorine concentration was fixed at 0-50 mol%. Simultaneously, the gels were prepared using a slow drying process at 40 ◦C under an air atmosphere, which was followed by grinding in a mortar. Gels were calcined at 300-350 ºC for structural characterization (XRD, N_2 adsorption, and XPS analysis).

3.2.2. Characterization of sol-gel

Organosilica sols were measured using a DLS analyzer (Zetasizer nano, ZEN3600, Malvern Co., Malvern, UK). A KBr plate was coated dropwise to obtain a measurement on the FT-IR spectrum (FT/IR-4100, JASCO, Tokyo, Japan) within a range of 400-4000 cm^{-1} to evaluate the functional groups in the organosilica network structure. X-Ray diffraction (D2 PHA-SER Bruker, Berlin, Germany) measurement was carried out to analyze the microstructure characteristics of xerogel powders for the organosilica network structures. N_2 adsorption measurements were conducted using a BELMAX (MicrotracBEL corp., Osaka, Japan). X-ray photoelectron spectroscopy (XPS, Shimadzu, Kyoto, Japan) was used to investigate the fluorine status in the organosilica network structure. To conduct the N_2 adsorption isotherms and XPS spectra, all samples were evacuated for 12 h at 200 ºC prior to starting the measurement.

3.2.3 Fabrication of organosilica membranes

Fluorine-doped and undoped pendant- and bridged-type organosilica membranes were fabricated using a porous alumina (porosity 50%, average pore size; 1μm, length; 100 mm, inner and outer diameter 8-10 mm, respectively) tube supplied by the Nikkato Corporation, Osaka, Japan. First, a porous tube was coated with large (2 μm) and small (0.2 μm) alumina particles diluted with a SiO_2-ZrO_2 sol followed by calcination at 550 ºC under an air atmosphere. Then an intermediate layer with an average pore size of 1-2 nm was coated with a SiO_2-ZrO_2 sol, diluted with distilled water to control the concentration (0.5-1 wt%), and calcined at 550 ºC. Finally, organosilica pendant- and bridged-type top separation layers were deposited onto the intermediate layers, which then were calcined at 300-350 ºC under a N_2 atmosphere.

3.2.4. Single-gas permeation measurement

Figure 2-1 depicts the experimental apparatus used for single-gas permeation measurements. Each gas (He (0.26 nm), H_2 (0.28 nm), CO_2 (0.33 nm), N_2 (0.36 nm), CH_4 (0.38 nm), CF_4 (0.48 nm), and SF_6 (0.55 nm)) with high purity was fed from the outer surface of the membrane at 200-400 kPa, and the permeate side was maintained at atmospheric pressure. In the present study, a high level of feed pressure (400 kPa) was applied to the permeation measurement of CF_4 and SF_6 molecules for accurate measurement due to the low permeation rate of these molecules. It should be noted that these molecules permeated by Knudsen diffusion, so that permeance was independent of feed pressure. Prior to evaluating the permeation measurements, each membrane was pre–

treated at 200 ºC under a N_2 flow for 8 h to remove the adsorbed water. Gas-permeation measurements were carried out at temperatures ranging from 50-200 ºC. It should be noted that the experimental deviations of less than 5% were recorded, and all membranes were fabricated 2-3 times to confirm reproducibility.

3.3. Results and discussion

3.3.1. Physicochemical properties of pendent-type organosilica

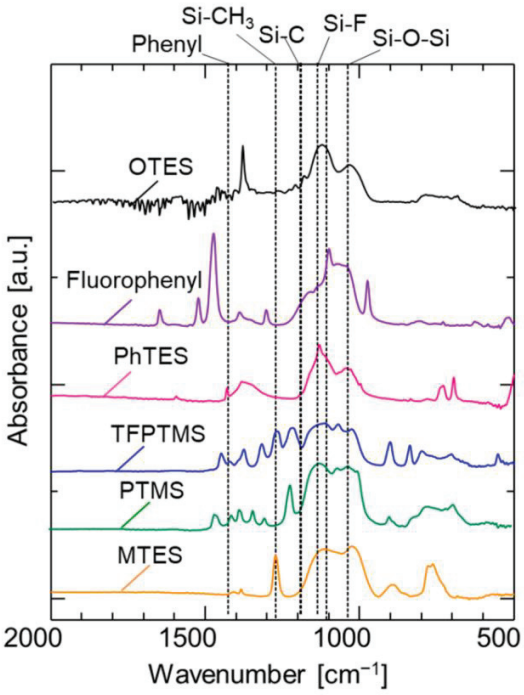

Fig. 3-1. FT-IR spectra of various pendant-type organosilica films calcined at 300 ºC under a N_2 atmosphere.

Figure 3-1 indicates the FT-IR spectra of various pendant-type organosilica structures coated onto a KBr plate and calcined at 300 ºC. The peaks at approximately 1050 cm^{-1} are

ascribed to the Si-O-Si bonds irrespective of the pendant-type organosilica structure, and show the completed hydrolysis/condensation reactions during sol-gel preparations [25,26]. Absorption peaks at approximately 1100-1200 cm^{-1} correspond to the Si-C bonds in the organosilica network structures. The absorption peak around 1280 cm^{-1} is associated with the Si-CH_3 groups and confirm the stability of the methyl groups following calcination at 300 ºC. Another peak corresponding to the phenyl group was observed around 1430 cm^{-1} in the PhTES sample [23]. The overall results demonstrate that the chosen calcination temperature is appropriate for membrane fabrication to avoid structural degradation.

Powder XRD analyses were performed on various pendant-type organosilica gels calcined at 300 ºC under a N_2 atmosphere to confirm the crystalline/microporous structure as shown in Fig. 3-2. The resulting diffraction patterns indicated a prominent broad peak at ~ 2θ = 20º, and this trend is independent of the pendant-type structure (C_1-C_8). This broad peak is attributed to the amorphous silica and is likely due to the main organosilica network chain. Meanwhile, the XRD patterns of all samples exhibited a sharp peak at ~ 2θ = 10º, which can be assigned to the well-ordered uniform network structure that could be associated with the pendant organic chain [31]. It should be noted that the peak shift to the slightly lower degree of 2θ = 20º could have been associated with variation in pore size, which will be discussed in the following sections.

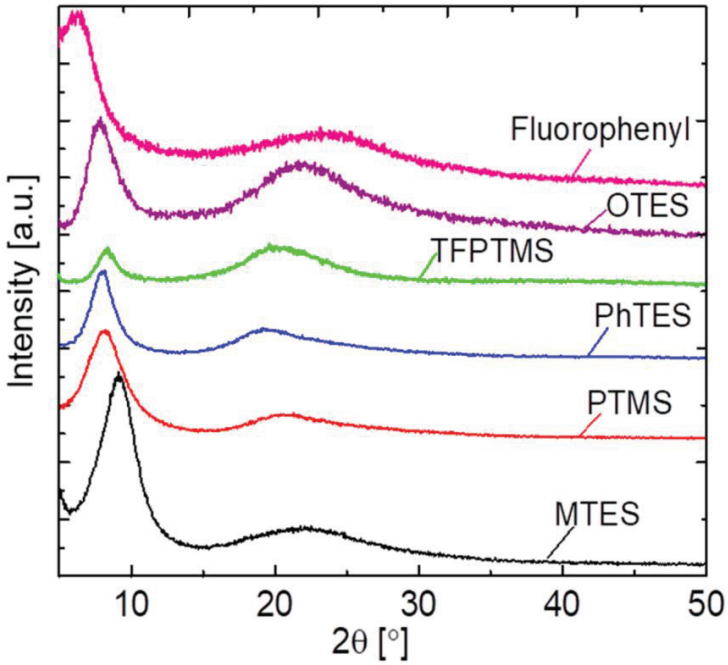

Fig. 3-2. XRD patterns of various pendent-type silica-derived gels calcined at 300 ºC under a N_2 atmosphere.

Fig. 3-3 illustrates the N_2 adsorption isotherms at 77 K of pendant-type organosilica gels calcined at 300 °C under a N_2 atmosphere. The pendant-type alkoxysilane showed a negligible amount of adsorbed N_2 irrespective of the carbon number (C_1-C_8), which indicates that pendant-type organosilica possess non-porous structures and a limited number of pores that are accessible to the adsorbed gas. The pendant-type organic chain present in the silica structure is thermally stable at the desired calcination temperature of 300 °C, which might be the reason for it not adsorbing a considerable amount of N_2. The pendant organic chains acted like barriers among the silica micropores by occupying space in the silica network structure, which would have made the pores relatively inaccessible to N_2 [23]. It is obvious that the decomposition of organic chains could result in the formation

of new micropores that would be accessible to N_2; this micropore regeneration could only be achieved, however, at the expense of the instability of the network structure [24].

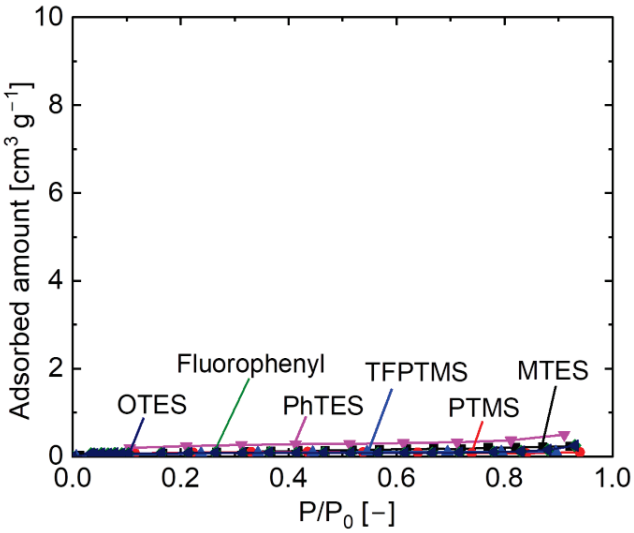

Fig. 3-3. N_2 adsorption isotherms at 77 K for various pendant-type organosilica-derived gels calcined at 300 ºC under a N_2 atmosphere.

Water-contact-angle measurements were carried out to observe the hydrophobic/hydrophilic properties of pendant-type alkoxysilane as shown in Fig. 3-4. All samples showed a water-contact angle that was higher than 80◦, which demonstrated the hydrophobicity of the organosilica structures. The contact angle increased as the carbon number increased from C_1 to C_8, which further revealed that stable organic chains decrease the silanol (Si-OH) density. In contrast, conventional silica shows a very low water-contact angle due to the excessive amount of silanol groups present in the silica matrix. The successful incorporation of organic moieties increased both network hydrophobicity and thermal stability [23].

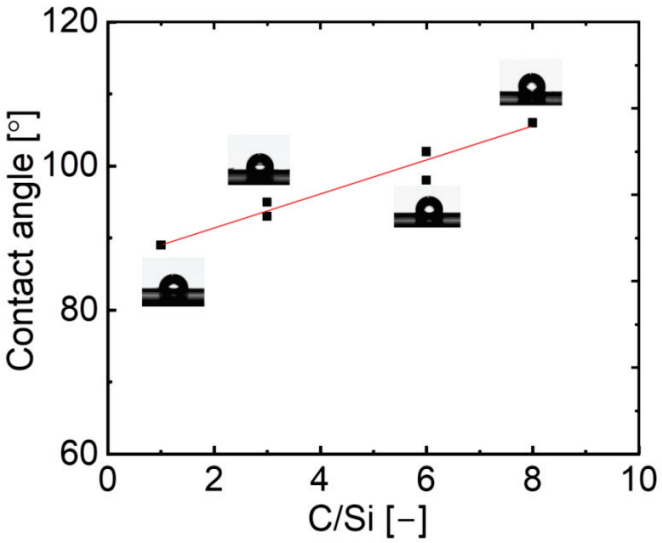

Fig. 3-4. Water contact angle of various pendent-type organosilica films calcined at 300 ºC under N_2 atmosphere.

3.3.2. Pore size controllability of organosilica membranes

It is quite difficult to obtain an exact pore size distribution of porous membranes for gas separation. The only way to estimate the pore size distribution is to take several measurements of gas permeances as a function of the differences in the molecular sizes of gas molecules. In the present study, the average pore size was roughly estimated according to the molecular size dependence of gas permeances. Fig. 3-5 shows the relationship between H_2/N_2 selectivity and the carbon number, and also shows the H_2 permeance of organosilica membranes at 200 ºC.

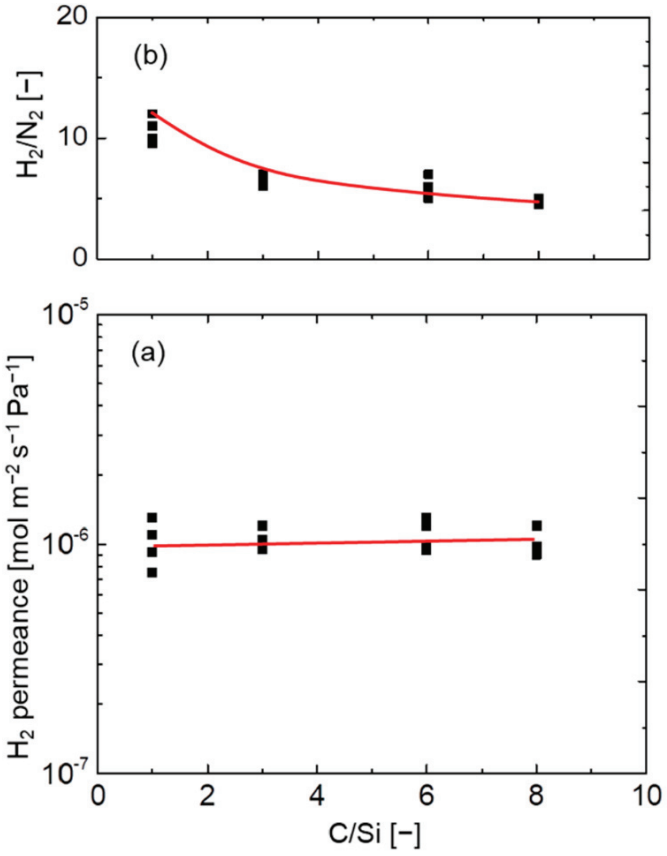

Fig. 3-5. Relationship between the C/Si ratio and H_2 permeance (a) and H_2/N_2 selectivity (b) at 200 ºC for pendant-type organosilica membranes calcined at 300 ºC under a N_2 atmosphere.

The permselectivity (H_2/N_2) of organosilica membranes corresponds to the respective pore size, and clearly decreases with an increase in the carbon number (C_1 to C_3). This indicates there is a somewhat loose network formation with an increase in the carbon number, and network pore size slightly decreases as the carbon number in the pendant side chain increases from C_3 to C_8. In general, membranes with a larger pore size show a higher level of H_2 permeance, which can be ascribed to the low resistance against permeate

molecules. Even though these membranes were prepared using mono–silicon alkoxysilane that consists of pendant groups with carbon numbers that varied from C_1 to C_8, the permeation properties of the membranes showed an approximately similar pore size with a comparable H_2 permeance even with a higher carbon number attached to the silicon atom (Si). It should be noted that an increase in the H_2 permeance of pendant-type organosilica network structures occurs at the expense of the removal of methyl groups after firing at an elevated temperature of 550 ºC [32].

To further evaluate the network pore size of organosilica membranes, a comparative study was carried out based on the relationship between the C/Si ratio and H_2/N_2 permselectivity, as well as the hydrogen activation energy E_p (H_2). It should be noted that the C/Si ratio of bridged-type membranes is half that of pendant types. Fig. 3-6a features the relationship between pendant- and bridged-type organosilica membranes at 200 ºC. In bridged-type organosilica membranes, the permeance ratio of H_2/N_2 was largely decreased as the carbon number increased between the two Si atoms, which could have been a result of the formation of a loose network structure [33,34]. On the contrary, pendant-type organosilica membranes showed a somewhat enlarged pore size with permeance ratios of H_2/N_2 that were lower than those of bridged-type structures, where higher H_2/N_2 selectivity was observed.

Fig. 3-6b illustrates the relationship between the C/Si ratio and hydrogen activation energy, E_p (H_2), for pendant- and bridged-type organosilica membranes. Non-adsorptive

hydrogen (H_2) is considered a suitable gas to evaluate pore size based on activation energy (E_p), and H_2 permeance is less affected by the presence of pinholes.

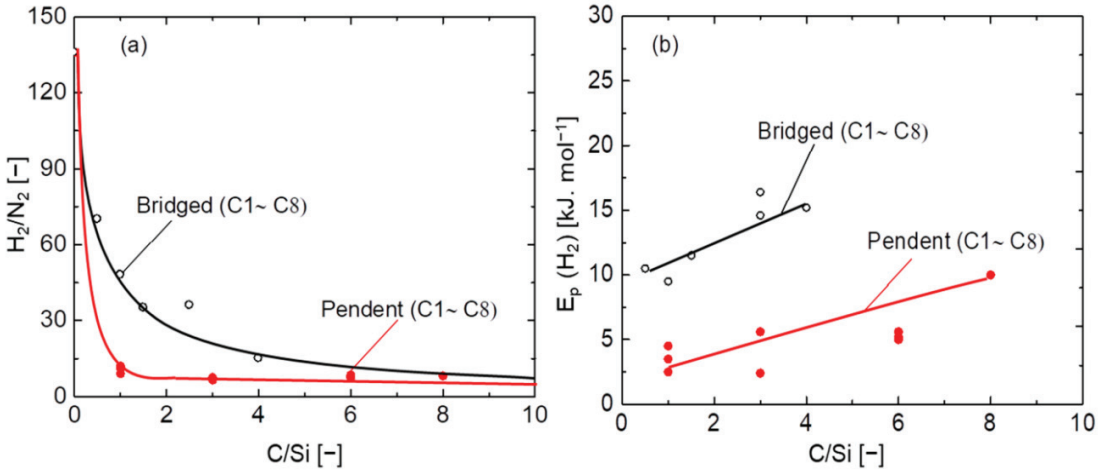

Fig. 3-6. Relationship between C/Si ratio, H_2/N_2 selectivity at 200 ºC (a), and activation energy (b) for pendant- and bridged-type organosilica membranes calcined at 300-350 ºC under a N_2 atmosphere.

The activation energies (E_p) were obtained using a modified gas–translational model (m-GT) [19,21]. In the bridged-type organosilica network structures, activation energies (E_p) increased as the C/Si ratio increased, which indicates that a smaller pore size required higher activation energy for molecules to diffuse through the micropores. Despite the network pore size of organosilica consisting of higher carbon linking units (BTESP, BTMSH, and BTESO), the flexibility of the organic chains could have affected the permeance of molecules to the point that the main chain could not effectively control the micropore structure. That would have resulted in higher levels of activation energies (E_p) for the membranes with long–chain organic linking units [21]. A similar phenomenon could

be in play with the pendant–type organosilica network structure wherein activation energies (E_p) are increased with increases in the C/Si ratio. However, compared with bridged-type organosilica network structures, pendant-type structures show a somewhat lower level of activation energy (E_p), due to the formation of a looser network.

Fig. 3-7 shows the schematic image of the effect that carbon–linking units exert on the network pore sizes of pendant- and bridged-type organosilica structures. The network pore size of bridged-type organosilica membranes demonstrates a dependence on carbon-linking units; as the carbon-linking units between two Si atoms increased, the network pore size of these membranes increased. An increase in the carbon number resulted in flexible linking units that subsequently led to a failure to maintain microporous properties, and a reduction in permeation properties. Conversely, the pendant-type alkoxysilane structure showed a similar pore size, although the carbon number was higher. A possible reason for the enlarged network pores in the pendant alkoxide structure could have been the existence of hydrophobic pendant side chains, which could have aggregated in the pore wall, and would have resulted in an enlarged network pore size.

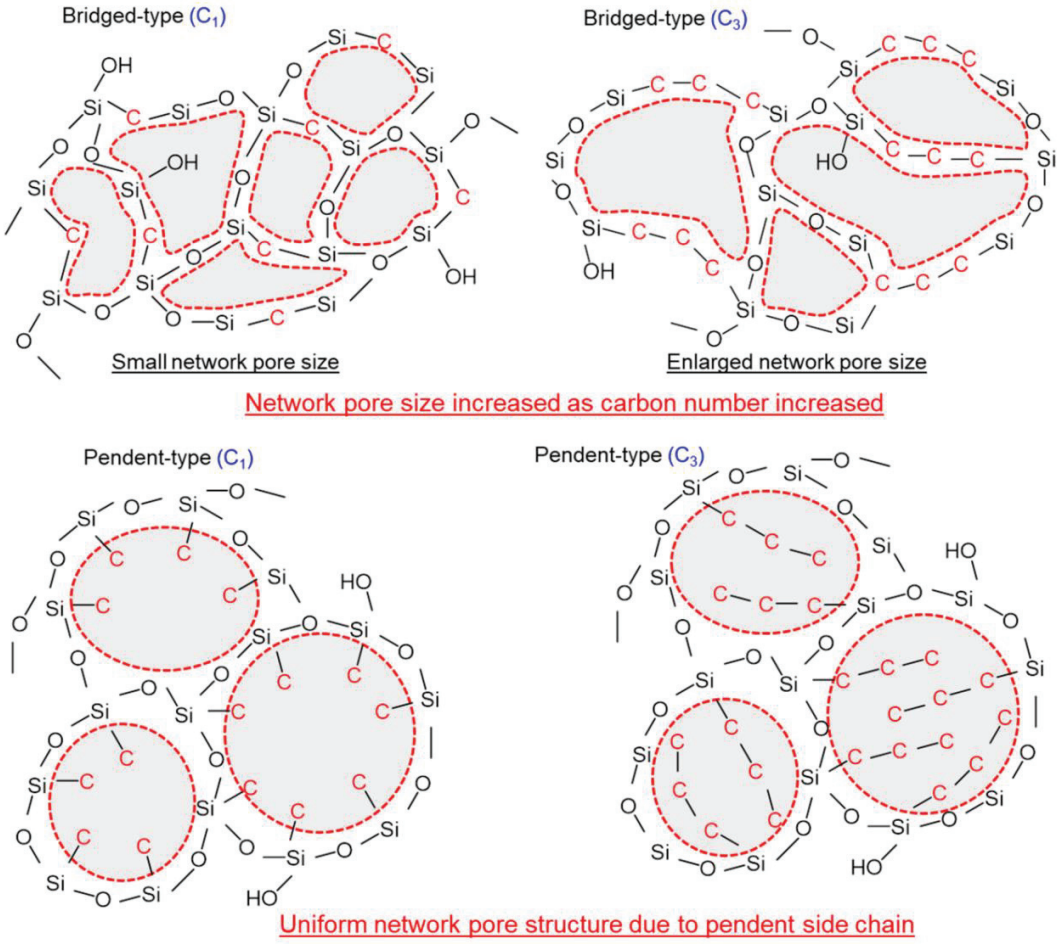

Fig. 3-7. Effect of C/Si ratio exerts on pendant-type and bridged-type organosilica network pore sizes.

3.3.3. The effect of fluorine doping exerts on a pendent-type organosilica network structure (C_1, C_3)

Fig. 3-8 shows the FT-IR spectra of fluorine-doped (F/Si = 1/9) and undoped pendant type (MTES and PTMS) organosilica network structures before/after calcination at 300 ºC. A Si-O-Si peak around 1100 cm^{-1} was observed in all samples irrespective of the fluorine

doping, which indicates the completion of hydrolysis/condensation reactions during the sol-gel process. Another peak centered around 900 cm^{-1} is ascribed to the silanol groups (Si-OH) present in the sample. However, no apparent difference was observed in the absorption peaks of silanol groups (Si-OH) in either fluorine-doped or undoped samples.

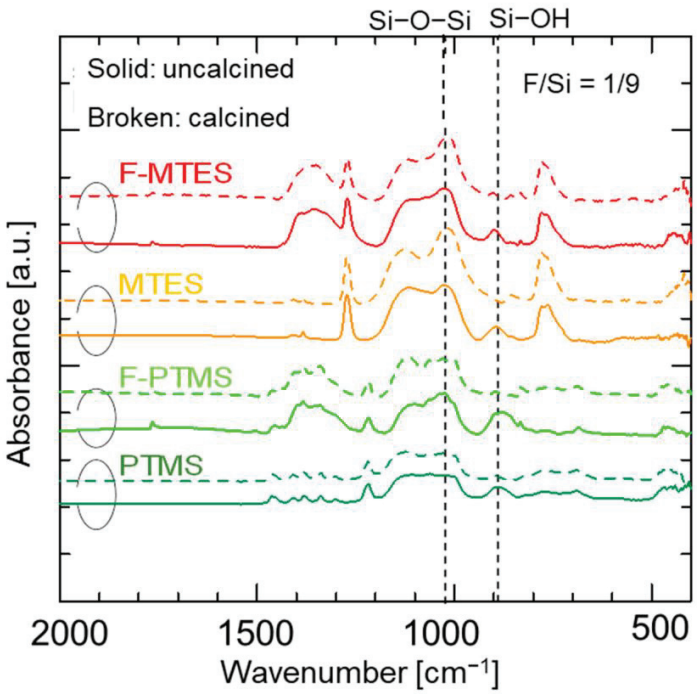

Fig. 3-8. FT-IR spectra of fluorine-doped (F-MTES, F-PTMS) and undoped (MTES, PTMS) pendant-type organosilica films before/after calcination at 300 ºC under a N_2 atmosphere.

Table 3-1 summarizes the Si-OH/Si-O-Si peak-area ratios of fluorine-doped and undoped samples before/after calcination. The results indicating a slight decrease in silanol groups (Si-OH) after fluorine doping were obtained for both forms of pendant-type organosilica network structures. It should be noted that various studies have reported that

fluorine significantly decreases the silanol density (Si-OH) of conventional silica (TEOS) and bridged-type organosilica (BTESM, BTESP) network structures [25-27]. This effectiveness of fluorine is associated with a decrease in the silanol density (Si-OH) perturbed by the presence of Si-F and C-F groups in the bridged-type organosilica network structures [35]. However, the present status of fluorine effectiveness in the pendant-type organosilica network structure seemed to be lessened by the existence of pendant-chain aggregation, which might have restricted the chemical bond formation of fluoride ions with silicon (Si-F) and carbon (C-F), as reported in fluorine-doped silica network structures [26].

Table 3-1. Si-OH/Si-O-Si peak area ratio for F-doped/undoped pendent organosilica films calcined at 300 ºC under N_2 atmosphere.

	Before calcination	After calcination
MTES	0.24	0.005
F-MTES	0.19	0.001
PTMS	0.38	0.007
F-PTMS	0.33	0.003

Fig. 3-9 depicts the XRD patterns of fluorine-doped (F/Si = 1/9) and undoped pendant–type organosilica gels calcined at 300 ºC under a N_2 atmosphere. The XRD pattern of organosilica gels exhibited two peaks at ~ 2θ = 20º and at ~ 2θ = 9º, respectively. The first peak corresponds to the amorphous structure of the main siloxane chain (Si-O-Si) in all samples irrespective of the doped fluorine, and the second sharp peak (~ 2θ = 9º) is ascribed to the formation of a highly ordered organosilica network structure due to the

existence of pendant organic groups. No significant effect was observed in fluorine-doped samples in terms of the peak shift, although previous studies have reported that fluorine-doped samples showed a peak shift to the lower degree of 2θ, which revealed an enlarged Si-O-Si bond angle caused by the Si-F groups present in the fluorine-doped organosilica network structures [25,26]. These results are consistent with the FT-IR spectra, wherein no obvious change in peak shift (blue shift) was observed after fluorine doping into pendant-type organosilica structures.

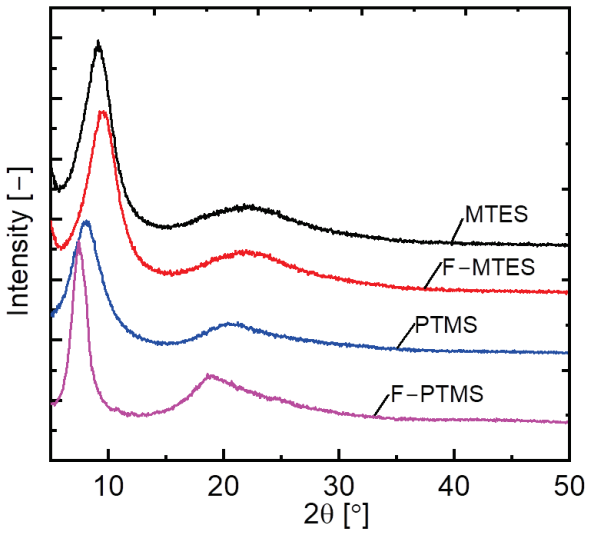

Fig. 3-9. XRD pattern of fluorine-doped and undoped pendent-type organosilica gels calcined at 300 ºC under N_2 atmosphere.

Microporous properties were evaluated via N_2 adsorption isotherms for fluorine–doped (F/Si = 1/9) and undoped pendant-type organosilica gels calcined at 300 ºC, as shown in Fig. 3-10a. A negligible amount of N_2 adsorption was observed in undoped samples, which indicated that most of the pores were inaccessible and corresponded to

a non-porous network structure. N_2 adsorption slightly improved in fluorine-doped samples, which suggests that micropores were generated after fluorine incorporation into the pendant-type organosilica network structure. A possible reason for the improved adsorption properties of F-doped samples is that the reduced silanol density (Si-OH) was affected by the fluoride ions.

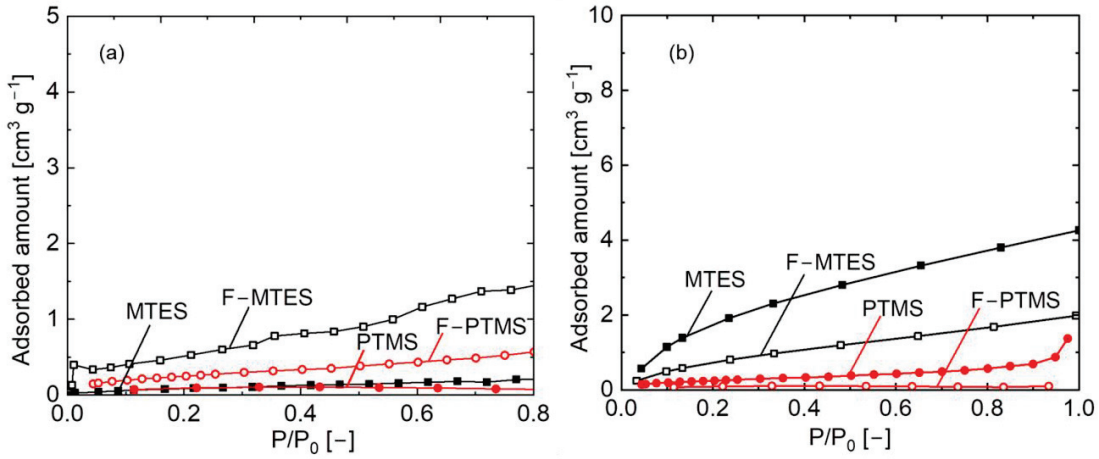

Fig. 3-10. N_2 adsorption isotherms at 195 ºC (a) and H_2O adsorption isotherms at 25 ºC (b) for fluorine-doped (F/Si = 1/9) and undoped (MTES,PTMS) pendant-type organosilica gels calcined at 300 °C under a N_2 atmosphere.

A similar effect of increased microporosity after fluorine doping was observed in the non–porous BTESP network structure. A high uptake of N_2 adsorption was observed in fluorine-doped BTESP samples, whereas undoped BTESP samples showed a non-porous structure. This change in the microporous properties of F-BTESP samples is associated with a decrease in silanol density (Si-OH), which was perturbed by Si-F and C-F bonds and the subsequent network structure resulted in a high surface area and micropore volume [27].

Thus far, these results are consistent with the observation of physicochemical properties (FT-IR), where a small change in silanol density (Si-OH) was seen in fluorine-induced pendant-type organosilica samples, and F-doped gels simultaneously showed improved N_2 adsorption properties.

Fig. 3-10b shows H_2O adsorption isotherms at 25 °C for fluorine-doped (F/Si = 1/9) and undoped pendant-type organosilica gels calcined at 300 °C under a N_2 atmosphere. Prepared samples (MTES and PTMS) showed H_2O adsorption onto pendant-type organosilica surfaces. Conversely, fluorine-doped gels displayed a negligible amount of H_2O adsorption, which is an indication of an increase in the hydrophobicity of fluorine-doped gels. The incorporation of fluorine into hydrophobic pendant-type organosilica further improved the hydrophobic/hydrophilic properties. Several studies have reported similar results of increased hydrophobicity with the addition of fluoride ions into silica matrix by showing the very low amount of H_2O adsorbed by comparison with undoped sample [26, 36, 37].

Fig. 3-11a shows the XPS spectra ranging from 0-1200 eV for fluorine-doped (F/Si = 1/9) and undoped pendant-type organosilica gels calcined at 300 ºC under a N_2 atmosphere. Organosilica-derived gels demonstrated Si peaks (100 and 150 eV), a C 1s peak (280 eV), and an O 1s peak (520 eV) irrespective of fluorine doping. An F 1s peak around 690 eV was detected only in fluorine-doped gels, which confirms the existence of fluorine in the F-doped pendant-type organosilica gels.

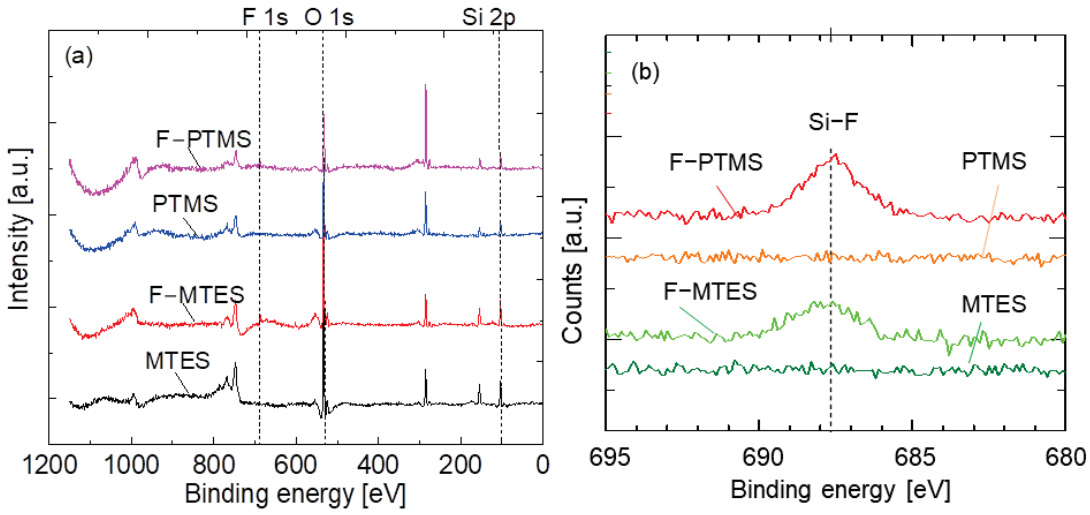

Fig. 3-11. XPS spectra in the range of 0-1200 eV (a) and F 1s spectra (b) for fluorine doped and undoped pendent-type organosilica gels calcined at 300 ºC under N_2 atmosphere.

Fig. 3-11b represents the narrow spectra of the F 1s peak, which ranged from 695 to 680 eV for both fluorine-doped and undoped pendant-type organosilica gels calcined at 300 ºC. As-prepared samples showed no peak intensity indicating Si-F bonds. On the other hand, a peak was detected as Si-F (688 eV) in all fluorine-containing organosilica network structures. The existence of fluorine as Si-F and C-F bonds has also been reported in bridged organosilica (BTESM, Si-C_1-Si; and BTESP, Si-C_3-Si) network structures [26,27].

3.3.4. Network pore-size evaluation of pendent- and bridged-type organosilica membranes

Fig. 3-12 shows the relationship between fluorine concentration (F/Si) and gas permeation properties (H_2 permeance, H_2/N_2, and E_p of H_2) at 200 ºC for fluorine-doped and undoped pendant-type (a) and bridged-type (b) organosilica membranes calcined at 300

ºC. Approximate similar H_2 permeance values were observed for both pendant-type organosilica membranes irrespective of the carbon number (C_1 and C_3). After fluorine incorporation (0-50 mol %), permeation properties were not significantly improved, and permselectivity corresponding to the network pore size remained unchanged as well as the E_p (H_2). These results indicate that the network pore size of both pendant-type membranes (C_1 and C_3) was almost independent of fluorine concentration.

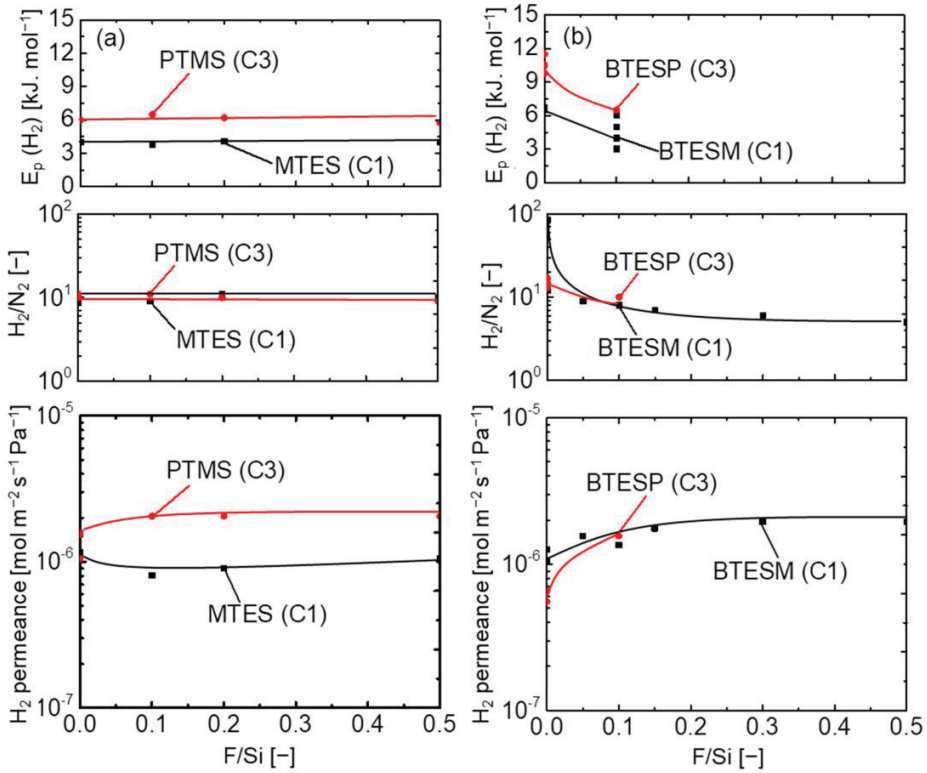

Fig. 3-12. Effect of doped fluorine concentration on the network pore sizes of pendant- and bridged-type organosilica membranes calcined at 300-350 ºC under a N_2 atmosphere.

On the other hand, bridged-type organosilica membranes showed a strong dependence on the carbon number present between two Si atoms. The effect of carbon linking units was apparent when the BTESM (Si-C_1-Si) with a single carbon showed a higher level of H_2 permeance compared with that of BTESP (Si-C_3-Si), with three carbons between two silicon atoms. Although previous studies have reported that permeation properties were improved as the carbon number increased, the flexibility of organic linking units could have decreased the H_2 permeance in BTESP membranes [21,37]. Long-chain organosilica membranes are known to block pores due to space occupation, and these are not considered effective for the fabrication of highly permeable gas–separation membranes. After fluorine (NH_4F) incorporation, improved permeation properties have been reported irrespective of the organic linking units, which demonstrated an enlarged network pore size that was caused by Si-F and C-F bonds [27,35]. H_2/N_2 selectivity and E_p (H_2) decreased as the fluorine concentration increased (F/Si = 0-5/5), which indicates a loose network formation. Network pore sizes of organic/inorganic silica membranes have been controlled effectively with appropriate fluorine concentration. These results further proved that the significance of fluorine in bridged-type organosilica is independent of the Si precursor.

Fig. 3-13 shows the schematic illustration of fluorine-doped organosilica pendant-type and bridged-type network structures. The catalytic effect of fluoride ions is the progression of hydrolysis/condensation reactions, as well as a reduction in the silanol density (Si-OH). Herein, bridged organosilica structures showed a cleavage of Si-C [38-41] bonds, which later formed C-F; simultaneously, this hydrophobic bond interaction reduced the OH groups. This dissociation energy of Si-C bonds could have resulted in cleavage and the

subsequent formation of hydrophobic C-F bonds. This chemical bond formation affected the desired pore size and improved the permeation properties of bridged-type organosilica membranes. On the contrary, no change in network pore size was observed in fluorine–doped pendant-type organosilica structures. The possible reason for the fluorine ineffectiveness could be explained by the aggregation of pendant organic groups in the micropores, which might have restricted the fluorine bond formation to Si-C and C-F.

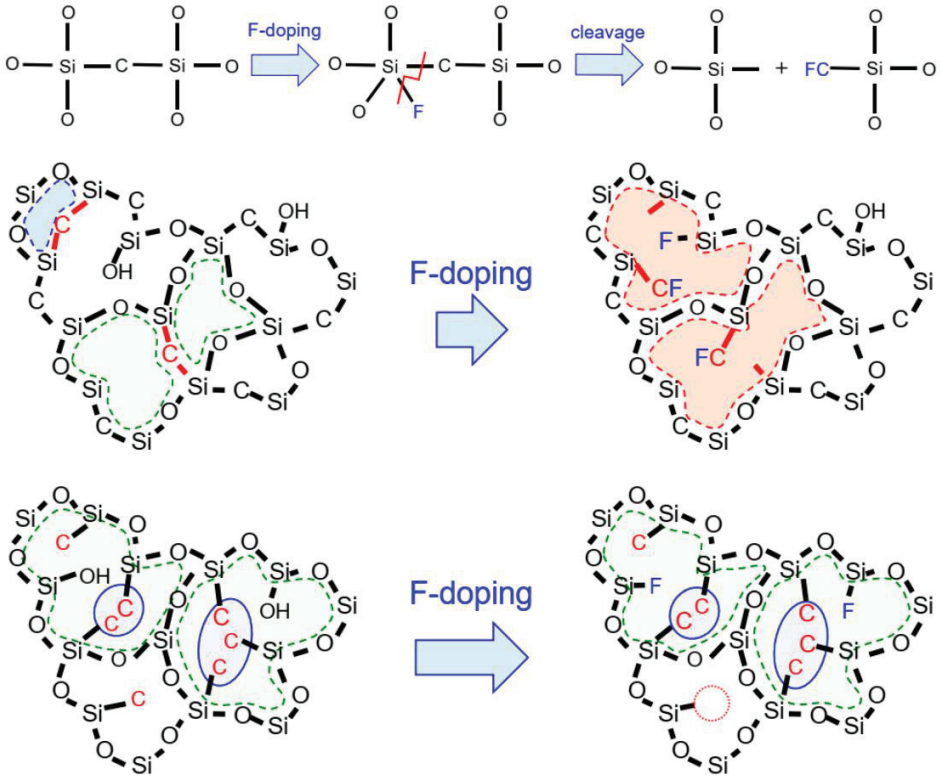

Fig. 3-13. A schematic image of the effect that fluorine doping exerts on pendant-type and bridged-type organosilica network structures calcined at 300-350 ºC under a N_2 atmosphere.

3.4. Conclusions

A series of pendant alkoxysilane structures with various carbon numbers (C_1-C_8) were used to fabricate sol-gel derived organosilica membranes to evaluate the effects of the C/Si ratio and fluorine doping. Initially, this investigation was focused on the effect that carbon-linking (pendant-type) units exert on a microporous structure and how this affects the gas–permeation properties of pendant-type organosilica membranes. Gas permeation results were compared with those of bridged-type organosilica membranes (C_1-C_8). Subsequently, we also evaluated the effect that fluorine doping (NH_4F) exerts on pendant–type [methytriethoxysilane (MTES), propyltrimethoxysilane (PTMS)] and bridged-type [1,2-bis(triethoxysilyl)methane (BTESM) bis(triethoxysilyl)propane (BTESP)] organosilica structures with similar carbon numbers (C_1 and C_3).

The pendant-type organosilica membranes showed a slightly looser network structure with a decrease in H_2/N_2 selectivity compared to those of bridge-type organosilica membranes. Activation energy (E_p) increased as the carbon number increased in both types of membranes, which indicates increased space occupation by pendant side chains as the C/Si ratio increased, and increased network flexibility in bridged-type organosilica membranes. However, permeation results revealed that pendant-type organosilica membranes demonstrated a larger pore size in comparison with bridged-type organosilica membranes, due to the lower values of activation energies (E_p) which is evidence of a loose network formation.

Fluorine-doped pendant-type organosilica membranes showed pore sizes similar to those of undoped organosilica membranes with comparable selectivity (H_2/N_2) and E_p (H_2). Those results are ascribed to the existence of pendant side chains, which could have restricted the effectiveness of fluorine and allowed the pore size to remain unchanged. Conversely, fluorine significantly improved the permeation properties of bridged–type organosilica membranes (H_2/N_2); the F/Si ratio was increased due to the formation of a loose network formation caused by the Si-F and C-F groups present in the network structure.

After several experiments, all membranes continued to exhibit considerable stability in characteristics such as molecular size dependence and temperature dependence of gas permeance. These good results notwithstanding, long-term separation performance of these membranes will be conducted in our future work.

References

1. H. J. Kim, H. C. Yang, D. Y. Chung, I. H. Yang, Y. J. Choi, J. K. Moon, Functionalized mesoporous silica membranes for CO_2 separation applications. J. Chem. 2015 (2015) 202867.

2. J. H. Moon, C. H. Lee, Hydrogen separation of methyltriethoxysilane templating silica membrane. AIChE J. 53 (2007) 3125–3136.

3. H. J. Moon, Y. J. Park, M. B. Kim, S. H. Hyun, C. H. Lee, Permeation and separation of a carbon dioxide/nitrogen mixture in a methyltriethoxysilane templating silica/α-alumina composite membrane. J. Membr. Sci. 250 (2005) 195-205.

4. Y. Gu, S. T. Oyama, High molecular permeance in a poreless ceramic membrane. Adv. Mater. 19 (2007) 1636-1640.

5. M. D. Jia, B. Chen, R. D. Noble, Falconer, J.L. Ceramic-zeolite composite membranes and their application for separation of vapor/gas mixtures. J. Membr. Sci. 90 (1994) 1-10.

6. Z. A. E. P. Vroon, K. Keizer, M. J. Gilde, H. Verweij, A. J. Burggraaf, Transport properties of alkanes through ceramic thin zeolite MFI membranes. J. Membr. Sci. 113 (1996) 293-300.

7. R. Krishna, L. J. P. Van den Broeke, The Maxwell-Stefan description of mass transport across zeolite membranes. Chem. Eng. J. Biochem. Eng. J. 157 (1995) 155-162.

8. J. M. van de Graaf, F. Kapteijn, J. A. Moulijn, Methodological and operational aspects of permeation measurements on silicalite-1 membranes. J. Membr. Sci. 144 (1998) 87-104.

9. G. Xomeritakis, S. Naik, C. M. Braunbarth, C. J. Cornelius, R. Pardey, C. J. Brinker, Organic-templated silica membranes: I. Gas and vapor transport properties. J. Membr. Sci. 215 (2003) 225-233.

10. R. M. de Vos, H. Verweij, High-selectivity, high-flux silica membranes for gas separation. Sci. 279 (1998) 1710-1711.

11. N. W. Ockwig, T. M. Nenoff, Membranes for hydrogen separation. Chem. Rev. 107 (2007) 4078-4110.

12. G. R. Gavalas, C. E. Megiris, S. W. Nam, Deposition of H_2-permselective SiO_2 films. Chem. Eng. Sci. 44 (1989) 1829-1835.

13. Y. Iwamoto, Precursors-derived ceramic membranes for high-temperature separation of hydrogen. J. Ceram. Soc. Jpn. 115 (2007) 947-954.

14. M. W. J. Luiten, N. E. Benes, C. Huiskes, H. Kruidhof, A. Nijmeijer, Robust method for micro-porous silica membrane fabrication. J. Membr. Sci. 348 (2010) 1-5.

15. D. Lee, L. Zhang, S. T. Oyama, S. Niu, R. F. Saraf, Synthesis, characterization, and gas permeation properties of a hydrogen permeable silica membrane supported on porous alumina. J. Membr. Sci. 231 (2004)117-126.

16. M. Nomura, M. Seshimo, H. Aida, K. Nakatani, S. Gopalakrishnan, T. Sugawara, S. I. Nakao, Preparation of a catalyst composite silica membrane reactor for steam reforming reaction by using a counter diffusion CVD method. Ind. Eng. Chem. Res. 45 (2006) 3950-3954.

17. S. Kim, G. R. Gavalas, Preparation of H_2 permselective silica membranes by alternating reactant vapor deposition. Ind. Eng. Chem. Res. 34 (1995) 168-176.

18. B. K. Sea, M. Watanabe, K. Kusakabe, S. Morooka, S. S. Kim, Formation of hydrogen permselective silica membrane for elevated temperature hydrogen recovery from a mixture containing steam. Gas Sep. Purif. 10 (1996) 187-195.

19. M. Guo, J. Qian, R. Xu, X. Ren, J. Zhong, M. Kanezashi, Boosting the CO_2 capture efficiency through aromatic bridged organosilica membranes. J. Membr. Sci. 643 (2022) 120018.

20. M. Kanezashi, T. Matsutani, T. Wakihara, H. Nagasawa, T. Okubo, T. Tsuru, Preparation and gas permeation properties of fluorine-silica membranes with controlled amorphous silica structures: Effect of fluorine source and calcination temperature on network size. ACS App. Mater. Int. 9 (2017) 24625-24633.

21. M. Kanezashi, Y. Yoneda, H. Nagasawa, T. Tsuru, Gas permeation properties for organosilica membranes with different Si/C ratios and evaluation of microporous structures. AIChE J. 63 (2017) 4491-4498.

22. J. Campaniello, C. W. Engelen, W. G. Haije, P. P. Pex, J. F. Vente, Long-term pervaporation performance of microporous methylated silica membranes. Chem. Comm. (2004) 834-835.

23. G. Li, M. Kanezashi, T. Tsuru, Preparation of organic-inorganic hybrid silica membranes using organoalkoxysilanes: The effect of pendant groups. J. Membr. Sci. 379 (2011) 287-295.

24. N. K. Raman, C. J. Brinker, Organic “template” approach to molecular sieving silica membranes. J. Membr. Sci. 105 (1995) 273.

25. M. Kanezashi, T. Matsutani, T. Wakihara, H. Tawarayama, H. Nagasawa, T. Yoshioka, T. Tsuru, Tailoring the subnano silica structure via fluorine doping for development of highly permeable CO_2 separation membranes. ChemNanoMat 2 (2016) 264-267.

26. M. Kanezashi, M. Murata, H. Nagasawa, T. Tsuru, Fluorine doping of microporous organosilica membranes for pore size control and enhanced hydrophobic properties. ACS Omega 3 (2018) 8612-8620.

27. I. Rana, H. Nagasawa, K. Yamamoto, T. Gunji, T. Tsuru, M. Kanezashi, Effect of fluorine doping on the network pore structure of non-porous organosilica bis (triethoxysilyl) propane (BTESP) membranes for use in molecular separation. J. Membr. Sci. 644 (2022) 120083.

28. D. L. Martens, J. Motuzas, S. Smart, J. C. D. da Costa, Structural investigation of cobalt oxide seeded silica xerogels under harsh hydrothermal condition. J. Sol-Gel Sci. Technol. 98 (2021) 470-477.

29. S. Smart, J. F. Vente, J. D. da Costa, High temperature H_2/CO_2 separation using cobalt oxide silica membranes. Int. J. Hyd. Ener. 37 (2012) 12700-12707.

30. E. S. Mirza, B. Topuz, Nanoscale tailoring on thin bimetallic organo-oxide membranes for H_2/CO_2 separation. Sep. Purif. Technol. 280 (2022) 119801.

31. G. G. Paradis, D. P. Shanahan, R. Kreiter, H. M. van Veen, H. L. Castricum, A. Nijmeijer, J. F. Vente, From hydrophilic to hydrophobic HybSiVR membranes: A change of affinity and applicability. J. Membr. Sci. 428 (2013) 157-162.

32. H. L. Castricum, A. Sah, M. C. Mittelmeijer-Hazeleger, C. Huiskes, E. Johan, Microporous structure and enhanced hydrophobicity in methylated SiO_2 for molecular separation. J. Mater. Chem. 17 (2007) 1509-1517.

33. I. Agirre, P. L. Arias, H. L. Castricum, M. Creatore, E. Johan, G. G. Paradis, J. F. Vente, Hybrid organosilica membranes and processes: Status and outlook. Sep. Purif. Technol. 121 (2014) 2-12.

34. M. Kanezashi, Y. Kazuya, Y. Tomohisa, T. Toshinori, Design of silica networks for development of highly permeable hydrogen separation membranes with hydrothermal stability. J. Amer. Chem. Soc. 131 (2009) 414-415.

35. M. Takenaka, H. Nagasawa, T. Tsuru, M. Kanezashi, Hydrocarbon permeation properties through microporous fluorine-doped organosilica membranes with controlled pore sizes. J. Membr. Sci. 619 (2021) 118787.

36. I. Rana, H. Nagasawa, T. Tsuru, M. Kanezashi, Tailoring the structure of a sub-nano silica network via fluorine doping to enhance CO_2 separation and evaluating CO_2 separation performance under dry or wet conditions. J. Membr. Sci. 658 (2022) 120735.

37. R. Inoue, M. Kanezashi, H. Nagasawa, K. Yamamoto, T. Gunji, T. Tsuru, Pore size tuning of bis (triethoxysilyl) propane (BTESP)-derived membrane for gas separation: Effects of the acid molar ratio in the sol and of the calcination temperature. Sep. Purif. Technol. 242 (2020) 116742.

38. J. M. Lee, S. J. Kim, J. W. Kim, P. H. Kang, Y. C. Nho, Y. S. Lee, A high resolution XPS study of sidewall functionalized MWCNTs by fluorination. J. Ind. Eng. Chem. 15 (2009) 66-71.

39. L. A. Zazzera, J. F. Moulder, XPS and SIMS study of anhydrous HF and UV/Ozone-modified silicon (100) surfaces. J. Electrochem. Soc. 136 (1989) 484.

40. W. Zhang, M. Dubois, K. Guérin, P. Bonnet, H. Kharbache, F. Masin, A. Hamwi, Effect of curvature on C-F bonding in fluorinated carbons: From fullerene and derivatives to graphite. Phys. Chem. Chem. Phys. 12 (2010) 1388-1398.

41. P. Xu, F. Wang, G. Fan, X. Xu, P. Tang, Hypervalent iodine (III) -mediated oxidative fluorination of alkylsilanes by fluoride ions. Ang. Chem. 129 (2017) 1121-1124.

Chapter 4

Catalytic effect of trifluoroacetic acid on the CO_2 transport properties of organic-inorganic hybrid silica membranes

4.1. Introduction

The drastic increase in anthropogenic CO_2 emissions is a major source of global warming. Therefore, CO_2 capture from pre/post-industrial emissions has become a crucial activity that currently is accomplished via processes that utilize cryogenic separation, CO_2 sorbents, and amine-based chemisorption. Amongst these processes, membrane separation offers promising results with low energy requirements, cost effectiveness, and easy to operate manners [1-5]. In particular, amorphous silica (tetraethoxylsilane) outperforms polymer and zeolite membranes by offering outstanding chemical-thermal stability and flexibility of pore-size tuning. Silica (SiO_2) membranes have an ultramicroporous structure (< 7Å) that allows only small molecules (He/H_2) to permeate, and rigorous contemplation for the tuning of pore sizes is required in order to accomplish CO_2/N_2 separation [6, 7].

It is noteworthy that enhanced CO_2 transport within the membrane matrix depends not only on the pore size (diffusivity/physisorption), but also on the affinity that penetrant molecules (solubility/chemisorption) demonstrate with the membrane matrix, which also is an essential parameter because preferentially adsorbed CO_2 assisted by CO_2-philic sites could block the permeance of unwanted molecules (N_2, CH_4...etc.). Hence, exclusive functional groups (primary, secondary, and tertiary amines) that possess a strong affinity for CO_2 polar molecules have been extensively utilized for silica surface modification.

Alkyl amine-functionalized membranes exhibit superior CO_2 transport with the dual benefits of induced CO_2-philic sites as well as a controlled network pore structure [8, 9]. These functional groups generally are incorporated via post-synthesis, impregnation, and co-condensation processes [10, 11]. More specifically, widely used primary ($-NH_2$) amines (3-aminopropyltriethoxysilyl, APTES) demonstrate superior CO_2 chemisorption properties and favorable practical applications. In addition, primary amines ($-NH_2$) on the tip of an organosilane are more approachable for CO_2 polar molecules by comparison with secondary (-NH-) and tertiary (-N-) amines, wherein CO_2 molecules would have minimal accessibility to active sites of amines [12, 13]. Ko et al. [14] studied the effect of amine type on CO_2 adsorption capacity, and the results were ranked in the following order: primary > secondary > tertiary at 25 ºC.

Nonetheless, a defect-free membrane surface has been difficult to obtain with pure APTES due to the faster condensation rates of amine-organic-silane. Thus far, the only alternative to use in the fabrication of a defect-free membrane has been an organic-inorganic silica structure with suitable APTES content [15]. The obtained hybrid silica (tetraethoxysilane, TEOS and APTES) network structure, however, undergoes densification due to the aminopropyl groups, and the resultant membranes exhibit low permeation properties [16]. Further, recent studies have also revealed a carbamate formation that results from the acid-base reaction between CO_2 and amines (NH_2). In that reaction, a zwitterion (COO^-) forms after the adsorption of CO_2 inside the pore walls and reacts with adjacent amines to consequently generate a stable carbamate (NH_3^+), which requires a high level of energy that hinders complete CO_2 desorption [17]. The drawbacks associated with the

aminopropyl groups in the TEOS-APTES network structure have made it a challenge to fabricate highly CO_2-permeable TEOS-APTES membranes with diminished carbamate formation (that increases the energy footprint) and minimal densification (that is responsible for low permeance).

Therefore, herein, we propose a novel strategy to tailor the network pore structure of TEOS functionalized with APTES in the presence of trifluoroacetic acid (TFA). Fig. 4-1 illustrates the possible network structure formation from the co-condensation of TEOS and APTES with different catalysts and CO_2 permeation via an amine-modified silica surface. To the best of our knowledge, no one has reported the catalytic efficiency that TFA (which contains terminal CF_3 groups) exerts on the network pore structure of TEOS-APTES membranes. Composite hybrid TEOS-APTES gels were employed to investigate the CO_2 adsorption properties and the results were compared with conventional catalysts. Subsequently, composite membranes were fabricated to evaluate the binary (CO_2/N_2) gas-separation performance.

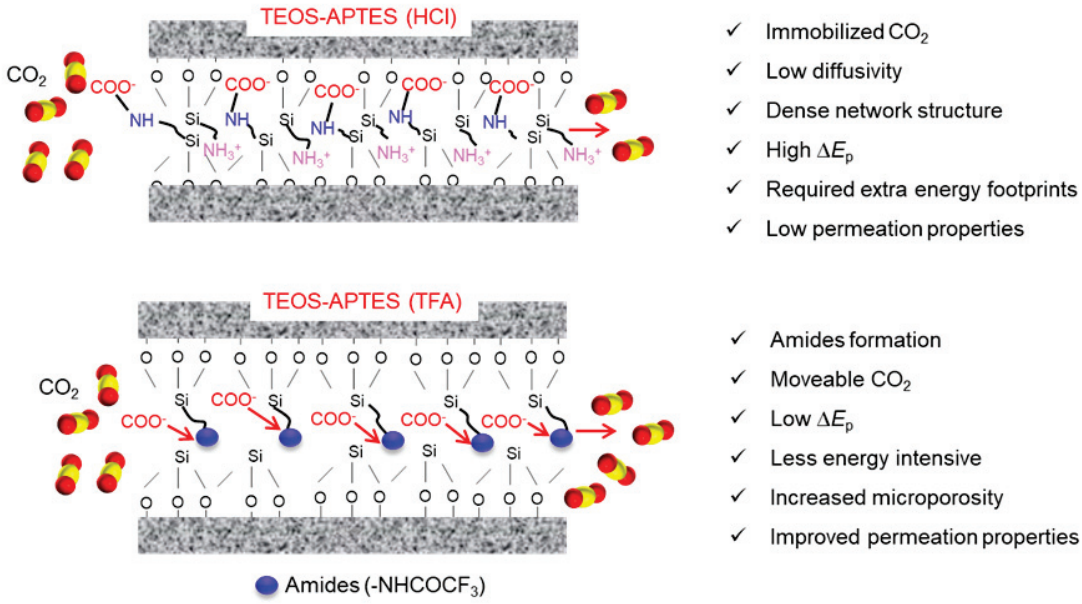

Fig. 4-1. CO_2 transport mechanism across the hybrid amine-silica composite membranes matrixes calcined at 250 ºC under a N_2 atmosphere.

4.2. Experimental section

4.2.1. Materials

TEOS was purchased from Thermo Fisher Scientific, USA, and used as received without further purification. APTES, TFA, and HCl were purchased from Tokyo Chemical Industry Co., Ltd. (TCI), Japan, and Nacalai Tesque, Inc., Kyoto, Japan, respectively. Deionized water was used to accomplish the hydrolysis reactions during sol-gel processing.

4.2.2. Sol/gel preparation and characterization

Silica sols were prepared via the commonly used sol-gel method [18]. A specific amount of TEOS was added to ethanol (EtOH) and left to stir for 5 minutes at 25 ºC. After that, water (H_2O) and catalysts (HCl & TFA) were added dropwise into the solution to achieve a

final molar ratio of TEOS/water/TFA, HCl of 1/200/5 (TFA) or 0.3 (HCl), and the TEOS/APTES concentration was controlled at 9.5/0.5. The final weight% of Si precursor was controlled at 2.0 wt%. It should be noted that a high TFA molar ratio = 5 was employed to avoid gelation during the hydrolysis/condensation reactions due to the amine basicity. Subsequently, the silica gel was prepared under an air atmosphere at 40 ºC, and this gel was calcined at 250 ºC under a N_2 atmosphere.

Particle size distribution was measured using a DLS analyzer (Malvan Zetasizer Nano ZS). Fourier transform infrared (FT-IR) analyses that ranged from 400-4,000 cm^{-1} were conducted via a FT-IR spectrometer (FT/IR-4100, Jasco, Japan). X-ray photoelectron spectroscopy (XPS, JEOL RE series JES-RE1X ESR spectrometer, Shimadzu, Japan) was used for the elemental analysis of TEOS-APTES (TFA) samples. A BELMAX (BELJAPAN INC.) was utilized to perform microporous analysis (N_2 adsorption at 77 K) for all gels prepared in this work. It is noteworthy that each sample was pre-treated at 200 ºC for at least 12 h to desorb the water. CO_2 adsorption/desorption isotherms were measured at 25 ºC. In order to establish the cross-sectional morphology of the TEOS-APTES (TFA) membrane, Field Emission-Scanning Electron Microscopy (FE-SEM, Hitachi S-4800, Japan) was used and samples were vacuumed overnight at 50 ºC.

4.2.3. Membrane fabrication and gas separation evaluation

Particle and intermediate layers were obtained by following our recent study [19]. To obtain a defect-free top separation layer, a 2 wt % TEOS-APTES sol (diluted with EtOH to reduce the concentration at 0.25 wt %) was coated 5-6 times, which was then followed by

calcination at 250 ºC under a N_2 atmosphere. Measurements for the single-gas permeance of hybrid silica membranes were conducted at 50-200 ºC using the experimental apparatus that appears in Fig. 2-1. In the single system, high purity gases (He, H_2, CO_2, N_2, CH_4, CF_4, and SF_6) were fed from the outer surface of the membrane at an absolute pressure of 200 kPa while the permeate side was controlled at atmospheric pressure. Prior to the start of the gas permeation evaluation, each membrane was pre-treated at 200 ºC to desorb water from the membrane surface. The actual permeate flow was measured via the use of a film-flow meter (SF-U, Horiba Ltd., Japan).

Subsequently, CO_2/N_2 binary gas mixtures (50/50 and 10/90) were evaluated at 50-200 ºC by maintaining upstream and downstream pressures of 100-200 kPa and 8-10 kPa, respectively. A vacuum pump was attached to the permeate side while conducting binary gas separation. Gas chromatography (GC-14B, Shimadzu, Japan) attached with a TCD detector (column: Unibeads 1S80/100, GL Science, Japan; column temperature: 75 ºC) was used to analyze the CO_2/N_2 compositions in the feed, retentate, and permeate streams.

In a similar manner, a binary gas mixture (CO_2/N_2 = 10/90) under wet conditions was fed into the membrane cell at an upstream pressure of 200 kPa while evacuating the permeate side via vacuum pump. Each gas was passed through the water evaporator at 25 ºC (H_2O partial pressure = 3 kPa) prior to being fed into the membrane module.

4.3. Results and discussion

4.3.1. Amine-silica (composite) sol/gel characterization

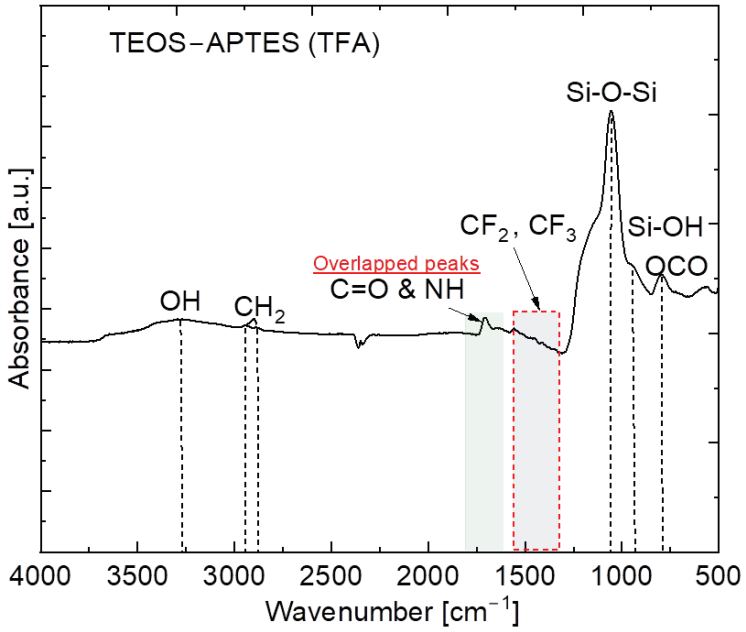

Fig. 4-2. FT-IR spectra for composite (TEOS-APTES) structure after calcined at 250 ºC under N_2 atmosphere.

Fig. 4-2 shows the chemical structure of TEOS-APTES (TFA) films calcined at 250 ºC under a N_2 atmosphere. The absorption peaks around 1,043 cm^{-1} and 940 cm^{-1} can be ascribed to the Si-O-Si [20] and Si-OH [21], respectively. The symmetrical/asymmetrical vibrational peak observed at around 2,800-3,000 cm^{-1} corresponds to propyl groups (Si-CH_2). The broad peak around 3,000-3,800 cm^{-1} is attributed to the partially hydrated Si-OH and/or to a combination of Si-OH and H_2O. A sharp peak emerged at around 1,650 cm^{-1} [8] as an indication of amines (N-H) successfully incorporated into the silica matrix. However, this absorption peak was overlapped by carbonyl groups (C=O) of TFA, which also

appeared at around 1,600-1,700 cm^{-1} [22]. TFA contained terminal CF_3 bonds, and these essential functional groups were assigned as CF_2 and CF_3 at around 1,300-1,400 cm^{-1} [23, 24].

Fig. 4-3a shows the N 1s spectra ranging from 392 to 406 eV for composite TEOS-APTES (TFA) gel. A prominent nitrogen peak was observed centered on 399 eV. Generally, a peak centered on 401 eV would be assigned to an intermediate carbamate (NH_3^+) formation that is the result of protonated amines [25]. Calvo et al. [26] reported a similar protonation effect in an amine-silica network structure containing TFA and suggested that the peak of carbamate was dominated by CF_3 bonds due to the electronegativity effect and to a slight shift towards a higher binding energy following the formation of amides (-$NHCOCF_3$).

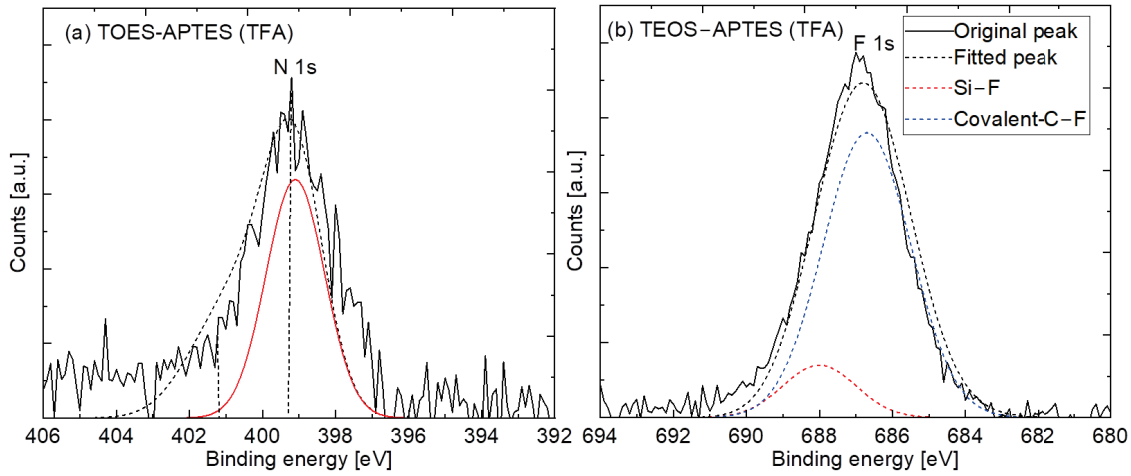

Fig. 4-3. Deconvolution of N 1s spectra (a) and F 1s spectra (b) for composite (TEOS-APTES) structure calcined at 250 ºC under N_2 atmosphere.

Fig. 4-3b shows the narrow F 1s spectra ranging from 680-694 eV for a TEOS-APTES (TFA) gel calcined at 250 ºC under a N_2 atmosphere. This fluorine existence is associated with TFA, which contains terminal CF_3 groups. Therefore, the peak centered at 687 eV is attributed to the existence of fluorine in the composite silica network structure. The deconvolution peaks centered at around 685.5 to 687 eV and 688 eV are ascribed to the C-F and Si-F bonds, respectively [27].

Fig. 4-4a shows the N_2 adsorption/desorption isotherms for pure APTES and composite TEOS-APTES gels with different catalysts. The APTES adsorbed a negligible amount of N_2, indicating a nonporous characteristic. On the contrary, the uptake of the adsorbed N_2 gas by the HCl-catalyzed sample slightly improved at low relative pressure and remained constant as the pressure increased from 0 to 1. Meanwhile, the TEOS-APTES (TFA) sample displayed a high uptake of adsorbed N_2 gas at low relative pressure, indicating a typical characteristic for a microporous structure as shown in Fig. 4-4b. This is ascribed to the existence of the CF_3 groups that formed as a result of chemical reaction between functional groups and trifluoroacetic acid as shown in Eq. 4-1. These bonds might have increased structure rigidity and intermolecular mobility enhanced simultaneously by following the increased micropore volume. These results were further confirmed by non-local density functional theory (NLDFT), as shown in Table 4-1.

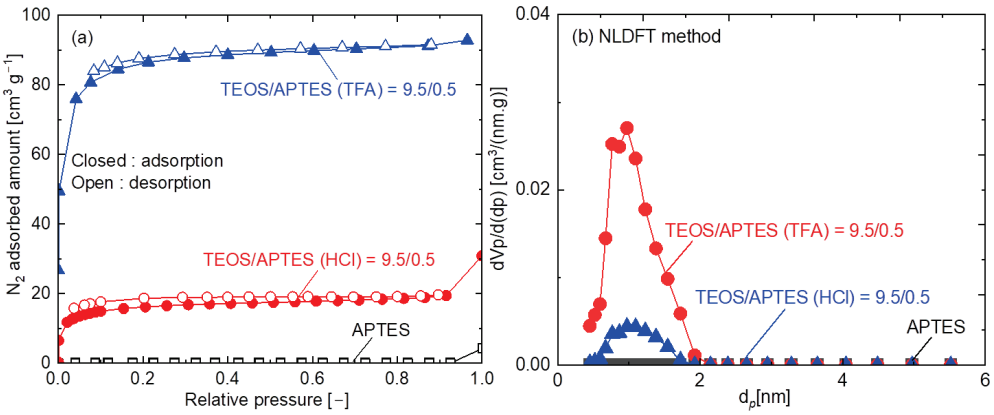

Fig. 4-4. N_2 adsorption/desorption isotherms (a) and pore size distribution obtained via NLDFT (b) for APTES and composite (TEOS-APTES) powders calcined at 250 ºC under N_2 atmosphere.

Table 4-1. Micropore volume obtained by NLDFT method for amine-silica gels calcined at 250 ºC under N_2 atmosphere.

Micropore volume (V_p cm^3 g^{-1})		
APTES	TEOS-APTES (HCl)	TEOS-APTES (TFA)
-	0.05	0.18

The following equation demonstrates the chemical reactions of trifluoroacetic acid and HCl with amine functional groups, which corresponds to the formation of amides (Eq. 4-1) and salt (Eq. 4-2) formation, respectively [16, 22]. The final reaction product could be explained as of groups contained with CF_3 bonds and simultaneously amide (-$NHCOCF_3$) formation (Eq. 4-1).

$$-\mathrm{Si}-\mathrm{C_3H_6NH_2} + \mathrm{CF_3COOH} \rightarrow -\mathrm{Si}-\mathrm{C_3H_6NHCOCF_3} + \mathrm{H_2O} \qquad (4\text{-}1)$$

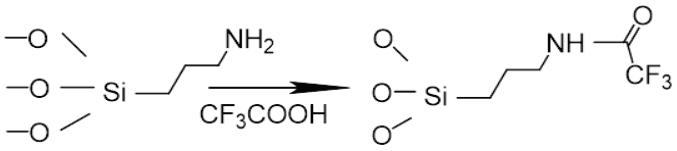

For HCl:

$$-\mathrm{Si}-\mathrm{C_3H_6NH_2}+\ \mathrm{HCl}\ \rightarrow -\mathrm{Si}-\mathrm{C_3H_6NH_3^+}\ \mathrm{Cl^-} \qquad (4\text{-}2)$$

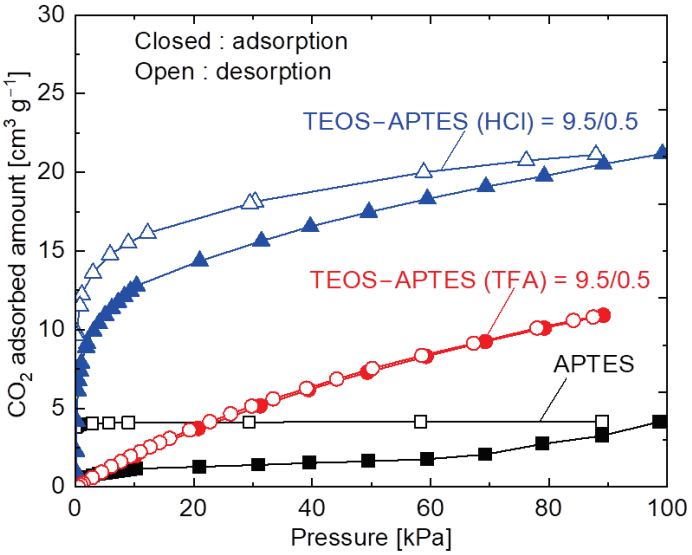

Fig. 4-5. CO_2 adsorption isotherms for APTES and composite (TEOS-APTES) powders calcined at 250 ºC under N_2 atmosphere.

Fig. 4-5 shows the CO_2 adsorption/desorption isotherms for APTES and composite TEOS-APTES gels. Unlike other materials, pure APTES exhibited irreversible adsorption/desorption with a typical hysteresis loop, which is a characteristic of the strong CO_2-amine interaction of a stable carbamate that results in an incomplete desorption of CO_2. TEOS-APTES (HCl) gel exhibited a similar hysteresis loop, but a higher uptake of

adsorbed CO_2 was observed. TEOS-APTES (TFA) gel, however, demonstrated a reversible adsorption/desorption profile. Generally, this suggests a lessened degree of carbamate formation and/or an unstable carbamic species where a structure experiences reversible adsorption/desorption. This novel approach, however, suggests that a newly formed species (-$NHCOCF_3$) is responsible for the complete desorption of CO_2.

4.3.2. Single gas permeation evaluation of composite membrane

Fig. 4-6 summarizes the temperature dependence (50-200 ºC) of He, CO_2, and N_2 permeance that is required to obtain activation energy (E_p). The TEOS-APTES (TFA) membrane displays superior permeance irrespective of the permeating molecules, and this superior permeance is assisted by enhanced molecular sieving via increased microporosity. He and N_2 (non-adsorptive molecules) permeance was decreased with decreasing temperature irrespective of the membrane type, which indicates an activated diffusion. However, the slope of temperature dependence was much higher for APTES in comparison with other membranes.

CO_2 showed activated diffusion for APTES and TEOS-APTES (HCl) membranes. These results indicate the higher activation energy (E_p) required for molecules to permeate these membranes, as shown in Table 4-2, and this is attributed not only to the dense structure caused by the flexibility of pendent side chains, but also to carbamate formation due to the existence of primary amines [11]. However, CO_2 permeance showed a surface diffusion mechanism in TEOS-APTES (TFA) membranes, which could be ascribed to the

relatively mild affinity that the newly formed species (amides) exhibit for CO_2 (solubility selectivity) [28] as shown in Eq. 4-1.

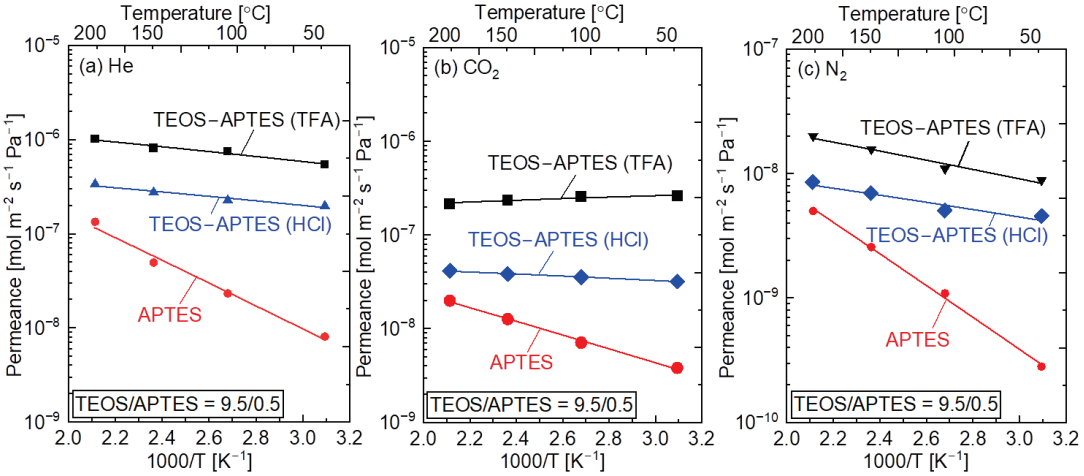

Fig. 4-6. Temperature dependence (50-200 ºC) of He, CO_2, and N_2 for APTES and composite (TEOS-APTES) membranes calcined at 250 ºC under N_2 atmosphere.

Table 4-2. Activation energies (E_p) of He, CO_2, and N_2 for APTES and composite TEOS-APTES membranes calcined at 250 ºC under N_2 atmosphere.

Activation energies (kJ mol^{-1})			
	APTES	TEOS-APTES (HCl)	TEOS-APTES (TFA)
He	22	8	6
CO_2	12	4	−3.6
N_2	17	10	7

Fig. 4-7 shows the pore size as examined via a modified gas translational model (GT) for APTES and composited TEOS-APTES membranes. The results indicate that TEOS-

APTES (HCl) exhibit similar pore size as of TEOS-APTES (TFA) membrane. However, CO_2-philic sites (-$NHCOCF_3$) as shown in Eq. **1**, and micropore volume is different for TEOS-APTES (TFA) membrane.

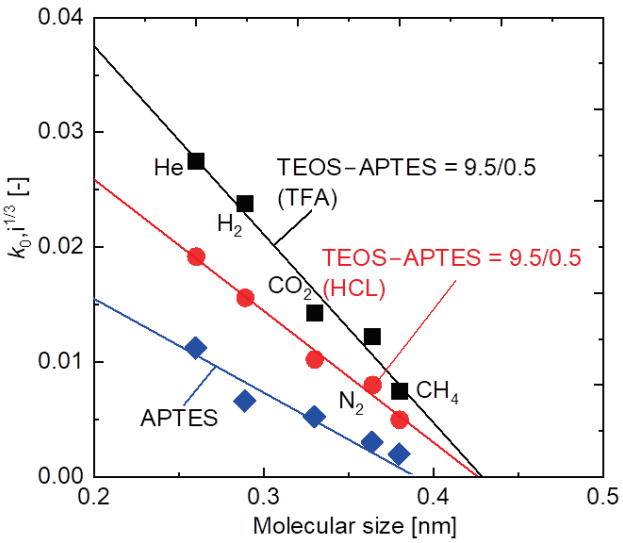

Fig. 4-7. Relationship between $k_{0,i}^{1/3}$ and molecular size (d_i) for APTES and composite TEOS-APTES membranes calcined at 250 ºC under N_2 atmosphere.

Fig. 4-8a depicts the relationship between $E_p(CO_2)$ and $E_p(CO_2) - E_p(N_2)$, which is essential to better understand the CO_2 separation potential of composite silica membranes [29]. TEOS-APTES (TFA) membranes demonstrate the lowest values of $E_p(CO_2)$, and the difference between $E_p(CO_2)$ and $E_p(N_2)$ indicates a higher level of CO_2/N_2 separation potential for these membranes when compared with other membranes, as displayed in Fig. 4-8a. This further emphasizes that TFA dramatically improves the molecular sieving properties, which generally undergo densification due the aminopropyl groups, and, therefore, permeation follows a solution-diffusion mechanism. These results were further

confirmed by a higher level of CO_2/N_2 selectivity for the TEOS-APTES (TFA) membrane, as shown in Fig. 4-8b.

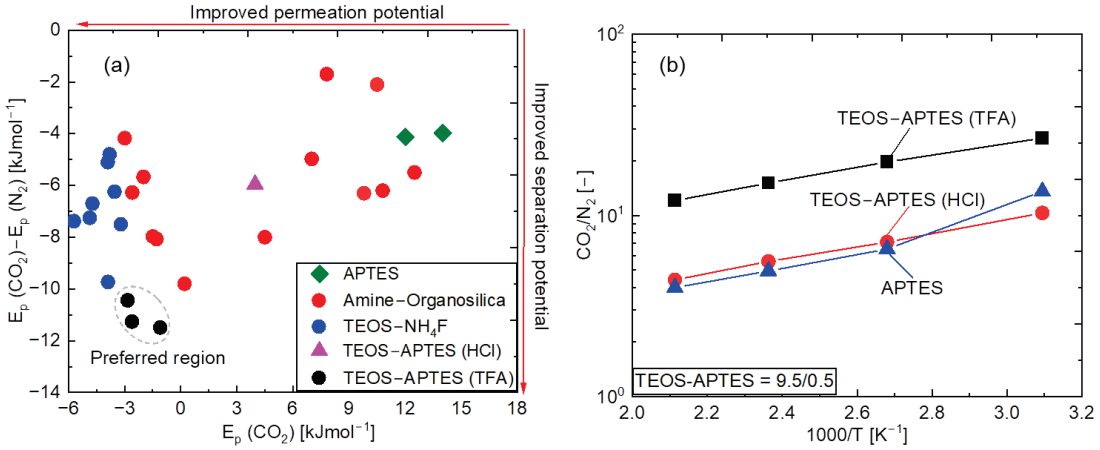

Fig. 4-8. Relationship between E_p (CO_2) and E_p (CO_2) – E_p (N_2) [27, 45, 46] (a) ideal CO_2/N_2 selectivity (b) for APTES and composite (TEOS-APTES) membranes calcined at 250 ºC under N_2 atmosphere.

4.3.3. Binary (CO_2/N_2) separation performance of composite membranes

Fig. 4-9 shows the temperature dependence of a TEOS-APTES (TFA) silica membrane for both single and binary (5/5) gas permeance. In the present study, the surface diffusion and activated diffusion mechanisms of CO_2 and N_2 permeance, respectively, demonstrated a similar dependence on temperature, irrespective of the separation system (single/binary). However, divergence in CO_2 permeance for single and binary separation systems apparently increased as the temperature was decreased from 200 to 50 ºC and this effect became more obvious in binary (5/5) separation when measured at a low temperature of 50 ºC. This trend could be explained by an increase in the CO_2 adsorption properties at 50 ºC,

which was followed by an enhancement of the effects of surface diffusion and a resultant network structure that exhibited a high CO_2 permeance of 3.8×10^{-7} mol m^{-2} s^{-1} Pa^{-1} with CO_2/N_2 selectivity of 35 when using a binary (5/5) separation system.

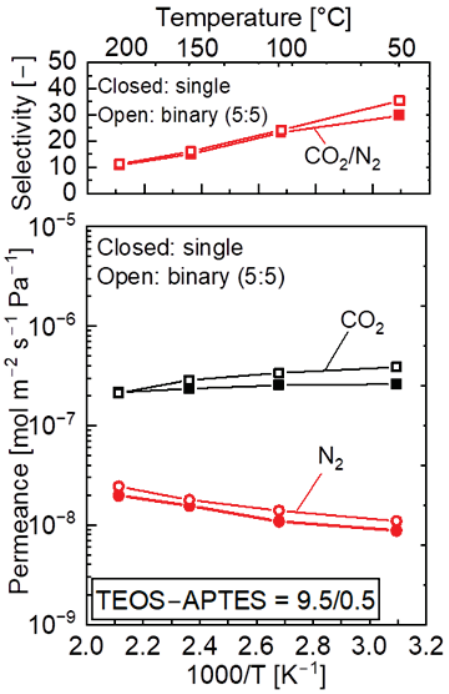

Fig. 4-9. Temperature dependence of single/binary gas separation for composite TEOS-APTES (TFA) membrane calcined at 250 ºC under N_2 atmosphere.

Fig. 4-10a displays the partial-pressure dependence on CO_2 permeance at 50 ºC for the TEOS-APTES (TFA) silica membrane. With the occurrence of a high level of partial pressure in the feed (where the network structure is saturated by the preferential adsorption of CO_2 molecules), CO_2 permeance is lower by comparison with a feed under a low level of partial pressure, which indicates the effect of surface diffusion.

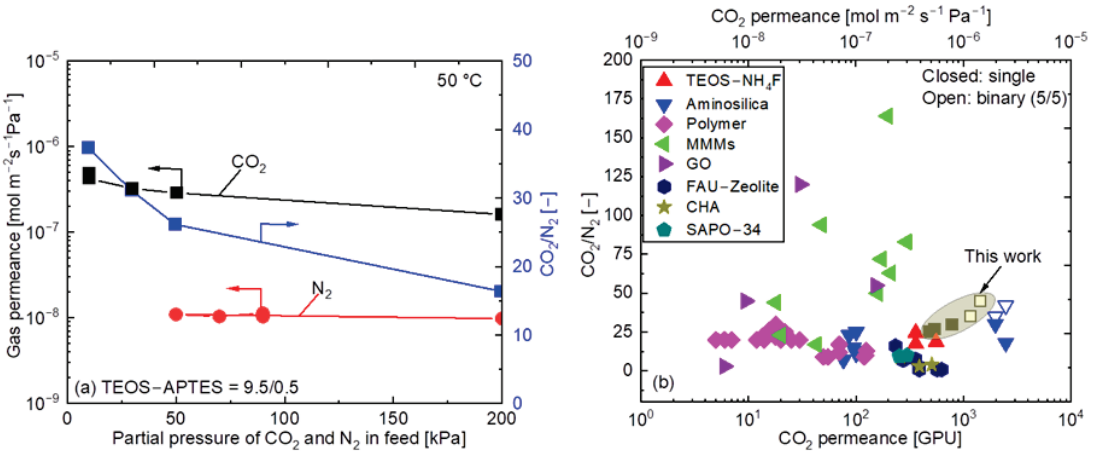

Fig. 4-10. Gas permeation properties: (a) partial-pressure dependence of CO_2 and N_2 permeance along with CO_2/N_2 selectivity for TEOS-APTES (TFA) membranes at 50 ºC; (b) relationship between CO_2 permeance and CO_2/N_2 selectivity for composite TEOS-APTES (TFA) membranes and recently reported state-of-the-art membranes.

Fig. 4-10b shows the relationship between CO_2 permeance and the CO_2/N_2 separation factors for TEOS-APTES (TFA) and other reported membranes at 50 ºC. TEOS-APTES (TFA) demonstrated a CO_2 permeance of more than 1,000 GPU and CO_2/N_2 selectivity of 35, which is superior to many state-of-the-art amine-silica membranes. It should be noted that a CO_2 permeance of more than 1,000 GPU (1 GPU = 3.5×10^{-10} mol m^{-2} s^{-1} Pa^{-1}) with moderate selectivity (~20) is acceptable for industrial applications [8]. This greater separation potential for TEOS-APTES (TFA) membranes could be the result of enhanced microporosity as well as interactions with CO_2 and amides, which facilitates gas transport within the membrane matrix.

4.3.4. Single/binary (CO_2/N_2 = 1/9) separation performance under wet conditions

The time courses for CO_2 and N_2 permeance were measured for TEOS-APTES (TFA) in order to evaluate the hydrothermal stability under dry and wet conditions (H_2O partial pressure = 3 kPa), as shown in Fig. 4-11. Apparently there was no change in the gas permeance for either CO_2 or N_2 under wet conditions. These results indicate considerable hydrothermal stability for the TEOS-APTES (TFA) membrane, which is attributed to the hydrophobic organic chain as well as to the extensive use of TFA that increased the hydrophobicity of the silica surface [26].

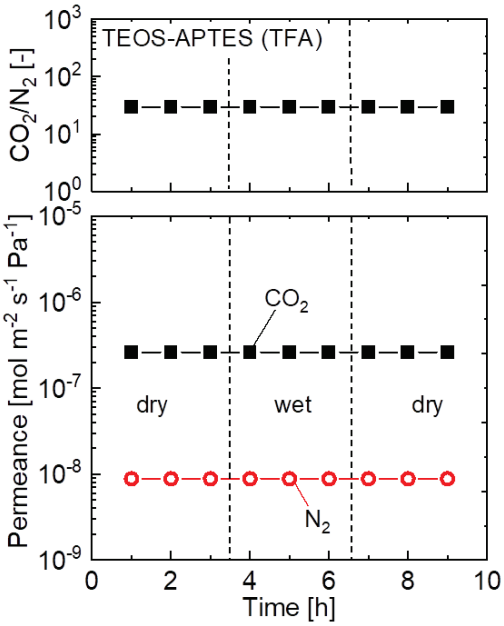

Fig. 4-11. Time course for CO_2 and N_2 permeance for the TEOS-APTES (TFA) membrane under both dry and wet conditions (H_2O partial pressure = 3 kPa).

Table 4-3 shows the performance of the TEOS-APTES (TFA) membrane at 50 ºC before/after exposure to relative humidity (RH) of 30-40% at 25 ºC for 50 days. CO_2 and

N_2 permeance showed considerable membrane stability over a period of 50 days. Sayari et al. [30] reported similar results from the steam exposure (RH: 0-74%, 303-423K) of amine-contained sorbents. The obtained results reveal that CO_2 adsorption increases with exposure to water vapor, which further establishes the stability of the amine surface under harsh conditions. Mebane et al. [31] explained that water vapor facilitated the stabilization of CO_2 reactive intermediates. Miyamoto et al. [32] concluded that the length of the alkyl chain could have a significant effect on the CO_2 separation performance of silica materials that contain amines.

Table 4-3. Single gas permeance at 50 ºC for TEOS-APTES (TFA) membrane before/after exposure to relative humidity (RH) of 30-40% for 50 days.

As prepared membrane			After 50 days exposure (RH: 30-40%)		
Permeance [mol m^{-2} s^{-1} Pa^{-1}]		α [−]	Permeance [mol m^{-2} s^{-1} Pa^{-1}]		α [−]
CO_2	N_2	CO_2/N_2	CO_2	N_2	CO_2/N_2
2.6×10^{-7}	9.8×10^{-8}	29	2.2×10^{-7}	7.1×10^{-9}	31

Table 4-4 shows the single and binary (CO_2/N_2 = 10/90) gas separation performance for TEOS-APTES (TFA) membranes under dry and wet (H_2O partial pressure = 3 kPa) conditions. CO_2 permeance showed comparable results irrespective of a dry or wet system. This could be attributed to an increase in the CO_2 adsorption capacity of respective membrane surfaces in the presence of water vapors, as reported in several studies [30-32].

Table 4-4. CO_2/N_2 binary (10/90) separation performance of TEOS-APTES (TFA) membrane at 50 ºC under dry and wet (H_2O partial pressure = 3 kPa) conditions.

Dry system			Wet system		
Permeance [mol m^{-2} s^{-1} Pa^{-1}]		α [−]	Permeance [mol m^{-2} s^{-1} Pa^{-1}]		α [−]
CO_2	N_2	CO_2/N_2	CO_2	N_2	CO_2/N_2
4.2×10^{-7}	1.13×10^{-8}	37	4.8×10^{-7}	1.03×10^{-8}	45

4.4. Conclusions

Amide-functionalized silica membranes were fabricated for CO_2/N_2 separation via the use of tetraethoxysilane (TEOS) and amine-silica (3-aminopropyltriethoxysilyl, APTES) precursors in the presence of trifluoroacetic acid (TFA). The FT-IR spectra showed newly formed species as a result of special interactions generated among TFA and primary amines (NH_2), which was further demonstrated by reversible CO_2 adsorption/desorption isotherms. NLDFT revealed a pore size distribution for the TEOS-APTES (TFA) sample that exhibited a higher micropore volume compared with those of either the APTES or TEOS-APTES (HCl) network structures. Further, the developed composite membranes exhibited a CO_2 permeance of 3.8×10^{-7} mol m^{-2} s^{-1} Pa^{-1} and a CO_2/N_2 selectivity of 35 at 50 ºC during binary gas separation, which was facilitated by a functionalized dual network structure with size-sieving properties (tailored network) and CO_2-philic sites (amides). Finally TEOS-APTES (TFA) membrane was applied under wet conditions (H_2O partial pressure = 3 kPa) to evaluate the hydrothermal stability in both single and binary (CO_2/N_2 = 1/9) separation systems. Membrane showed considerable hydrothermal stability irrespective of the single/binary separation system.

References

1. K. Nakahiro, L. Yu, H. Nagasawa, T. Tsuru, M. Kanezashi, Pore structure controllability and CO_2 permeation properties of silica-derived membranes with a dual-network structure. Ind. Eng. Chem. Res. 60 (2021) 8527-8537.

2. K. Karakiliç, C. Huiskes, M. W. Luiten-Olieman, A. Nijmeijer, L. Winnubst, Sol-gel processed magnesium-doped silica membranes with improved H_2/CO_2 separation. J. Membr. Sci. 543 (2017) 195-201.

3. M. T. Ravanchi, T. Kaghazchi, A. Kargari, Application of membrane separation processes in petrochemical industry. Rev. Des. 235 (2009) 199-244.

4. H. L. Castricum, H. F. Qureshi, A. Nijmeijer, L. Winnubst, Hybrid silica membranes with enhanced hydrogen and CO_2 separation properties. J. Membr. Sci. 488 (2015) 121 128.

5. S. Karimi, Y. Mortazavi, A. A. Khodadadi, A. Holmgren, D. Korelskiy, J. Hedlund, Functionalization of silica membranes for CO_2 separation. Sep. Purif. Technol. 235 (2020) 116207.

6. M. Asaeda, S. Yamasaki, Separation of inorganic/organic gas mixtures by porous silica membranes. Sep. Purif. Technol. 25 (2001) 151-159.

7. K. Kusakabe, S. Sakamoto, T. Saie, S. Morooka, Pore structure of silica membranes formed by a sol-gel technique using tetraethoxysilane and alkyltriethoxysilanes. Sep. Purif. Technol. 16 (1999) 139-146.

8. M. Guo, M. Kanezashi, H. Nagasawa, L. Yu, J. Ohshita, T. Tsuru, Amino-decorated organosilica membranes for highly permeable CO_2 capture. J. Membr. Sci. 611 (2020) 118328.

9. L. Yu, M. Kanezashi, H. Nagasawa, M. Guo, N. Moriyama, K. Ito, T. Tsuru, Tailoring ultramicroporosity to maximize CO_2 transport within pyrimidine-bridged organosilica membranes. ACS App. Mater. Int. 11 (2019) 7164-7173.

10. Y. Sakamoto, K. Nagata, K. Yogo, K. Yamada, Preparation and CO_2 separation properties of amine-modified mesoporous silica membranes. Micro. Meso. Mater. 101 (2007) 303-311.

11. L. Yu, M. Kanezashi, H. Nagasawa, T. Tsuru, Fabrication and CO_2 permeation properties of amine-silica membranes using a variety of amine types. J. Membr. Sci. 541 (2017b) 447-456.

12. B. Wadi, C. Li, V. Manovic, P. Moghadam, S. A. Nabavi, Contributions of CH_4-amine interactions by primary, secondary, and tertiary amines on CO_2/CH_4 separation efficiency. Chem. Eng. J. (2023) 142117.

13. L. Mafra, T. Čendak, S. Schneider, P. V. Wiper, J. Pires, J. R. Gomes, M. L. Pinto, Amine functionalized porous silica for CO_2/CH_4 separation by adsorption: Which amine and why. Chem. Eng. J. 336 (2018) 612-621.

14. Y. G. Ko, S. S. Shin, U. S. Choi, Primary, secondary, and tertiary amines for CO_2 capture: Designing for mesoporous CO_2 adsorbents. J. Coll. Int. Sci. 361 (2011) 594-602.

15. S. Araki, T. Satoh, H. Doi, H. Yano, Y. Miyake, Properties of amino-functionalized silica membranes for the dehydration of water/ethanol mixtures. Des. Water Treat. 7 (2009) 12-17.

16. G. Xomeritakis, C. Y. Tsai, C. J. Brinker, Microporous sol-gel derived aminosilicate membrane for enhanced carbon dioxide separation. Sep. Purif. Technol. 42 (2005) 249-257.

17. B. A. McCool, W. J. Desisto, Amino-functionalized silica membranes for enhanced carbon dioxide permeation. Adv. Fun. Mater. 15 (2005) 1635-1640.

18. M. Kanezashi, T. Matsutani, T. Wakihara, H. Tawarayama, H. Nagasawa, T. Yoshioka, T. Tsuru, Tailoring the subnano silica structure via fluorine doping for development of highly permeable CO_2 separation membranes. ChemNanoMat. 2 (2016) 264-267.

19. I. Rana, H. Nagasawa, T. Tsuru, M. Kanezashi, Tailoring the structure of a sub-nano silica network via fluorine doping to enhance CO_2 separation and evaluating CO_2 separation performance under dry or wet conditions. J. Membr. Sci. 658 (2022) 120735.

20. A. Grill, Porous pSiCOH ultralow-k dielectrics for chip interconnects prepared by PECVD. Ann. Rev. Mater. Res. 39 (2009) 49-69.

21. H. Ishida, J. L. Koenig, Fourier transform infrared spectroscopic study of the silane coupling agent/porous silica interface. J. Coll. Inter. Sci. 64 (1978) 555-564.

22. M. Jafarzadeh, E. Soleimani, P. Norouzi, R. Adnan, H. Sepahvand, Preparation of trifluoroacetic acid-immobilized Fe_3O_4@ SiO_2-APTES nanocatalyst for synthesis of quinolones. J. Fluor. Chem. 178 (2015) 219-224.

23. S. Fujihara, C. Mochizuki, T. Kimura, Formation of LaF_3 microcrystals in sol–gel silica. J. Non-Cryst. Solid. 244 (1999) 267-274.

24. A. M. Mailhot, A. Elyamani, R. E. Riman, Reactive atmosphere synthesis of sol-gel heavy metal fluoride glasses. J. Mater. Res. 7 (1992) 1534-1540.

25. S. Suzuki, S. B. Messaoud, A. Takagaki, T. Sugawara, R. Kikuchi, S. T. Oyama, Development of inorganic-organic hybrid membranes for carbon dioxide/methane separation. J. Membr. Sci. 471 (2014) 402-411.

26. A. Calvo, M. Joselevich, G. J. Soler-Illia, F. J. Williams, Chemical reactivity of amino-functionalized mesoporous silica thin films obtained by co-condensation and post-grafting routes. Micro. Meso. Mater. 121 (2009) 67-72.

27. M. Takenaka, H. Nagasawa, T. Tsuru, M. Kanezashi, Hydrocarbon permeation properties through microporous fluorine-doped organosilica membranes with controlled pore sizes. J. Membr. Sci. 619 (2021) 118787.

28. D. Deng, Y. Cui, D. Chen, N. Ai, Solubility of CO_2 in amide-based brønsted acidic ionic liquids. J. Chem. Therm., 57 (2013) 355-359.

29. L. Yu, M. Kanezashi, H. Nagasawa, T. Tsuru, Role of amine type in CO_2 separation performance within amine functionalized silica/organosilica membranes: A review. App. Sci. 8 (2018) 1032.

30. A. Sayari, Y. Belmabkhout, Stabilization of amine-containing CO_2 adsorbents: dramatic effect of water vapor. J. Amer. Chem. Soc. 132 (2010) 6312-6314.

31. D. S. Mebane, J. D. Kress, C. B. Storlie, D. J. Fauth, M. L. Gray, K. Li, Transport, zwitterions, and the role of water for CO_2 adsorption in mesoporous silica-supported amine sorbents. J. Phys. Chem. C. 117 (2013) 26617-26627.

32. M. Miyamoto, A. Takayama, S. Uemiya, K. Yogo, Gas permeation properties of amine loaded mesoporous silica membranes for CO_2 separation. Des. Water Treat. 34 (2011) 266-271.

Chapter 5

Conclusions and outlook

This dissertation is devoted to the development of fluorine induced microporous silica membranes for CO_2 separation. Various characterizations were conducted to clarify the network pore structure and surface morphologies of employed materials. In order to obtain highly permeable CO_2 selective silica membranes, network pore structure of several monomers was tailored via fluorine doping to increase the molecular sieving effect as well as the controlled CO_2 adsorption properties of respective fluorine doped materials. The present research emphasizes the development of fluorine induced organic-inorganic silica membranes with high CO_2 permeation properties. This novel strategy will have far reached effect on the development of CO_2 selective silica membranes. The main conclusions and outlook of this dissertation were summarized as follows.

5.1. Conclusions

(a) A strategy was proposed to control the network pore structure of conventional silica via fluorine doping to fabricate highly permeable membranes for CO_2 separation. Various fluorine concentrations (F/Si=0.1/9.9, 0.3/9.7, 0.5/9.5, 1/9, 2/8) were doped via a sol-gel method to allow examination of the effect that fluorine exerts on a silica network structure. Physicochemical analysis revealed that fluorine effectively improved the hydrophobic/hydrophilic properties by eliminating the factors (Si-OH) involved in the formation of a dense silica structure.

Fluorine-doped silica membranes fabricated with different concentrations of fluorine showed consistent results according to structural characterization. For example, an F/Si ratio of 0.5/9.5 showed a loose network structure by comparison with a smaller fluorine content (F/Si=0.1/9.9). Fluorine doping precisely enlarges the network pore size in a sub-nano range. Due to a reduction in Si-OH in a network structure, however, CO_2 adsorption is decreased as the concentration of doped fluorine increases. A fluorine-doped silica membrane with an F/Si ratio of 0.1/9.9 showed the highest permeance ratio of 50 with CO_2 permeance of 1.6×10^{-7} mol m^{-2} s^{-1} Pa^{-1} at 50 ºC.

In a wet system (200-300 ºC, H_2O partial pressure: 3 kPa), fluorine-doped silica membranes were quite stable, irrespective of the concentration of the doped fluorine. Under steam with a high level of partial pressure (300 ^{o}C, H_2O partial pressure: 30 kPa), the concentration of doped fluorine strongly affected the hydrothermal stability. The F-SiO_2 membrane with an F/Si ratio of 0.1/9.9 showed drastic decreases for all examples of permeance. On the contrary, when fluorine content was increased, it was apparent that the change in pore size distribution accordingly suppressed the hydrothermal stability and the membranes with F/Si ratios of 0.3/9.7 & 0.5/9.5 showed steady values for gas permeance in both dry and wet systems.

(b) A series of pendant alkoxysilane structures with various carbon numbers (C_1-C_8) were used to fabricate sol-gel derived organosilica membranes to evaluate the effects of the C/Si ratio and fluorine doping. Initially, this investigation was focused on the effect that carbon-linking (pendant-type) units exert on a microporous structure and how this affects the gas-

permeation properties of pendant-type organosilica membranes. Gas permeation results were compared with those of bridged-type organosilica membranes (C_1-C_8). Subsequently, we also evaluated the effect that fluorine doping (NH_4F) exerts on pendant–type [methytriethoxysilane (MTES), propyltrimethoxysilane (PTMS)] and bridged-type [1,2-bis(triethoxysilyl)methane (BTESM) bis(triethoxysilyl)propane (BTESP)] organosilica structures with similar carbon numbers (C_1 and C_3).

The pendant-type organosilica membranes showed a slightly looser network structure with a decrease in H_2/N_2 selectivity compared to those of bridge-type organosilica membranes. Activation energy (E_p) increased as the carbon number increased in both types of membranes, which indicates increased space occupation by pendant side chains as the C/Si ratio increased, and increased network flexibility in bridged-type organosilica membranes. However, permeation results revealed that pendant-type organosilica membranes demonstrated a larger pore size in comparison with bridged-type organosilica membranes, due to the lower values of activation energies (E_p) which is evidence of a loose network formation.

Fluorine-doped pendant-type organosilica membranes showed pore sizes similar to those of undoped organosilica membranes with comparable selectivity (H_2/N_2) and E_p (H_2). Those results are ascribed to the existence of pendant side chains, which could have restricted the effectiveness of fluorine and allowed the pore size to remain unchanged. Conversely, fluorine significantly improved the permeation properties of bridged–type organosilica membranes (H_2/N_2); the F/Si ratio was increased due to the formation of a

loose network formation caused by the Si-F and C-F groups present in the network structure.

After several experiments, all membranes continued to exhibit considerable stability in characteristics such as molecular size dependence and temperature dependence of gas permeance. These good results notwithstanding, long-term separation performance of these membranes will be conducted in our future work.

(c) Amide-functionalized silica membranes were fabricated for CO_2/N_2 separation via the use of tetraethoxysilane (TEOS) and amine-silica (3-aminopropyltriethoxysilyl, APTES) precursors in the presence of trifluoroacetic acid (TFA). The FT-IR spectra showed newly formed species as a result of special interactions generated among TFA and primary amines (NH_2), which was further demonstrated by reversible CO_2 adsorption/desorption isotherms. NLDFT revealed a pore size distribution for the TEOS-APTES (TFA) sample that exhibited a higher micropore volume compared with those of either the APTES or TEOS-APTES (HCl) network structures. Further, the developed composite membranes exhibited a CO_2 permeance of 3.8×10^{-7} mol m^{-2} s^{-1} Pa^{-1} and a CO_2/N_2 selectivity of 35 at 50 ºC during binary gas separation, which was facilitated by a functionalized dual network structure with size-sieving properties (tailored network) and CO_2-philic sites (amides). Finally TEOS-APTES (TFA) membrane was applied under wet conditions (H_2O partial pressure = 3 kPa) to evaluate the hydrothermal stability in both single and binary (CO_2/N_2 = 1/9) separation systems. Membrane showed considerable hydrothermal stability irrespective of the single/binary separation system.

5.2. Outlook

We have demonstrated the CO_2 permeation properties of fluorine induced microporous silica membranes. Fluorine effectively controlled the network pore sizes of silica membranes which showed excellent CO_2/N_2 separation performance following the high molecular sieving effect. However, the obtained pore size distribution for some of the organosilica membranes was not effective for CO_2/N_2 separation. Therefore, a careful attention required to develop CO_2 selective silica membranes for future applications while considering this strategy. It is worth noticing that chosen strategy was not subject to apply for industrial trial in terms of CO_2/N_2 separation efficiency. Hence, it is vital to further explore the possibilities of CO_2/N_2 separation efficiency of fluorine induced silica membranes on industrial scale by employing the approach described in this research study. Thus far, CO_2 affinity and network pore size controlled by using fluorine contained amino-silica precursors could be another alternative technique. Last but not the least, the assessments of the affinity between CO_2 and silica membranes is currently conducted through qualitatively measuring the single-component adsorption isotherms, which is far from the real conditions of binary separations of CO_2/N_2 mixtures. The binary gas sorption properties or a measurement of breakthrough may provide us more useful information for better understanding the separation mechanism of CO_2/N_2 through fluorine induced silica membranes.

List of publications

Journal articles

1. **Ikram Rana,** Hiroki. Nagasawa, Toshinori Tsuru, Masakoto Kanezashi*, Tailoring the structure of a sub-nano silica network via fluorine doping to enhance CO_2 separation and evaluating CO_2 separation performance under dry or wet conditions. *J. Membr. Sci.* 658 (2022) 120735.

2. **Ikram Rana,** Hiroki Nagasawa, Kazuki Yamamoto, Takahiro Gunji, Toshinori Tsuru, Masakoto Kanezashi*, Effect of fluorine doping on the network pore structure of non-porous organosilica bis (triethoxysilyl) propane (BTESP) membranes for use in molecular separation. *J. Membr. Sci.* 644 (2022) 120083.

3. **Ikram Rana,** Takahiro Nagaoka, Hiroki Nagasawa, Toshinori Tsuru, Masakoto Kanezashi*, The effect of C/Si ratio and fluorine doping on the gas permeation properties of pendant-type and bridged-type organosilica membranes. *Membranes* 12 (2022) 991.

4. **Ikram Rana,** Hiroki Nagasawa, Toshinori Tsuru, Masakoto Kanezashi*, Catalytic effect of trifluoroacetic acid on the CO_2 transport properties of organic-inorganic hybrid silica membranes. *J. Membr. Sci. Lett*. 3 (2023) 100047.

Academic proceedings

1. **Ikram Rana,** Hiroki. Nagasawa, Toshinori Tsuru, Masakoto Kanezashi*, Effect of fluorine doping on non-porous bis (triethoxysilyl) propane (BTESP) network structure. *Annual meeting of Society of Chemical Engineers Japan (Scej)*, March 16-18, 2022. (Oral)

2. **Ikram Rana,** Hiroki. Nagasawa, Toshinori Tsuru, Masakoto Kanezashi*, Effect of fluorine doping on CO_2 permeation properties of silica membranes, *15th International conference on catalytic membrane reactors (ICCMR-15)*, August 01-06, 2022, Tokyo, Japan. (Oral)

3. **Ikram Rana,** Hiroki. Nagasawa, Toshinori Tsuru, Masakoto Kanezashi*, Tailoring the structure of a sub-nano silica network via fluorine doping to enhance CO_2 separation and evaluating CO_2 separation performance under dry or wet conditions, *Membrane symposium of Japan,* Nov 09-10, 2022, Kobe, Japan. (Oral)

Acknowledgment

First and foremost, I would like to express my deepest appreciation to my supervisor, Prof. Masakoto Kanezashi, for providing me the opportunity to come to Hiroshima University and extend sincere gratitude for his patient guidance throughout my PhD study. His profound knowledge and continuous assistance benefited me for the pursuit of scientific research. I am very grateful to his insightful and helpful advices on both the research work and the career planning. I am very thankful to Prof. Toshinori Tsuru and Prof. Hiroki Nagasawa for sparing no efforts to provide precious suggestions on my research work and the dissertation. I would like to express my gratitude to Prof. Kazuki Yamamoto and Prof. Takahiro Gunji for synthesizing the organosilica monomers for membrane fabrications. I would also like to thanks to Prof. Oshita and Prof. Fukui in my dissertation committee for reading my thesis in their busy schedule. I am thankful to my supporter, Mr. Takahiro Nagaoka, for his assistance in my research work and daily life, when I came to Japan. I would like to thanks all other group members in the Separation Engineering Lab, for their endless help. Specially, I would like to express my appreciation to Dr. Sulaiman O. Lawal for helping me out during my research work. I would like to thank my beloved parents, the only inspiration to me. Finally, I highly appreciate the financial support from the Japanese Government (Monbukagakusho, MEXT) scholarship.

July 2023

Ikram Rana